Investigation of the "Unit Cell" Concept for Air-to-Liquid Heat Exchanger Research and Development

---

A Thesis presented to
the Faculty of the Graduate School
at the University of Missouri-Columbia

In Partial Fulfillment
of the Requirements for the Degree

Master of Science

---

by
SEAN C. STAED

Dr. James Bryan, Thesis Supervisor

AUGUST 2007

The undersigned, appointed by the dean of the Graduate School, have examined the thesis entitled,

INVESTIGATION OF THE UNIT CELL CONCEPT FOR AIR-TO-LIQUID HEAT EXCHANGER RESEARCH AND DEVELOPMENT

presented by Sean C. Staed, a candidate for the degree of master of science, and hereby certify that, in their opinion, it is worthy of acceptance.

Professor James Bryan

Professor Gary Solbrekken

Professor T.R. Marrero

This thesis is dedicated to my parents. For all of the support and encouragement they have given to me throughout the years of my life.

ACKNOWLEDGEMENTS

The author acknowledges the financial support of Advanced Heat Transfer LLC and to Outokumpu-Heatcraft who provided the comparative data for the standard size coils and the Unit Cell coils for testing. Acknowledgements must be made to members of these companies who were in direct contact with the author specifically, Mike Heidenreich, Hailing Wu and Bill Winebrenner. Also thanks must be given to Dr. James Bryan for his guidance and knowledge throughout the Unit Cell project. Finally for the University of Missouri-Columbia and to Joshua Hensley and Bryan Samuels who helped in production of the air handler system.

TABLE OF CONTENTS

LIST OF FIGURES

Figure **Page**

LIST OF TABLES

Table **Page**

NOMENCLATURE

A	Coil cross-section area, m^2 (ft^2)
C	Constant or correction factor
C_p	Specific heat, kJ/kg·°C (Btu/lb_m·°F)
D	Inside tube diameter, m (ft)
h	Enthalpy, kJ/kg (Btu/lb_m)
M	Molecular mass, g/mol (lb_m/mol)
$\dot{m}$	Mass flow rate, kg/s (lb_m/h)
n	Number of moles
p	Pressure kPa (in. of H_2O)
ΔP	Pressure drop kPa (in. of H_2O)
Q	Heat transferred, W (Btu/h)
q''	Heat flux, W/m^2 (Btu/h · ft^2)
Re	Reynolds Number
T	Temperature, °C (°F)
U	Overall heat transfer coefficient, W/m^2 · ° C (Btu/h ·ft^2 · ° F)
$\dot{V}$	Volumetric flow rate, m^3/s (ft^3/min)
$\vec{v}$	Face velocity, m/s (ft/min)
W	Air humidity ratio, kg/kg (lb_m/lb_m)
X	Mol fraction

Greek Symbols

μ	viscosity, micropoise
ρ	density, kg/m^3 (lb_m/ft^3)
v	specific volume, m^3/kg (ft^3/lb_m)

Subscripts

actual	actual
dry	dry air
duct	duct
H_2O	water
in	inlet
LFE	Laminar Flow Element
lm	log mean
out	outlet
s	saturation
sensible	sensible
std, standard	standard
wb	wet bulb
wet	wet air
ws	water vapor saturation

ABSTRACT

This study investigated the validity of the Unit Cell concept to explore the performance of air-to-liquid heat exchangers. The Unit Cell concept will test only a 15.24 cm by 15.24 cm portion of a full sized prototype coil, to predict airside and heat transfer performance. This reduction in prototype size will allow for reduced costs and time for researching and development of heat exchangers. To validate a working model of the Unit Cell concept, a testing apparatus and procedure has been developed to test the small sized coils. Tests have shown that pressure drop across the Unit Cell coil can be matched within 6.27% and overall heat transfer can be matched within 6.37% of the full sized standard coil. By matching the available standard sized coil results, the Unit Cell concept has been confirmed and will provide a basis for improving heat exchanger testing.

1. INTRODUCTION

Air-to-refrigerant and air-to-liquid heat exchangers are a commonplace in today's society, from simple home appliances to intricate industrial equipment. As that market continues to expand and craves for more efficient and complex heat exchangers, it is imperative to develop new technology and research methods to test new types of heat exchangers. Even with advances in analytical and numerical tools, heat exchanger manufacturers have repeatedly turned to experimental data for coil improvements and model verification. However, the generation of experimental data can be relatively costly and time consuming.

In the past, scaled-up experimental models have been employed to predict heat transfer and flow characteristics. Yun and Lee [1,2] investigated airside heat transfer characteristics and pressure drop of fin-and-tube heat exchangers using a three times scaled-up model. In these investigations they studied the effect of slit parameters such as fin pitch, pattern angle, slit height and slit length. Byun, Lee, Jeon and Mok [3] invoked a similar method in enlarging a finned tube heat exchanger as much as four times to estimate pressure drop and heat transfer characteristics of four different kinds of fins: louver, double side split, single side split and plain fin. Likewise Kang and Kim [4] performed a study on how heat transfer and flow characteristics of air cooled heat exchangers enlarged three times compare well with standard sizes. All the studies mentioned above deal with enlarging a coil 3-4 times its practical size. While these tests reduce the cost of producing a prototype coil, the redundancy of producing multiple expensive dies for both fundamental testing and for production coils is undesirable. By

testing coils using a Unit Cell model, which tests similarly geometrid coils at a reduced face area, one similar die can be produced while benefiting from the same reduced costs of prototype coils.

The main goal of this work is to develop the "Unit Cell" concept to accommodate the research and development of new air-to-liquid heat exchangers. The "Unit Cell" concept is a method to predict and map the pressure drop and heat transfer characteristics of a standard (full-size) heat exchanger by testing a smaller version, specifically a 15.24 cm by 15.24 cm (6.00 in. by 6.00 in.) section or a face area of 0.0232 m^2 (0.25 ft^2). A coil of this size will also be conducive to CFD analysis, further improving coil R&D efforts. The dimensional requirements for a heat exchanger test, prescribed by ARI 410-2001 5.2.1 [5], are presented as:

> "All cooling and heating coil Laboratory Tests shall be conducted with a representative coil having a face area of 2 to 10 ft^2 [0.19 to 0.93 m^2]."

The Unit Cell method will test a coil whose size will be an order of magnitude lower than what is conventionally prescribed, while still imposing the rest of the ARI testing requirements.

In theory a standard coil regardless of its full scale size should have the same heat flux and pressure drop of its Unit Cell counterpart under the same operating conditions. Scaled-up models must address similitude relations and scale their data accordingly to match standard results. But the advantage in the Unit Cell model is that many of heat transfer and flow characteristics can be compared directly at a 1:1 ratio, rather than at a scaled parameter. In practice matching many of the operating conditions may be difficult. If the Unit Cell testing can be validated and practical, it can be beneficial to the industry by reducing the total cost of prototypes and expediting development time

through outsourcing testing to smaller labs. Unit Cell tests will offer an alternative method of verification of analytical and numerical models. On a more investigatory level, the decreased test time can lead to a better understanding of major role players in overall coil efficiency relative to the coil's tube and fin geometry.

Three specific objectives were required to accomplish the goal.

1. Design and build a wind tunnel to accurately facilitate air-side flow and heat transfer measurements.
2. Design and build a liquid loop to accurately facilitate liquid-side flow and heat transfer measurements.
3. Develop and validate Unit Cell method against available full size coil data.

2. EXPERIMENTAL SETUP

The following sections provide detailed descriptions of the wind tunnel and liquid loop systems designed and developed to enable the "Unit Cell" method.

2.1 The Air Handler and Liquid Loop

A multifunctional small-scale wind tunnel was developed to primarily support in the verification and testing of the Unit Cell concept. The testing apparatus consists of a temperature and humidity controlled wind tunnel and a recirculating liquid supply loop designed to provide reliable testing conditions procedures and numerous testing capabilities on both the air and water side of the system. Schematics of the entire testing system are presented in Figs. 1-3.

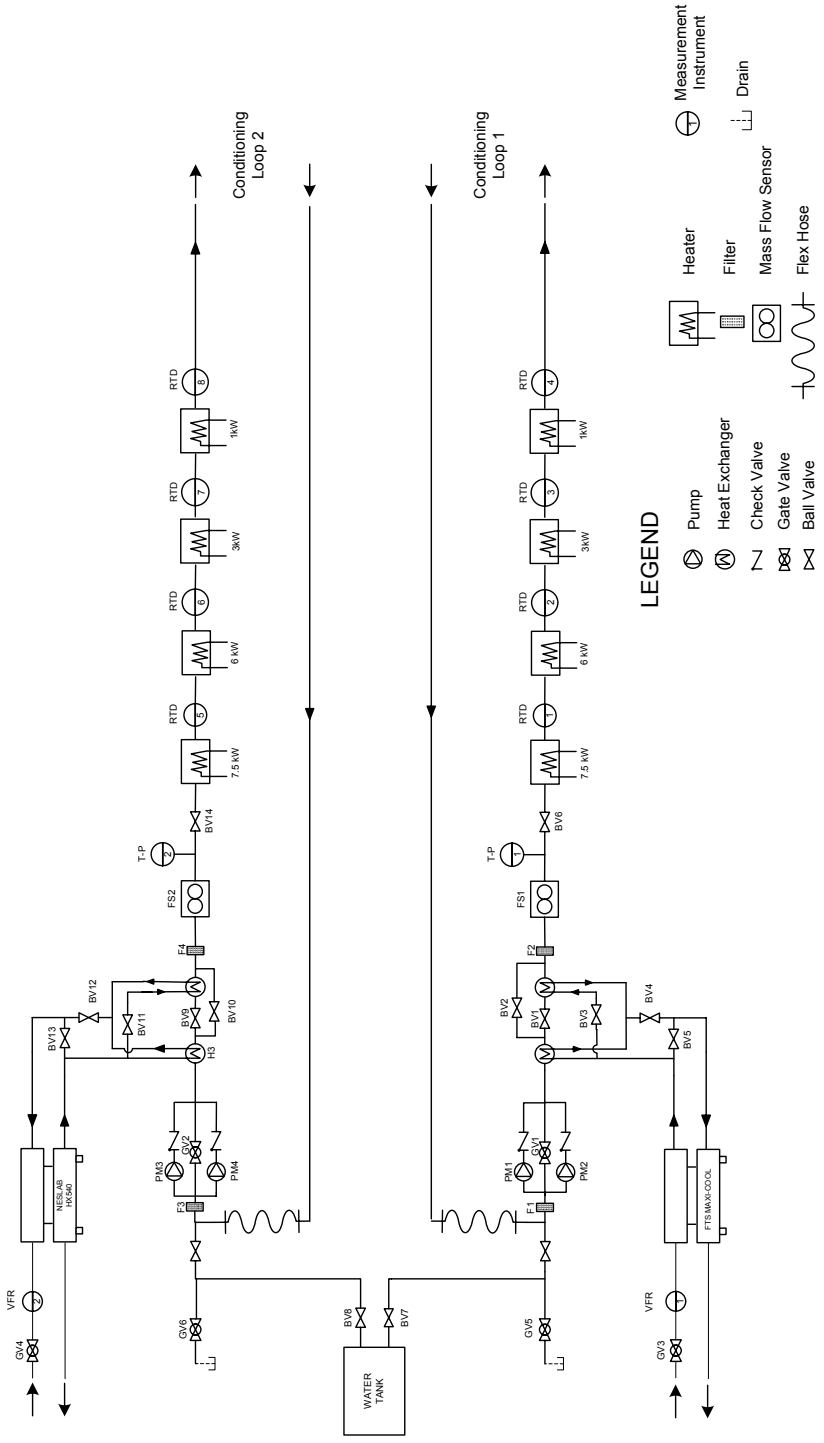

Fig. 1. Schematic of air-handler conditioning loops.

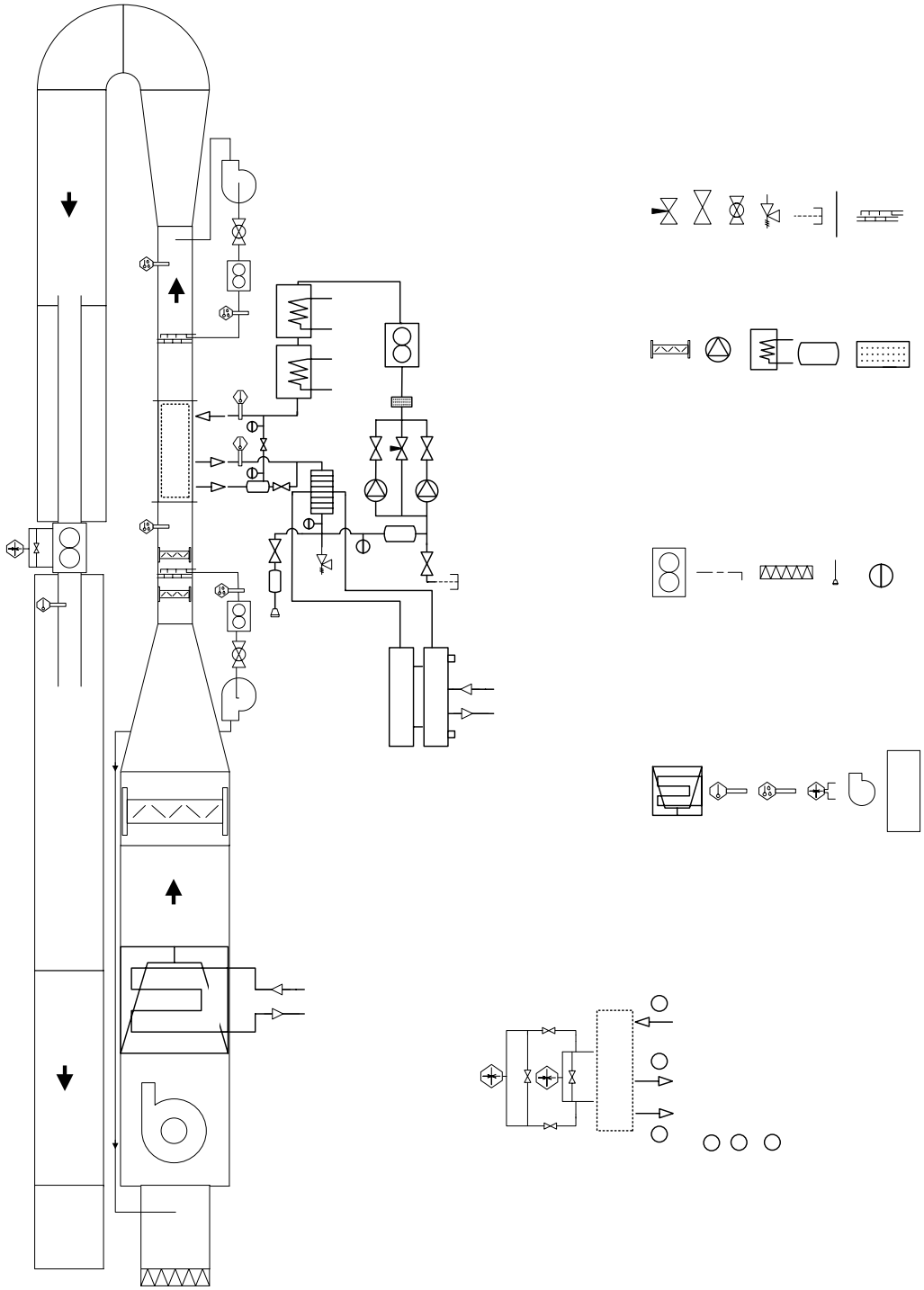

Fig. 2. Schematic of original air-handler and test liquid loop.

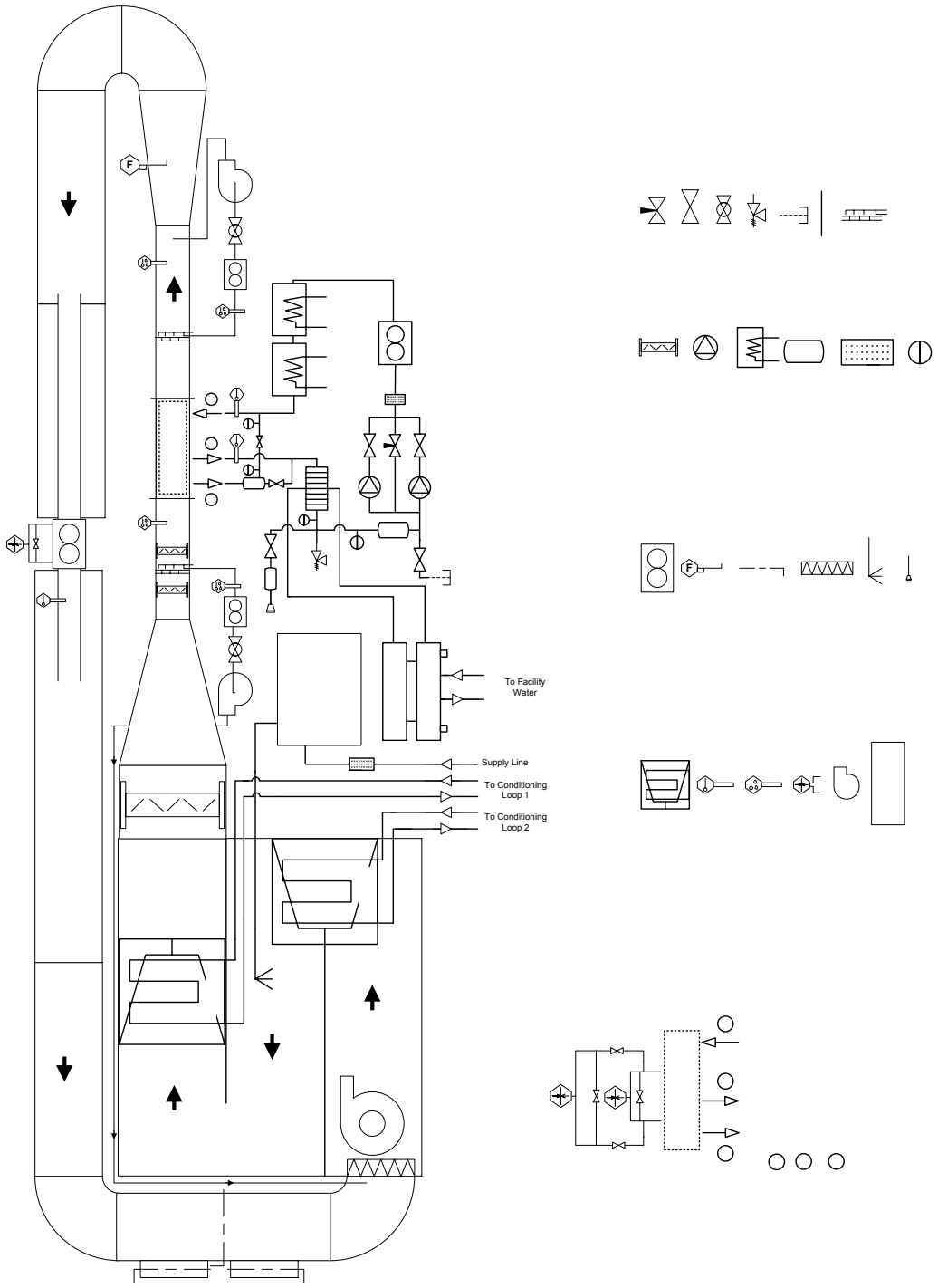

Fig. 3. Schematic of current air-handler and test liquid loop.

2.1.1 Wind Tunnel

The original air handler section relied on a ½ hp variable speed Trane blower for its air supply, Fig. 4. The blower was controlled by a PowerFlex® 4 controller. The original air handler had a steady controllable flow operation range of 0-5 m/s of air flow inside the 15.24 cm by 15.24 cm (6.00 in. by 6.00 in.) duct. The air temperature was controlled by a single A-coil connected to Air-Handler Conditioning Loop 1. However, two problems arose in dealing with the original air handler design. First, due to size restraints, the blower exit was located off-center creating a non-uniform flow field. Secondly, lack of a reliable humidifier lead to uncontrollable wet bulb conditions. Factoring seasonal weather conditions with ambient lab conditions a controllable humidity was unobtainable. A temporary wet filter was placed at the inlet of the wind tunnel to help increase the humidity of the system on dry days but again the overall control of this humidity metric was low.

Fig. 4. Original air handler used in early Unit Cell tests.

The new and current air-handler was designed with both the flow asymmetry and humidity control in mind, Fig. 5. The new handler was expanded to incorporate both a

second A-coil and a humidifier. The air enters the air handler through a baffle system which allows the wind tunnel to regulate the amount of air recirculated. The baffles can allow the wind tunnel to be run in an open loop configuration with or without air recirculation or in a completely closed loop configuration. Once in the air handler the air is moved through the wind tunnel by a 2 hp variable speed centrifugal fan. The fan is operated by a PowerFlex® 4 controller on the control panel. The air is blown into the Primary A-Coil which is temperature controlled by Conditioning Loop 1. The air then moves into the humidifying section of the air handler, where steam is supplied to the air to increase the overall humidity of the air. The steam is introduced into the system by a VaporStream® VLC 9-1 Humidifier which is manually regulated by a DriSteem® controller and a 0-10 VDC power supply. To prevent mold and mildew growth, which is accelerated by the presence of water moisture, the air handler is equipped with two UV lights. The air then moves through a second A-coil, the Set-Point Coil, for final temperature control. The Set-Point Coil temperature settings are supplied by Conditioning Loop 2.

Fig. 5. Current air handler.

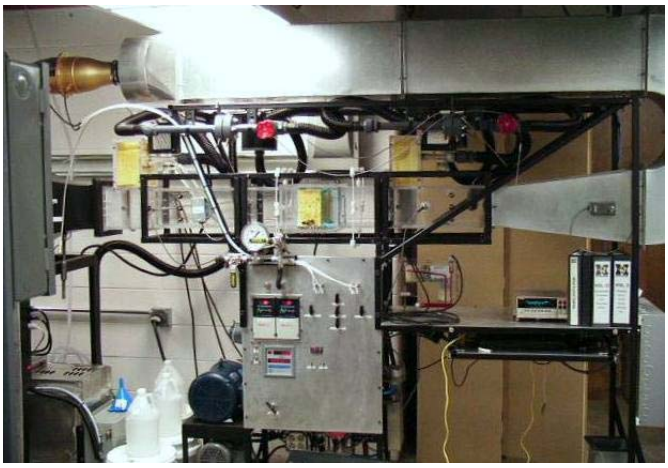

Fig. 6. Wind tunnel with instrumentation.

Once the air passes through the Set Point A-coil, the description of the wind tunnel, Fig. 6, is similar for both the original and current air handler designs. From the Set Point A-coil the air enters a series of static mixers and a 45.72 cm by 45.72 cm by 15.24 cm (18.00 in. by 18.00 in. by 6.00 in.) settling chamber alleviating any asymmetric flow. The air is then constricted in a contraction nozzle which reduces the air profile from the 45.72 cm by 45.72 cm (18.00 in. by 18.00 in.) to a 15.24 cm by 15.24 cm (6.00 in. by 6.00 in.) cross section. From there the air flows in a 15.24 cm by 15.24 cm (6.00 in. by 6.00 in.) clear acrylic duct. Once in the plastic duct, air is sampled for inlet dry bulb and wet bulb temperature measurements in between a series of screen and honeycomb straightening sections. The air's temperature and humidity is again measured by a secondary Dwyer® Probe. The air then enters the modular test section which contains the actual unit test coil and pressure taps for pressure drop measurements across it. The modular test section outlet air is again sampled for the outlet dry bulb and wet bulb temperature measurements.

The air then exits the acrylic duct work and enters a steel expansion section increasing the duct size from 15.24 cm by 15.24 cm (6.00 in. by 6.00 in.) to 30.48 cm by 30.48 cm (12 in. by 12 in). The air flow is measured by a laminar flow element (LFE) after the steel ducting turns 180° back towards the air handler. However, prior to entering the LFE the air flows through 101.6 cm (40.0 in.) PVC pipe with a 10.16 cm (4.00 in.) diameter so that fully developed flow will be present as for the LFE. On the outlet of the LFE a thermistor measures the dry bulb temperature. The air then flows to the return baffle and is either discarded form the system or recirculated by the series of baffles.

2.1.2 The Unit Cell Coils and Test Section

To test the coils accurately and comparatively it is necessary to develop a coil test section for easy mounting in the wind tunnel. The Unit Cell coils which are tested are pre-circuited to the designer's specifications with one inlet and outlet. The face area of the coils is nominally the specified 15.24 cm by 15.24 cm (6.00 in. by 6.00 in.); however, due to limitations in the fin and tube sizing this face area can vary slightly. To allow for insertion into the test section, the coils are encased in an acrylic frame, Fig. 7, which can slide relatively easily in and out of the test section. Regardless of the actual test coil size, the casing only exposes the 15.24 cm by 15.24 cm (6.00 in. by 6.00 in.). test region to the air flow, thus making performance comparisons between each coil much easier. Standard construction and drawings of this encasing can be seen in the Appendix A.

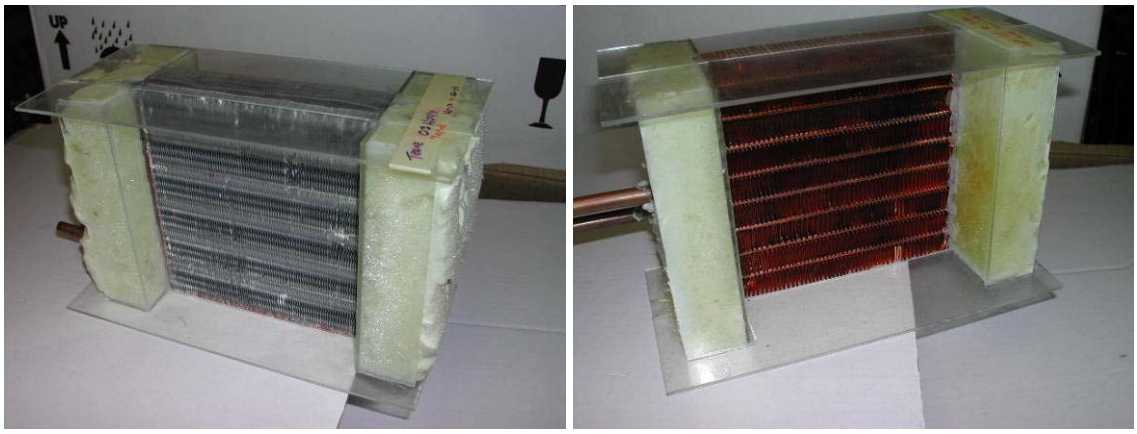

Fig. 7. Pictures of Unit Cell coils mounted inside fabricated acrylic casings.

The framed coils are inserted into the custom built test section shown in Fig. 8. The test section is modular and can be removed from the wind tunnel and replaced with other research sections when needed. The section measures a total of 55.88 cm (22 in.) in length and act as part of the wind tunnel ducting. The acrylic test section holds and insulates the coil during testing and also has the pressure taps and manifold tubing for pressure drop measurements. Once the coil is inserted into the test section it is sealed with vacuum tape to prevent any air flow out of the test section.

(a) **(b)**

Fig. 8. Modular test section: (a) Section without coil. (b) Section with coil.

2.1.3 Air Handler Conditioning Loops

To ensure that air flow through the test coil was at specified conditions, two single-phase resistive heating loops (see Fig. 1) were created to provide sufficient heating and cooling for the air handler A-coils. These loops, Conditioning Loop 1 and Conditioning Loop 2, were built similarly but are independent of one another to provide maximum control of the testing apparatus. The coils are connected to the conditioning loop by a length of flex hosing, which can be connected and disconnected to both the air handler and loop through quick disconnect fittings. The inlet of the conditioning loop doubles as a return from the A-coil and a fill valve of the system when it was connected to facility water. Once the water enters the inlet of the conditioning loop it flows down a long stretch of copper tubing prior to entering a filter which prevents particulate buildup in the system. The conditioning water leaves the filter and enters parallel 3-hp and 1-hp pumps. These pumps are controlled by two Allen-Bradely® 1305 variable speed controllers mounted on the control panel. The water exits the pumps and flows into two 25 kW Flat Plate® heat exchangers, Fig. 9. Conditioning Loop 1 is connected to a smaller 1 kW FTS® Maxi-Cool chiller, Fig. 10, while Conditioning Loop 2 is connected to a larger 50 kW HX540 NESLAB®, Fig. 11, chiller providing broader range of water temperatures. Once exiting the heat exchangers the water flow rate is measured by a Micro Motion® A351 Corriolis mass flow meter. A Micro Motion RFT 9739 controller is utilized to monitor flow on the loop's control panel. For final temperature control, the water enters a series of resistive heaters. The water flows first through a 7.5 kW heater and is followed by a 6kW, 3 kW, and 1 kW heater. At each heating element a RTD measures the water outlet temperature. These measurements are relayed back to

Watlow® 96 controller, which monitors the firing of the heater elements. The conditioning loop heaters are shown in Fig. 12. Once through the heater series, the water exits the system through another quick disconnect and flows into the flex hose heading toward an A-coil.

Fig. 9. Air handler conditioning loop Flat Plate® heat exchangers.

Fig. 10. Maxi-Cool chillers used for supplement heating and cooling for Air Handler Conditioning Loop and Unit Cell Liquid Loop.

Fig. 11. HX540 NESLAB® chiller used for cooling for Air Handler Conditioning Loop.

Fig. 12. Air handler conditioning loop heater section. Watlow® resistive heaters 1 kW, 3kW, 6kW, and 7.5kW.

2.1.4 Unit Cell Conditioning Loop

To test the performance of the Unit Cell coil, a 1.27 cm (0.50 in.) stainless steel recirculating liquid loop was built to provide controlled cooling and heating to the coil. The liquid used in the conditioning loops for all tests was distilled water. This water enters the loop from the test coil and enters a Flat Plate heat exchanger. Here the water is

cooled or heated depending on the settings of the FTS Maxi-cool, which is connected to the heat exchanger. From there the water flows to an accumulator up-stream of two pumps to ensure that the pumps have a positive pressure head at all times. The water is pumped through the system by a 1 hp and a 3 hp gear pump connected in parallel, Fig. 13. Each pump is controlled by a PowerFlex® 4 controller, which delivers each pump a 0-60 Hz frequency. The system has flow capabilities of reaching 10 kg/min, using the 1 hp pump, and 30 kg/min, using the larger 3 hp motor pump. The water is pumped through a filter before it flows through a Micro Motion® Model D mass flow meter used for monitoring the flow rate. After the water flows through the flow meter it enters the resistive heater section. Three 1 kW heaters are present for final temperature adjustment during cold water tests and for primary heating during hot water tests, as shown in Fig. 15. One 1 kW heater cannot be adjusted and fires at full power when turned on. The other two 1 kW heaters are coupled in series and connected to a Watlow® 96 controller which can vary the out put power from 0-100%. The water then flows out to the Unit Cell coil through 1.27 cm (0.50 in.) flexible hose. At both the entrance and exit of the Unit Cell coil, delrin couplers were constructed to connect the flexible hosing to the liquid loop and to house a thermistor for inlet and outlet water temperatures. The flex line leading to the couplers allowed for multiple types of coil configurations and manifolds, and also allowed for the connectors to be mounted directly onto the coil minimizing the heat loss between the inlet and outlet of the coil.

Fig. 13. Stacked 1-hp and 3-hp pumps for Unit Cell liquid loop.

Fig. 14. Micro Motion® flow meter used for water flow measurement.

Fig. 15. Heating section of Unit Cell liquid loop.

2.2 Instrumentation

To effectively evaluate each coil, the performance of each coil must be measured by various forms of instrumentation. All instrumentation and measurement apparatuses were built in accordance to ARI and ASRAE Standards. The instrumentation for the wind tunnel system was chosen primarily to maximize accuracy since total energy transfer of the small scale coils is in the 2000 W and lower range.

2.2.1 Air Side Temperature Measurement

Determining the total heat transfer and heat transfer coefficient for a prototype test heat exchanger requires an energy balance between the air and liquid side of the coil. To obtain the heat transfer on the air side of the test coil, accurate measurements of the inlet and outlet wet and dry bulb temperatures of the moist air must be acquired both entering and leaving the test coil. With these energy transfers from the Unit Cell coil exceptionally low, the air side temperature measurements need to be extremely accurate. The measurements are acquired using custom built systems, developed in accordance with ASHRAE Standard 33-2000 [6] and through constant upgrades of the wind tunnel, Fig. 16. The air temperature measurement system consists of an air sampling device, a measurement section, a valve and orifice plate for air flow regulation and a fan.

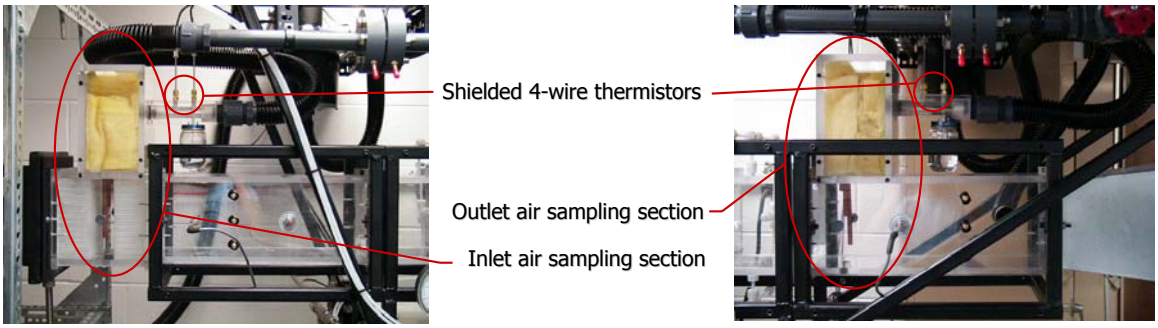

Fig. 16. Air sampling and dry and wet bulb temperature measuring devices.

To obtain air temperature measurements, 0.95 cm (0.38 in.) copper tubes are used to sample the moist air 55.88 cm (22.00 in.) upstream from the test section and 6.35 cm (2.50 in.) downstream from test section. The copper tubing is inserted into nylon compression fittings and comes together outside the wind tunnel in a series of elbow and T-fittings creating the sampling "tree". The goal of the tree is to collect an effective sample of air from the tunnel cross sections for measurement of dry and wet bulb temperatures. The original sampling tree design, collected air from four copper tubes with a series of holes drilled into the tubing, Fig. 17a. To account for pressure drop in the copper tubing the holes increased in size as they approached the center of the duct. However without much foresight, the large size of the holes near the walls of the duct resulted in more air being sampled along the duct walls. This poor sampling of air, lead to dissimilar results between air and water energy balance. A second design was considered as a simplification to the first. To account for any type of temperature stratification air was sampled at three locations inside the duct, two corners and the duct center, Fig. 17b.

While the current method does not completely eliminate the unbiased sampling it does provide a reasonably fair sampling of the cross-sectional area. More importantly the design has delivered acceptable energy balance calculations between the air and water side of the Unit Cell coil. To tests the overall effectiveness of the sampling tree, the tubing holes were methodically plugged one at a time and the measured temperature was compared. At a flowing air-ambient temperature difference of 12.56 °C, the measured dry bulb temperature as each hole was covered and uncovered varied less than ±0.05 °C for any configuration, well within an acceptable range of error and uncertainty.

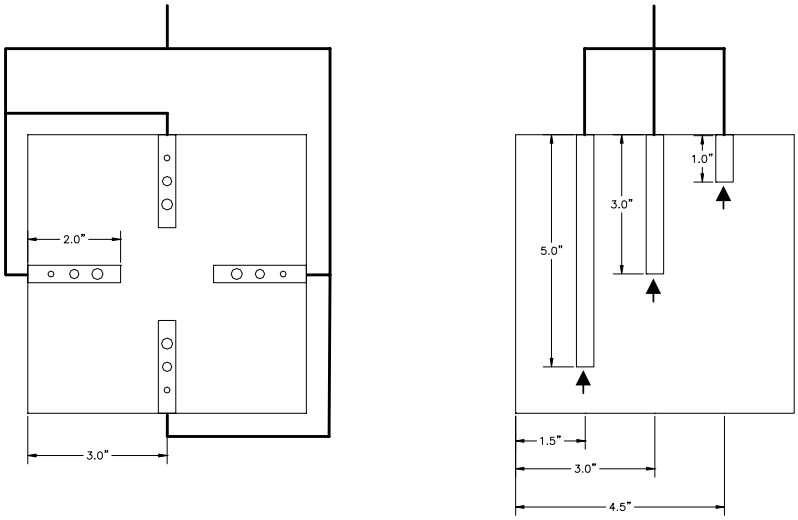

Fig. 17. Schematic of the air sampling device: (a) Original configuration (b) Current configuration.

Another aspect of the sampling tree which was changed from its original design was the tubing and manifold between the sampling tree and the measurement section. In the original configuration the nylon tubing and manifold which lead into the temperature measurement devices was excessively long and poorly insulated, Fig. 18a. By placing a temperature probe directly into the actual duct air stream and comparing its temperature to the sampled air temperature, failures in the air side temperature measurement system could be easily found. In fact the heat transfer in the sampling section was so great, at an air stream temperature of 30 °C; the sampling devices read only a temperature of 22 °C. To correct this problem the long tubing was replaced with only 2-inch sections of tubing and the manifold was encased in an acrylic box insulated with fiberglass insulation, Fig. 18b. This manifold design provided the air with sufficient insulation and mixed the air prior to entering the measurement section, allowing for accurate dry and wet bulb temperature measurements. Two Dwyer® Temperature/Humidity Probe have been placed in the center of the duct and are used to check for abnormalities in the system.

Temperature measurements from the probe, which only measures the temperature at the center of the duct, and the sampling system differ by only 0.4 °C.

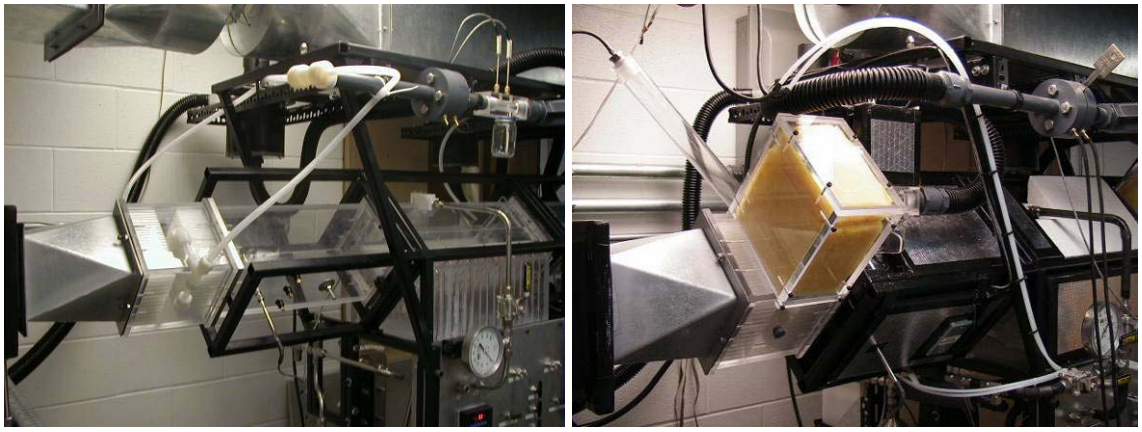

(a) (b)

Fig. 18. Air manifold design: (a) Original configuration (b) Current configuration.

Once the air exits the manifold it enters the acrylic measurement section. Each block consists of two 22.86 cm (9.00 in.) stainless-steel shielded 4-wire Thermoinc® thermistors, one collecting the dry bulb temperature measurement the other collecting the wet bulb temperature measurement. The thermistor probes are suspended by compression fittings, so that their tips are directly in the flow stream of the sampled air, Fig 17. For the wet bulb measurements, 7.62-12.70 cm (3.00-5.00 in.) cotton wicks are loosely slid over the probe. The end free the wick is suspended in a jar of distilled water. This allows the water to progress up the wick and an air saturation temperature can be measured. One issue with the airside temperature measurements is the reliability of the wet bulb probes. Improper handling and constant use of the cotton wicks causes them to dry out and compromise the temperature readings. Therefore, when installing the wet bulb thermistors, sanitary gloves are worn to help prevent oils and other contaminants contacting the cotton wicks. The dry out became increasingly evident during hot water tests in which the air temperatures would reach 70 ºC at times. During heating tests, only

sensible heat is transferred with no change to the humidity ratio. So, to minimize uncertainty the humidity ratio can be calculated using the inlet conditions and the outlet wet bulb temperature ignored. During cooling tests, to protect the probes from unnoticed dry out, the Dwyer® Humidity probes offer additional verification of the wet bulb temperature. To accurately measure the wet bulb temperatures, an air velocity across the probes tips is ensured between 3.6 m/s and 5.1 m/s in accordance to ASHRAE Standard 41.2 [7]. To supply this air velocity in the temperature measurement apparatus, air is pulled through each measurement apparatus by a 1/15 hp axial fan, Fig. 20. Upstream of each fan is an orifice plate and gate valve, for measurement and regulation of the air velocity, Fig 19. Differential pressure measurements in the orifice plate are monitored by an inclined manometer, to ensure that the correct air velocity flowing through each measurement apparatus. The sampled inlet air is returned to the air handler from the downstream side of the axial fan. The outlet sampled air is returned to the primary duct 30.48 cm (12.00 in.) downstream of the outlet sampling tree, so that the sampled air can be accounted for during air flow measurements.

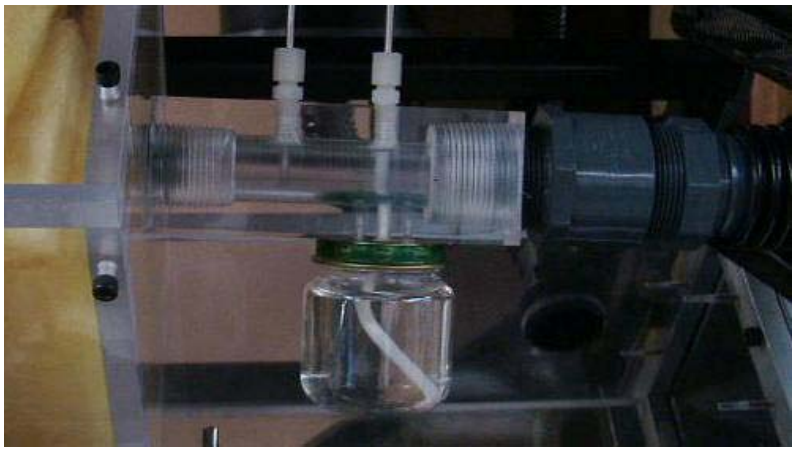

Fig. 19. Air dry and wet bulb temperature measurement system.

Fig. 20. Air blower for temperature measurement

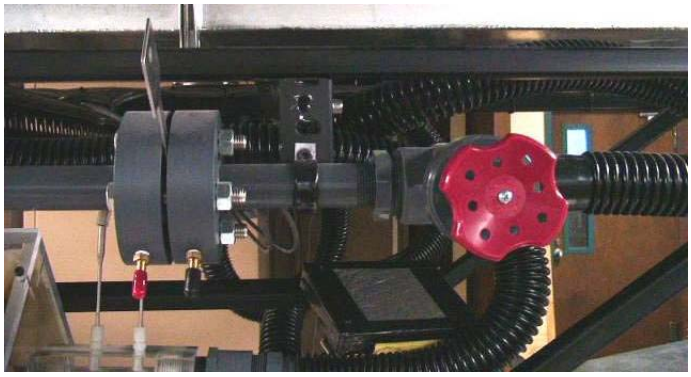

Fig. 21. Air flow regulation for temperature measurement.

To study the effects of air velocity inside the sampling sections on the probe temperature, two tests were performed by varying this velocity through the measurement section. In the first test, air velocity effects of cold air, air temperature below the ambient conditions, were tested; an inlet air dry bulb temperature between 12.5-14.5 ºC with an actual air flow velocity through the duct of 5.0 m/s. The second test used hot air, which flowed at a similar flow rate as the previous but at nominal dry bulb temperature of 34 ºC. The ambient temperature for both tests was 22.0 ºC. In the first test, comparisons between the exposed temperature probes to the insulated probes, original temperature measurement versus current temperature measurement, show a dramatic improvement in

the performance can be seen, Fig. 22. The non-insulated probes allowed shifts in the temperature measurements as the air flow through the measurement section was increased, Fig. 22. In fact there was a 2.85% difference between the measured air dry bulb temperature at 3.6 and 5.1 m/s. By switching the brass fittings to plastic and adding further insulation to the probe, this difference in temperature measurement was reduced to 0.38% for the acceptable air flow velocity region.

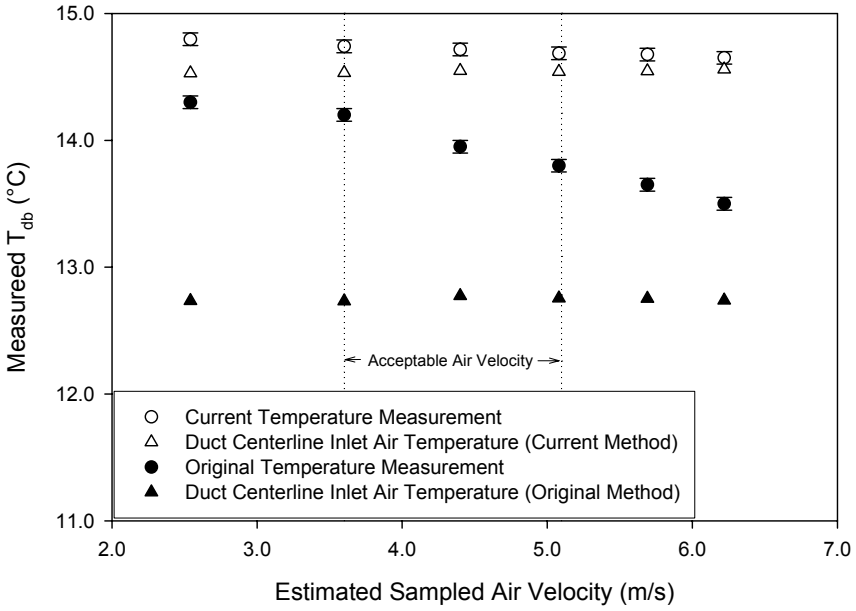

Fig. 22. Temperature versus estimated air flow velocity across the measurement probes. (Cold Air Test)

Similar trends were seen in the hot air tests, Fig. 23. At a lower air velocity the thermistor probes are more greatly affected by the ambient conditions than they are at high air flow rates. Thus, at low flow rates air temperatures drift toward the ambient. However with the addition of insulation to the probe, the variation in the measurements between 3.6-5.1 m/s through the measurement section is nominally less than 0.1 ºC, well within the allowable amount of uncertainty for heating tests.

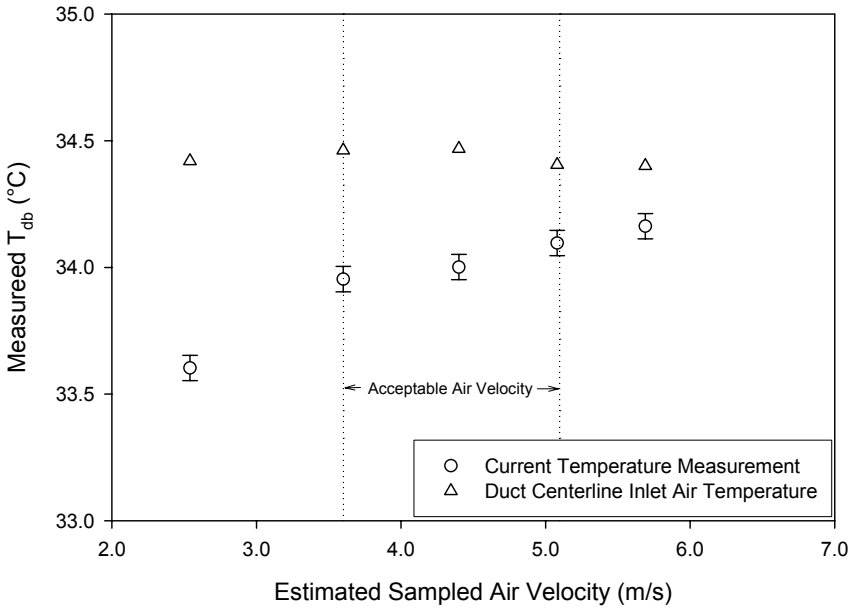

Fig. 23. Temperature versus estimated air flow velocity across the measurement probes. (Hot Air Test)

To minimize the ambient affects on the thermistor probes, the air velocity of 5.1 m/s was chosen as the standard for both the front and back sections. This corresponds to 49.81 Pa (0.20 inches of H_2O) pressure drop across the orifice plates. The increased velocity through the measurement apparatus also allows for the system temperatures to reach steady state more quickly than it would at low velocities. Since both the inlet and outlet sampling sections of the system were set at the same velocity, any other variations in probe temperature due to air velocity were assumed negligible.

Another source of measurement error dealt with the heat loss/gain through the measurement sections distorting temperature measurements. The long length of the stainless-steel thermistors allowed them to perform as cylindrical fins and skew the actual air temperature towards ambient conditions. To accommodate the unwanted energy transfer the fittings which held the probes in place where switched from brass to PVC and the length of the probes shafts were insulated with fiberglass. While this phenomena did ``not affect the air temperature measurements that were close to ambient conditions, at

high temperatures (40 °C) and low temperatures (15 °C), the difference between a non-insulated probe and insulated probe could be as much as 1.0 °C. Because heat loss issues were such a predominate problem in the temperature sampling and measurement section of the test apparatus, efforts were made to ensure that unwanted heat transfer on other portions of the system would be minimal. To limit the heat losses, fiberglass insulation was added to the wind tunnel between the inlet and outlet measurement sampling sections, Fig. 24. Using a thermal camera heat loss areas were systematically identified and insulated.

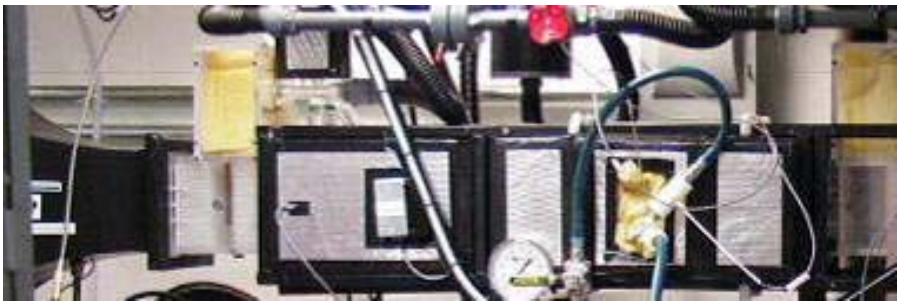

Fig. 24. Wind tunnel with insulation.

Even with changes in design and additional insulation, there is and will continue to be a limited amount of heat loss in the system. Because the amount of heat transfer from the Unit Cell coil to the air stream is such a small quantity, efforts must be made to consider any type of heat leak from the system. This is done by performing a baseline "zeroing" test, prior to a full scale Unit Cell test. For the "zero" test, the Unit Cell coil is disconnected from the recirculation loop and is exposed to normal air inlet conditions. Ideally the system should be under adiabatic conditions during "zeroing", and the inlet and outlet temperatures should be equal. However, a combination of variation in thermistor calibration, variation in the sampled air and heat transfer to or from the ambient causes the inlet and outlet temperatures to be slightly different. In many cases this difference in temperatures is less than the uncertainty of the thermistors themselves

and can be ignored. In instances where the temperature offset is significant, the difference inlet and outlet in the adiabatic temperature tests are added the outlet temperatures during normal tests. By offsetting the outlet temperatures by this difference the zeroing can account for the various forms of the system and calibration errors. This "zeroing" correction is done for both the dry and wet bulb temperature measurements. For a coil that transfers 2000 W (6824 Btu/h) of heat at an air velocity of 3.5 m/s, an adiabatic temperature difference of ±0.2ºC correlates to approximately 18 W (61 Btu/h), a heat transfer fluctuation of 1%. A 1% change in heat transfer can be a factor, when trying to obtain an air to water energy balance between 3-5%.

The accuracy for measuring air temperatures prescribed by ASHRAE Standard 33-2000 6.1.2 [6], is 0.3ºC for heating coils and 0.06ºC for cooling coils. The total uncertainty in air side temperature measurements is typically ±0.05º. When the thermistors "zeroed," this uncertainty increases slightly to ±0.08ºC for the outlet measurements. In all cases the measurement uncertainty for heating coil tests is deemed acceptable and in accordance with ASHRAE Standards. Only when the thermistors are "zeroed" and the cooling tests are performed, is the system unable to produce acceptable temperature measurements. Thus the air side temperature measurement instrumentation and methods are sufficient for the Unit Cell coil testing. The thermistors themselves have an accuracy of ±0.01 °C and a drift of less than 0.01 °C per year; therefore calibration is recommended at least once a year. Detailed calibration procedures and uncertainty analysis can be seen in the Appendix B.

2.2.2 Pressure Drop Measurement

Another important performance metric is the pressure drop across the heat exchangers. To measure the pressure drop across the heat exchanger coil a total of eight pressure taps, four upstream and four downstream, have been incorporated into the modular test section. The 0.15 cm (0.06 in.) taps were drilled flush to the wall centered along each wall face, 7.62 cm (3.00 in.) in front of the coil and 7.62 cm (3.00 in.) behind the coil as according to ASNI/ASHRAE 41.2 1987 [7]. On the outside of the test section 0.64 cm (0.25 in.) NPT pipe threads were carefully tapped into the backside of the pressure taps. Plastic compression fittings were inserted into the pipe threads and 0.64 cm (0.25 in.) plastic tubing was used to connect the four pressure taps together. These makeshift manifolds were created on both the upstream and downstream pressure taps.

The upstream manifold was connected to the high side of two Validyne DP-103 differential pressure transducers, while the downstream manifold was connected to the low side of the transducers. The transducers were connected together with 0.64 cm (0.25 in.) stainless steel tubing and equipped with bypass valves, Fig. 25. The transducers were connected to a CD280 Multi-Channel Carrier Demodulator, which converted the transducer output to a ±10VDC output for DAQ measurement. The use of two transducers allows for a broader range in measurement, one of the transducer acts for pressure drops 0-.086 kPa (0-0.35 in. of H_2O) and the other a higher range to 0.55 kPa (2.22 in. of H_2O). To protect the low pressure transducer during high pressure ranges, shut off valves were inserted before and after the transducer to avoid over pressuring and damaging the diaphragm. From ASHRAE Standard 33-2000 6.2.4 accuracy of pressure measurement is to be at least 0.001 kPa (0.005 in. of H_2O). With the current set up the

typical pressure drop uncertainty across the coil for a given test is at this 0.001 kPa requirement. Calibration curves and detailed calibration procedures of the transducers can be seen in the Appendix B.

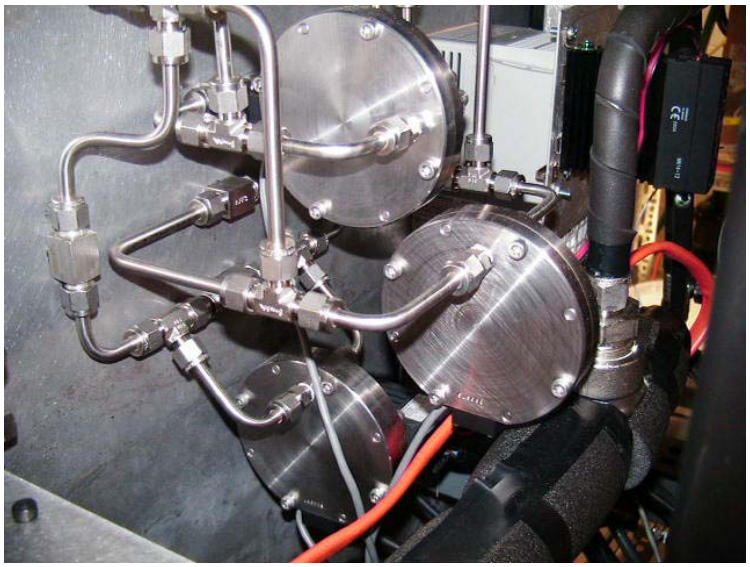

Fig. 25. Differential Pressure Transducers for measuring pressure drop across Unit Cell coil and through laminar flow element.

Small imperfections in the construction allowed air to bypass the coil disrupting the coils heat transfer but more importantly the pressure drop across it, Fig. 26. While these imperfects are also common in standard coil production, they only represent a small portion of the overall surface area on a full scale coil. However, in a small scale environment this bypass can sometimes represent up to 10% of the total surface area. To accommodate for the air bypass, the small gaps were plugged with silicone and adjustments were made to the overall surface area of the coil.

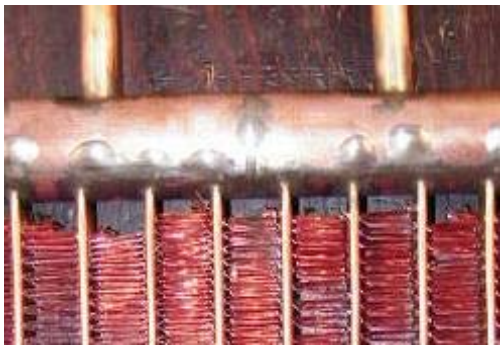

Fig. 26. Gaps between manifold and fins create a bypass for air flow.

2.2.3 Air Flow Measurement

In the original configuration of the wind tunnel, an iris orifice meter was used to measure the volumetric flow rate, Fig. 27. A pressure drop measurement across the meter was obtained by connecting the orifice meter to a DP-103 Validyne® Differential Pressure Transducer with a range of 0-0.55 kPa. The orifice transducer was connected to the same CD280 Multi-Channel Carrier Demodulator that the coil pressure drop transducers were connected to. The orifice meter cost efficient method for measuring a wide range of air flow rates without the construction or use of air flow nozzles. However, at low air flow rates the flow was not stable requiring a different approach to measure and control the air flow rate.

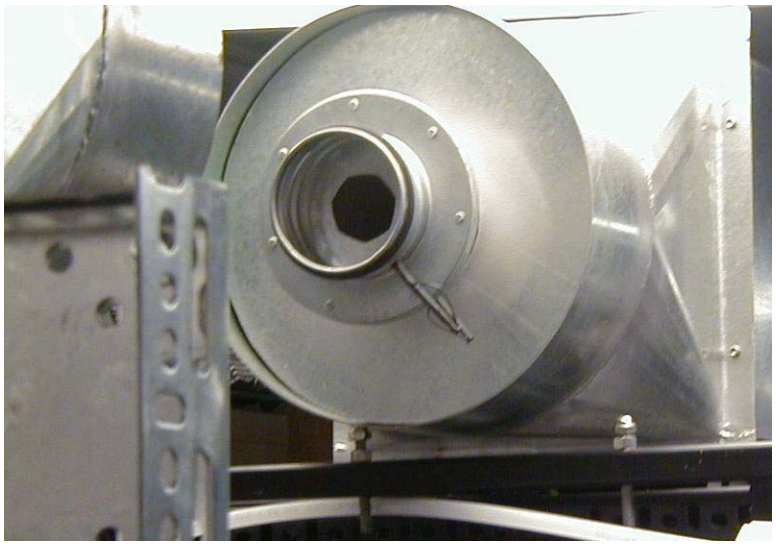

Fig. 27. Orifice meter originally used for air flow measurement.

The air flow rate is now measured using a Meriam® Laminar Flow Element (LFE) model 50MC2-4-1, Fig. 28. Because the air needs to be fully developed as it enters the LFE, the air flows through a 101.60 cm (40.00 in.) length of 10.16 cm (4 in.) diameter PVC pipe prior to the LFE entrance. A pressure drop measurement across the LFE is obtained by connecting the LFE to a DP-103 Validyne® Differential Pressure Transducer with a range of 0-0.55 kPa. The LFE transducer is connected to the same CD280 Multi-Channel Carrier Demodulator that the coil pressure drop transducers were connected to. For accurate volumetric flows in the LFE, both the properties of the entering air and its absolute pressure must be known.

The dry bulb temperature is measured by stainless-steel shielded 4-wire Thermoinc® thermistors whose probe tip was inserted directly into the air flow at the outlet of the LFE. Assuming that no moisture in the air is lost between the outlet of the coil and inlet of the LFE, the humidity ratio at the coil outlet and LFE entrance are assumed equal. With the dry bulb temperature and humidity ratio, all needed air properties can be calculated. The absolute pressure is measured by a Princo Fortin Tube

Mercurial Barometer, Fig. 29. For direct comparison to the Standard Coil data, all air flow rates are standardized to dry air at a temperature of 21.11 °C and standard barometric pressure of 101.3 kPa (29.92 in. of Hg).

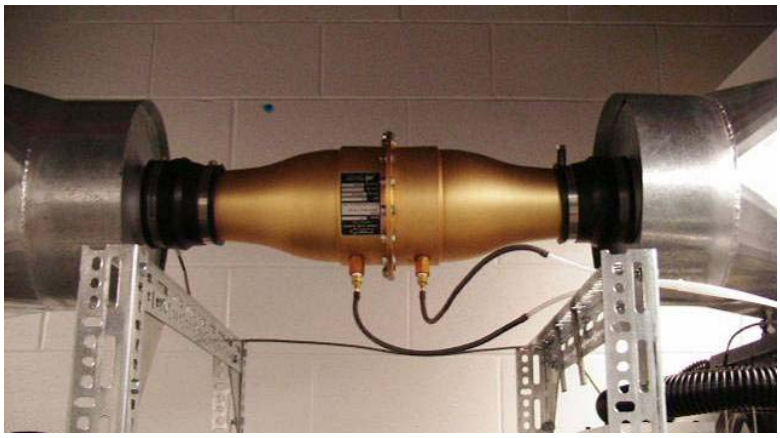

Fig. 28. Laminar Flow Element used for air volumetric flow rate measurements.

Fig. 29. Princo Fortin Tube Mercurial Barometer.

The actual volumetric flow rate is determined from the calibrated LFE using equations provided in the *Laminar Flow Elements: Installation and Operation Instructions* [8]. To obtain this flow rate, the differential pressure across the LFE and the outlet air temperature from the LFE was measured. Using the calibration curve from the LFE, Eq. (A11), the uncorrected flow rate, $\dot{V}_{LFE}$, can be solved. To correct for variations

in the calibration two correction factors must be considered. The first correction factor deals with the reference temperature of the *ΔP* sensor. Because the calibration curve is given at a water reference temperature of 4˚C, the ratio water densities at there reference temperatures must be multiplied to the pressure drop across the LFE.

$$C_{\Delta P} = \frac{\left(\text{density of } H_2O \text{ @ device temperature reference}\right)}{\left(\text{density of } H_2O \text{ @ } 4°C\right)} \tag{1}$$

The density of H_2O at the device reference temperature can be obtained using H_2O density tables for the ambient temperature, while also noting that the density of water at 4˚C is 999.969 kg/m^3 (62.426 lbs/ft^3).

To correct for vicious effects during calibration, the uncorrected flow rate is multiplied by the ratio of a viscosity correction factor:

$$C_\mu = \left(\frac{\mu_{std}}{\mu_f}\right) = \frac{\left(\text{viscosity of flowing gas at } 21.11°F\right)}{\left(\text{viscosity of flowing gas at flowing temperature}\right)}. \tag{2}$$

The μ_{std} or calibrated viscosity is given as 181.87 micropoise. The reference viscosity also in micropoise, μ_f, is much more involved and defined as:

$$\mu_f = \left(\frac{14.58 T_{db,LFE}^{\ 3/2}}{110.4 + T_{db,LFE}}\right) \times \left(\frac{\mu_{wet}}{\mu_{dry}}\right), \tag{3}$$

where $T_{db,LFE}$ is the LFE dry-bulb temperature in Kelvin, μ_{wet} is the viscosity of moist air and μ_{dry} is the viscosity of dry air. Through the use of the Southerland equation from Auld [9] the dry air viscosity can be given by,

$$\mu_{dry} = \frac{1.458 \times 10^{-6} \sqrt{T_{db,LFE}}}{1 + \frac{110.4}{T_{db,LFE}}} \tag{4}$$

again where the $T_{db,LFE}$ is the LFE dry-bulb temperature in Kelvin. The wet air viscosity can be estimated by curve fitting Kestin and Whitelaw's [10] data for the viscosity of wet air as a function of air temperature and mol fraction of water to air, Fig. 30.

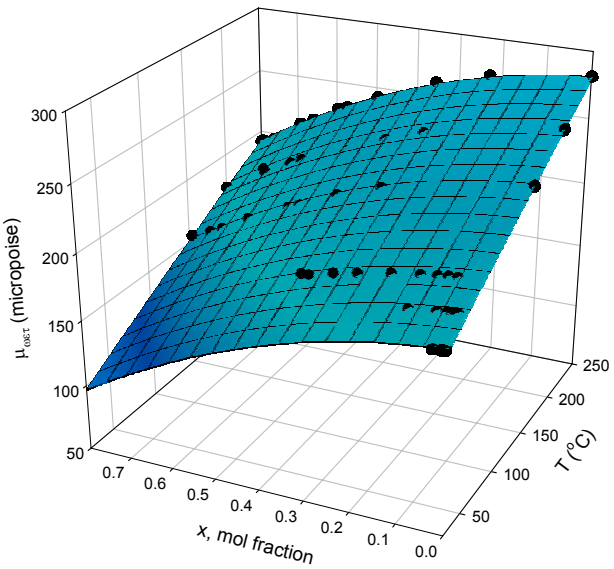

Fig. 30. Three dimensional plot of viscosity with respect to mol fraction of and dry bulb temperature.

Using Sigma Plot software for the three-dimensional curve fit option the equation for wet air viscosity is estimated as,

$$\mu_{wet} = 174.1648 + 0.4556T_{db,LFE} - 20.4213X - 0.0001T_{db,LFE}^{\ 2} - 113.3991X^2 \qquad (5)$$

where $T_{db,LFE}$ is the air temperature in °C and X is the mol fraction of water to air. The mol fraction of the air was calculated using

$$X = \frac{n_{H_2O}}{n_{air} + n_{H_2O}} = \frac{\dfrac{W}{M_{H_2O}}}{\dfrac{W}{M_{H_2O}} + \dfrac{1}{M_{air}}} \qquad (6)$$

where n_{H_2O} and n_{air} are the number of moles of water and air respectively, W is the humidity ratio and M_{H_2O} and M_{air} are the molecular mass of water and air. The

molecular mass of water is 18.016 g/mol while the molecular mass of air is 28.97 g/mol. Assuming there is one mole of air, the ratio of number of moles of water to the total number of moles can be estimated.

Multiplying this viscosity correction factor to the already pressure corrected LFE flow rate; the actual volumetric flow rate can be calculated. Thus the equation for the actual volumetric flow rate becomes,

$$\dot{V}_{actual} = C_{\mu} \times \dot{V}_{LFE}\left(\Delta P, C_{\Delta P}\right) \tag{7}$$

With the actual volumetric flow rate known the actual air face velocity through the test coil can be calculated using,

$$\vec{v}_{actual} = \frac{\dot{V}_{actual}}{A_{duct}}, \tag{8}$$

where A_{duct} is the cross-sectional area of the duct. The velocity calculated through the test coil assumes that the same volumetric flow rate through the LFE is the same as that of the test coil. Thus the air is treated as an incompressible fluid and the densities at the LFE and the test coil are assumed constant in the flow calculations. This assumption is valid for the LFE conditions up to 24.5 m/s (4,822.8 ft/min) and an air temperature of 66.7 °C (150 °F).

Similarly to the calculations of the actual air velocity, the standard air velocity can be calculated with the LFE volumetric flow rate and a series of calibration correction factors. The standard volumetric flow rate can be calculated by,

$$\dot{V}_{standard} = \dot{V}_{actual} \times C_T \times C_P \times C_{\rho} \tag{9}$$

where $\dot{V}_{actual}$ is the actual volumetric flow rate as described above, C_T is an air temperature correction factor, C_P is a pressure correction factor and C_{ρ} is an air density

correction factor. The temperature correction factor standardizes the flow rate to a standard temperature of 21.11 °C (70 °F). To calculate this temperature correction factor the ratio of the standard temperature to flowing temperature must be determined.

$$C_T = \left(\frac{T_{std}}{T_f} \right) = \frac{(\text{Absolute Standard Temperature})}{(\text{Absolute Flowing Temperature},)} \tag{10}$$

where T_{std} = 21.11 °C (70 °F) and T_f is the dry-bulb LFE temperature.

The pressure correction factor standardizes the flow to an atmospheric pressure of 101.3 kPa. This correction factor can be obtained by,

$$C_P = \left(\frac{P_f}{P_{std}} \right) = \frac{(\text{Absolute Inlet Line Pressure})}{(\text{Absolute Standard Pressure},)} \tag{11}$$

where P_{std} is the standard pressure of 101.3 kPa (29.92 in. of Hg) and P_f is the atmospheric line pressure. Because the absolute pressure is not measured directly it must be estimated. The absolute line pressure is estimated by adding the pressure drop through the LFE to the total ambient atmospheric pressure.

$$P_f \approx p + \Delta P_{LFE} . \tag{12}$$

Thus difference between the ambient atmospheric pressure and the pressure on the outlet of the LFE is assumed negligible. This assumption is later verified in the air side heat transfer calculations using the standard air velocity. The absolute pressure was measured using the mercurial barometer. To correct for variation in temperature the actual atmospheric pressure could be calculated by using the supplied correction equation,

$$p = p_{measured} + \left(18.9 \times 10^{-6}\right)\left(T_{amb} - 20\right)\left(p_{measured}\right), \tag{13}$$

where $p_{measured}$ is the measured atmospheric pressure in mm of Hg and T_{amb} is the ambient temperature in °C.

The final correction factor deals with the differences in air densities. Because the standardized air is assumed to be dry air, the air flow rate must be multiplied by the ratio of density of wet air, ρ_{wet} to the density of dry air, ρ_{dry}.

$$C_{\rho} = \left(\frac{\rho_{wet}}{\rho_{dry}} \right) \tag{14}$$

The density of moist air can be calculated using

$$\rho_{wet} = \frac{(1+W)p}{0.2871(T_{db,LFE} + 273.15)(1+1.6078W)} \tag{15}$$

where p is the atmospheric pressure in kPa, W is the humidity ratio, and $T_{db,LFE}$ is the LFE temperature in °C. A similar technique can be used to find the density of the dry air; however for the dry air case the humidity ratio is zero reducing the equation to,

$$\rho_{dry} = \frac{p}{0.2871(T_{db,LFE} + 273.15)}. \tag{16}$$

The standard air face velocity is calculated just as the actual air face velocity was calculated but uses the standard volumetric flow instead of the actual volumetric flow,

$$\vec{v}_{standard} = \frac{\dot{V}_{standard}}{A_{duct}}. \tag{17}$$

According to ASHRAE Standard 41.2-1987 [7] the accuracy of air flow measurement must be within 1.2% of the flow rate regardless of measurement method. Currently the LFE is has accuracy of 1-2%, with air flow stability within the system being the largest factor of uncertainty in the air flow measurement. Although the flow accuracy is at times outside of the ASHRAE Standard it is relatively close and much improved over the orifice meter. The calibration equations and uncertainty analysis can be seen in Appendix B.

2.2.4 Liquid Temperature Measurement

Like the air side temperature measurements, shielded 4-wire stainless-steel Thermoinc® thermistors are used to measure the inlet and outlet water temperatures. The thermistors measure the water temperatures inside two delrin plastic 'T' couplers, which are attached directly to the inlet and outlet of the coil. The thermistor probes are suspended in the couplers by 0.3175 cm (0.125 in.) compression fittings, so that the probe tips are directly in line of the water flow. The T-couplers provide thermal insulation for the water and transition the recirculation loop flow from 1.27 cm (0.50 in.) flex tube to the coil's tube diameter. Two areas of concern in the waterside temperature measurements were discovered during testing of the coils. Again as experienced with the airside thermistors, large amounts of heat was lost because of the probe lengths. To accommodate for this, the couplers and thermistor probes are surrounded in insulation during testing and the probe compression fittings were changed from brass to plastic. Secondly the orientation of the coupler affects the thermistor temperature readings. Due to the reduction in inside diameter of the delrin measurement coupler to the small diameter the connection fittings, air can become entrapped in the inlet coupler, if it is attached in line of the coil inlet. The entrapped air would shift the thermistors readings towards ambient conditions. To correct this problem the inlet coupler is rotated 90° to the vertical position during testing, Fig. 31. This allows any air in the system to either be flushed through the coil or become entrapped away from the thermistor.

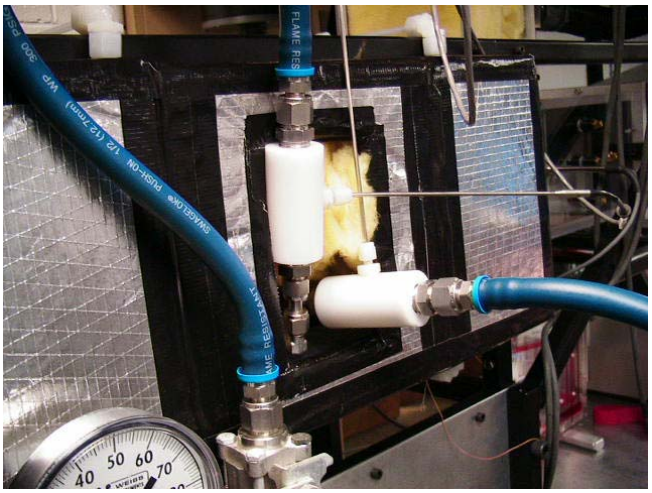

Fig. 31. Delrin plastic 'T' couplers and thermistor probes for water side temperature measurement. Inlet coupler is inverted to 90°.

Again like the air side temperature measurements a "zeroing" technique is employed for the water side temperature measurements, to help quantify any heat loss in the system. A baseline "zeroing" test, prior to a full scale Unit Cell test is performed by connecting the inlet and outlet couplers directly to one another by passing the Unit Cell coil. The recirculation loop is brought to the ideal inlet conditions of the actual test and the offset between the inlet and outlet water temperatures is recorded. The offset is added to the outlet temperature so that both the inlet and outlet temperatures should ideally read the same. The accuracy for measuring water temperatures prescribed by ASHRAE Standard 33-2000 6.1.2 [6], is 0.3ºC for all cases. The total uncertainty in water side temperature measurements is typically ±0.04ºC well within the allowable limit. When the thermistors are "zeroed," the uncertainty increases slightly to ±0.08ºC for the outlet temperature measurement. Calibration data and uncertainty analysis of the thermistors can be seen in the Appendix B.

2.2.5 Liquid Flow Measurement

The liquid mass flow rate is measured with a D25 MicroMotion® flow meter. The flow meter was connected to a Model 9712 Remote Flow Transmitter (RFT) which converted the flow meter output to a frequency output for DAQ measurement. The RFT was also coupled with a MicroMotion® Digital Rate Totalizer which displays mass flow rate on the wind tunnel control panel. The flow meter was selected for its high accuracy and low maintenance. The calibration of the Micro Motion flow meter took place outside of the laboratory so detailed calibration procedures are not available. The uncertainty for the water flow measurements tended to be less than 0.5% of the mass flow rate measurement.

2.3 Electrical System

The data acquisition (DAQ) system used in this experimental investigation was an Intergra Series Keithley 2701 Ethernet enabled DAQ. The DAQ was connected to an IBM ThinkPad Laptop through the computers Ethernet port. A Keithley 7708 multiplexer card was wired to read the multiple instruments discussed earlier. The 7708 multiplexer can accept up to 40 two wire voltage measurements, or 20 4-wire measurements. The Keithley DAQ and 7708 card were chosen for there ease of applicability and their capacity to run multiple instruments. The data acquisition system, the 2701 DMM and IBM laptop, are shown in Fig. 32.

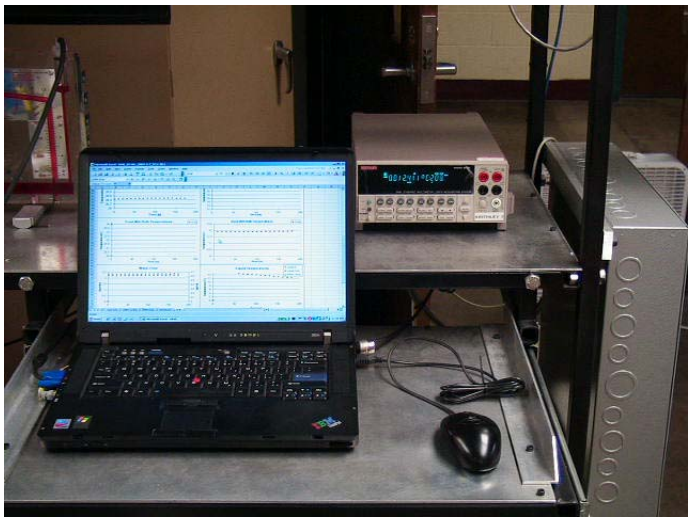

Fig. 32. Kiethley 2701 DAQ with 7708 multiplexer card.

3. EXPERIMENTAL METHODS

3.1 Test Procedure

To achieve a direct comparison between the standard coil and the Unit Cell coil the tests inlet conditions on the air and waterside need to be ideally matched. Using the data from the standard sized coils is assumed as the standard inlet coil settings. Even with the reduction of in size of the coils the inlet dry bulb temperature, inlet wet bulb temperature, standard air face velocity and inlet water temperature can compare directly to that of the Unit Cell coil. However, because of a reduction in the coil geometry, a large portion of water side circuitry was removed from the coil, thus making a direct comparison of mass flow rate of the coil impossible. Thus, the tube side Reynolds's Number, as defined by (18), is matched to compensate for the different coil circuitry.

$$\mathrm{Re} = \frac{\rho \vec{V} D_h}{\mu} \tag{18}$$

During each test the wind tunnel system is started according to the procedure in Appendix C. The test apparatus is monitored and adjusted until inlet conditions are satisfied. Once the system reaches steady-state, the DAQ records steady-state temperatures, pressures, and flows for a total of 20 min. This data is analyzed for Unit Cell verification and coil performance measurements.

3.2 Data Reduction

The overall heat transfer coefficient, *U*, at various air velocities is used to compare and validate the Unit Cell coil to that of the standard size coil. In determining

both the energy balance and overall heat transfer coefficient, the air side heat transfer rate can be calculated by using the actual air velocity and solving Eq. (19),

$$Q_{air} = \dot{m}_{air}\left(h_{in} - h_{out}\right) \tag{19}$$

where $\dot{m}_{air}$, is the mass flow rate of water and h_{in} and h_{out} represent the inlet and outlet air enthalpies, respectively. Equation 19 was obtained from ASHRAE Handbook-Fundamentals [11] as well as the subsequential equations 20-26. The enthalpy for both the inlet and outlet conditions is determined by

$$h = 1.006T_{db} + W(2501 + 1.805T_{db}) \tag{20}$$

where T_{db} is the dry bulb temperature in °C, of the air and W is the humidity ratio.

The humidity ratio, W, is determined by the dry and wet bulb temperatures and the atmospheric pressure. Again, during heating tests only sensible heating occurs and no moisture is added to the air; therefore, there is no change in the humidity ratio. With no change in the air moisture content and the high risk of the wick dry out on the wet bulb probes, the outlet humidity is assumed to be equal to that of the inlet side in enthalpy and supplementary calculations. To determine the humidity ratio of the moist air, the humidity ratio of moist air at saturation thermodynamic wet-bulb temperature must be determined through the equation,

$$W_{s,wb} = 0.62198\frac{p_{ws}}{p - p_{ws}} \tag{21}$$

where p is the atmospheric pressure in kPa and p_{ws} is the pressure of pure water in kPa. The pressure of pure water can be calculated by

$$\ln p_{ws} = C_1 / T_{wb} + C_2 + C_3 T_{wb} + C_4 T_{wb}^{\ 2} + C_5 T_{wb}^{\ 3} + C_6 \ln T_{wb} \tag{22}$$

$$C_1 = -5.8002206E + 03$$
$$C_2 = 1.3914993E + 00$$
$$C_3 = -4.8640239E - 02$$
$$C_4 = 4.1764768E - 05$$
$$C_5 = -1.4452093E - 08$$
$$C_6 = 6.5459673E + 00$$

where T_{wb} is the wet-bulb temperature in Kelvin and p_{ws} is the pressure of pure water again in kPa. Solving for the pressure of pure water in Eq. (22) the humidity ratio of moist air at saturation thermodynamic wet-bulb temperature can be calculated and used to define the humidity ratio of the moist air.

To solve for the humidity ratio Eq. (23) is used.

$$W = \frac{(2501 - 2.381T_{wb})W_{s,wb} - 1.006(T_{db} - T_{wb})}{2501 + 1.805T_{db} - 4.186T_{wb}}, \tag{23}$$

Using Eqns. (20) through (23), the enthalpies can be solved for both the inlet and outlet conditions. To finish calculating the heat transfer on the air side the actual mass flow rate must be determined. The mass flow rate of the air is calculated by using the volumetric flow obtained from the LFE and its calibration curve.

$$\dot{m}_{air} = \frac{\vec{v}_{actual}}{\nu} A, \tag{24}$$

where $\vec{v}_{actual}$ is the actual air face velocity provided by LFE, ν is the moist air viscosity and A is the cross-sectional area of the wind tunnel. The cross-sectional area of the duct is calculated to be 0.0232 m^3. As for the moist air viscosity, this can be calculated using the equation:

$$\nu = \frac{0.2871(T_{db,LFE} + 273.15)(1 + 1.6078W)}{p} \tag{25}$$

In Eq. (25) the $T_{db,LFE}$ represents the LFE dry-bulb temperature and W represents the humidity ratio at the outlet of the test coil. Solving for the air viscosity and the mass allows the air side heat transfer to be determined from Eq. (19).

An alternate air side heat transfer calculation was used as a validation that the equations and methods used for the system were correct and accurate. While the calculation for the total heat transfer is similar to that presented above, the standard mass flow rate is determined differently as described in section 2.2.3. Thus, the total air side heat transfer can be calculated by,

$$Q_{air} = \dot{m}_{air,standard}\left(h_{in} - h_{out}\right). \tag{26}$$

where $\dot{m}_{air,standard}$, is the standard mass flow rate of water and h_{in} and h_{out} represent the inlet and outlet air enthalpies, respectively. The standard mass flow rate can be calculated by dividing the standard volumetric flow by the standard's air specific volume.

$$\dot{m}_{air,standard} = \frac{\dot{V}_{standard}}{v_{standard}}, \tag{27}$$

The specific volume for a standard air of standard calibration conditions, 21.11 °C (70 °F) and 101.3 kPa (29.92 in. of Hg), is 0.0232258 m^3/kg.

In theory the actual mass flow rate should be equal to that of the standard mass flow rate. To help validate that the flow rates are being calculated correctly a comparison of actual mass flow rate versus standard mass flow rate can be made. At an inlet condition of 26.67 °C dry bulb and 24.82 °C wet bulb temperatures, the actual mass flow rate was calculated at 0.0893 kg/s. For the same test a standard mass flow rate was calculated at 0.0895 kg/s, a difference of 0.25% between the two. Because this difference

in mass flow rates is extremely low, the confidence in both the standard and actual flow measurements and calculations are assumed valid.

To validate the testing apparatus an energy balance between the air and liquid was determined. The liquid side heat transfer is much simpler to determine. To solve for this value the equation

$$Q_{H_2O} = \dot{m}_{H_2O} C_p \left(T_{in} - T_{out}\right), \tag{28}$$

where $\dot{m}_{H_2O}$ is the mass flow rate, T_{in} and T_{out} are the inlet and outlet water temperatures respectively and C_p is the specific heat of the water. The specific heat is acquired from tabular data from Incropera and DeWitt [12] using the average of the inlet and outlet temperatures. Comparing the two heat transfer rates, the overall effectiveness of the testing system can be analyzed.

In some instances it may be more useful to study the coils in terms of its heat transfer coefficient at various air velocities. The log-mean temperature difference for a counter-flow heat exchanger must be determined using by:

$$\Delta T_{lm} = \frac{\left(T_{db,in} - T_{H_2O,out}\right) - \left(T_{db,out} - T_{H_2O,in}\right)}{\ln\left(\dfrac{T_{db,in} - T_{H_2O,out}}{T_{db,out} - T_{H_2O,in}}\right)}. \tag{29}$$

The overall heat transfer coefficient, U, value can be determined by:

$$U = \frac{q_{sensible}}{A \Delta T_{lm}}. \tag{30}$$

where $q_{sensible}$ is the sensible heat transfer of the coil and A is the cross-sectional area of the coil. The calculation of the $q_{sensible}$ depends on the coil test performed. In heating tests, because only sensible heat is transferred, $q_{sensible}$ is calculated as the average of the air side and liquid heat transfers.

4. RESULTS AND DISCUSSION

In studying the performance of the Unit Cell, only the steady-state heat transfer and pressure drop were concerned and the transient heat characteristics ignored. To ensure every test was at steady-state, data was collected for each test for a total of at least 1000 seconds. Data in which the air side temperature fluctuation from the initial reading to the final reading was ±0.2°C or in which a steady oscillatory temperature measurement could be seen as shown in Fig. 33 was deemed as steady-state.

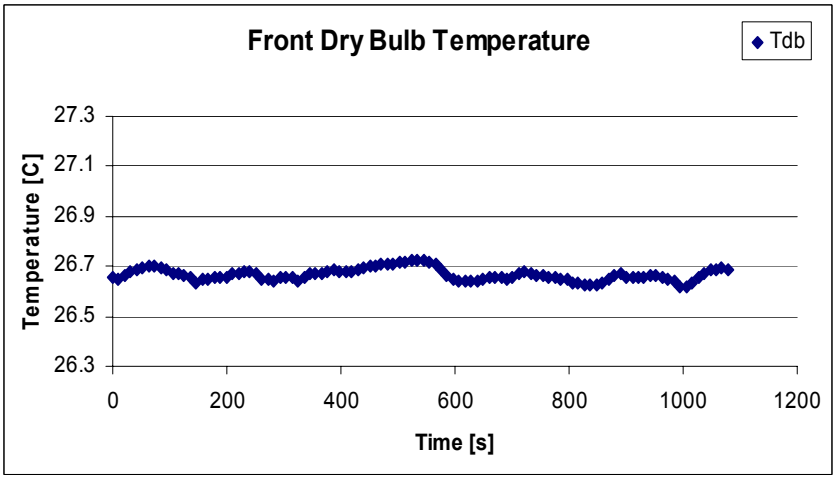

(a)

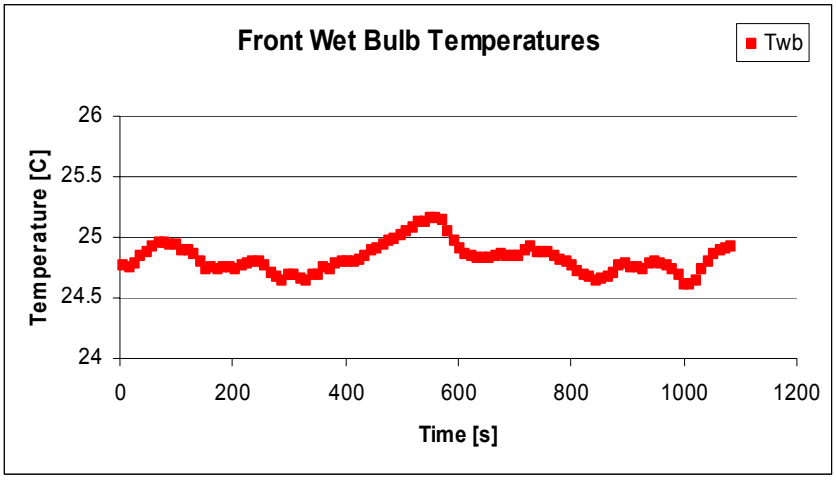

(b)

Fig. 33. Sample system data collection at steady-state: (a) Front dry bulb measurement. (b) Front wet bulb measurement.

Fluctuation in the dry bulb temperature measurements, tended to be much lower than that of the wet bulb temperature measurement. This variation in temperature manifested itself in the uncertainty of each measurement, but not outside an acceptable region as described in ASHRAE Standard 33-2000 11.9 [6]. Using the uncertainty calculations per Appendix B, the average temperatures in Fig. 33 are 26.67±0.046 °C for the dry bulb temperature and 24.82±0.056 °C for the wet bulb temperature. A similar method was used to determine when the water side temperatures were at steady state. In Fig. 34, a sample collection of steady state data for the water inlet temperature at 81.18±0.128 °C can be seen.

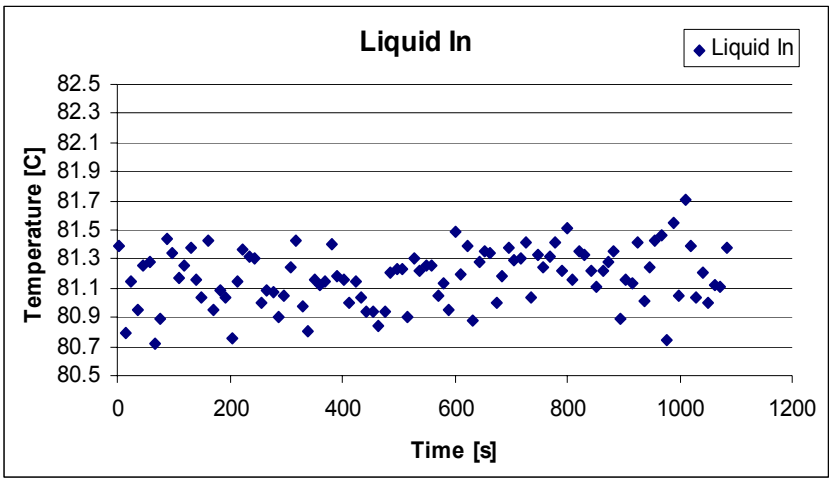

Fig. 34. Sample system data collection of liquid inlet temperature at steady-state.

When all temperatures were considered at steady state, necessary data was collected for a minimum of 100 data points, approximately 1000 s. This data was then averaged and used in the calculation of airside and heat transfer performance.

Before the Unit Cell concept can be verified it is necessary to show the test apparatus is both accurate and repeatable. The test apparatus performance can be quantified in terms of its energy balance between the air side and water side heat transfer

rates. As specified by the ASHRAE Standard 33-2000 11.9 [6], the total heat transfer balance shall fall between the following limits,

$$+5\% \geq \frac{100\left(Q_{air} - Q_{H_2O}\right)}{\frac{1}{2}\left(Q_{air} + Q_{H_2O}\right)} \geq -5\% . \tag{31}$$

Thus the energy balance between the air and water became the ultimate goal during build up the system. Using data from sensible heating tests of the Trane 03H047 Unit Cell coil, the air and water heat transfers as they vary with standard face velocity can be viewed in Fig. 35. For this test, the coil was subjected to inlet air dry and wet bulb temperatures of 26.7 °C and 22.5 °C, respectively. The actual air face velocity was adjusted from 1.5 m/s to 3.5 m/s which corresponds too 1.4 m/s 3.1 m/s standard air velocity. The inlet water conditions for the coil were a Re of 29,500 and an inlet water temperature of 82.2 °C.

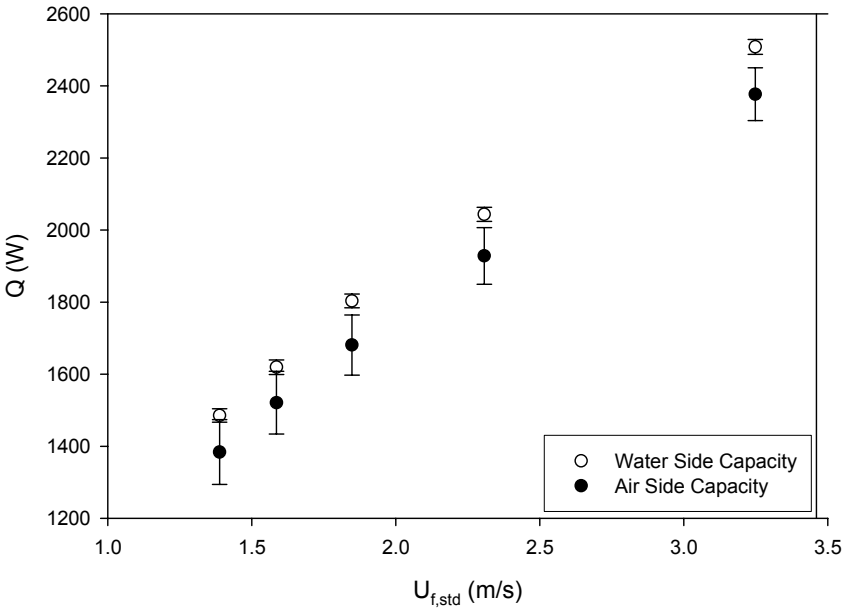

Fig. 35. Heat transfer vs. standard air face velocity results for the 03H047 Unit Cell coil. (Heating Test)

The energy balance for the sensible test varies from -5.4% to -8.3%, decreasing as the air face velocity increases. This range of data has been typical for all coils. During cooling tests the air side heat transfer is typically 5-8% higher than the water side heat transfer. Noting there is such fluctuation in the airside heat transfer, it is assumed that the water heat transfer value is more accurate than the airside measurement. There are two justifications for this theory:

1. To determine the airside heat transfer rate a total of six measurements must be made, 5 temperature measurements and 1 flow measurement. Conversely the waterside heat transfer rate can be determined by only three measurements, 2 temperature measurements and 1 flow measurement. With fewer measurements the variability in the measurements decreases.
2. Placement of the thermistor probes vary greatly between the two systems. The waterside thermistors are placed directly in the flow stream of the water, while on the airside air must be sampled and measured outside the flow stream, rather than inside the air duct providing more area for heat loss between coil and measurement location.

However these observations should not discredit the overall performance of the system. While this cannot be completely ignored and further improvements may be made to the system in the future, it is relatively close to the ±5% and will be assumed reasonable at this point.

Another important factor in dealing with the performance and accuracy of the testing system is the repeatability of the system. Two separate repeatability tests were performed on the Trane 03H047 test coil to determine the reliability of the system. No

two repeatability tests were performed in succession and the cotton socks on all wet bulb thermistors were replaced before each test. The test conditions for the repeatability study can be seen in Table 1. Test #1 conditions were chosen to replicate the conditions tested for the standard coil. The Test #2 conditions were similar to Test #1 only the inlet wet bulb temperature was increased to 22.6 °C. In both tests the coil was subjected to five different air flow rates between 1.5 and 3.5 m/s.

Table 1. Repeatability Test Parameter.

Test Parameter	Test #1	Test #2
$T_{db,in}$ (°C)	26.7	26.7
$T_{wb,in}$ (°C)	16.6	22.6
$\vec{v}_{air,act}$ (m/s)	1.5-3.5	1.5-3.5
$T_{H_2O,in}$ (°C)	82.2	82.2
$\dot{m}_{H_2O}$ (kg/min)	4.56	4.56

In both tests the repeatability of the system can be seen to be achieved, Figs 36-39. In Test #1 all measurements were within 3.00% of the previous test. For Test #2 there is a slightly discrepancy in water side heat transfer; however this same phenomena is not seen in the air side heat transfer rate. Because this higher heat transfer rate is only seen in one set of the water side measurements, the reason of the difference is mostly likely caused by air in the probe section as described above. If the water side heat transfer rate for Test #2 is disregarded the system conditions and results are shown as quite repeatable. The uncertainties for both repeatability tests can be seen in Table 2. The average uncertainty for each parameter is the average of uncertainty for all air flow rates. The maximum is the largest uncertainty from each test.

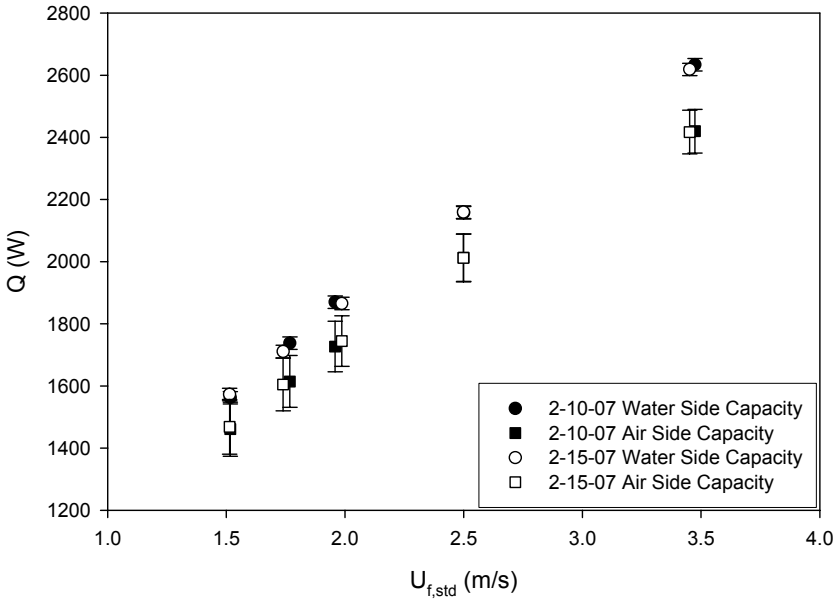

Fig. 36. Test #1 repeatability energy transfer results for the 03H047 Unit Cell coil.

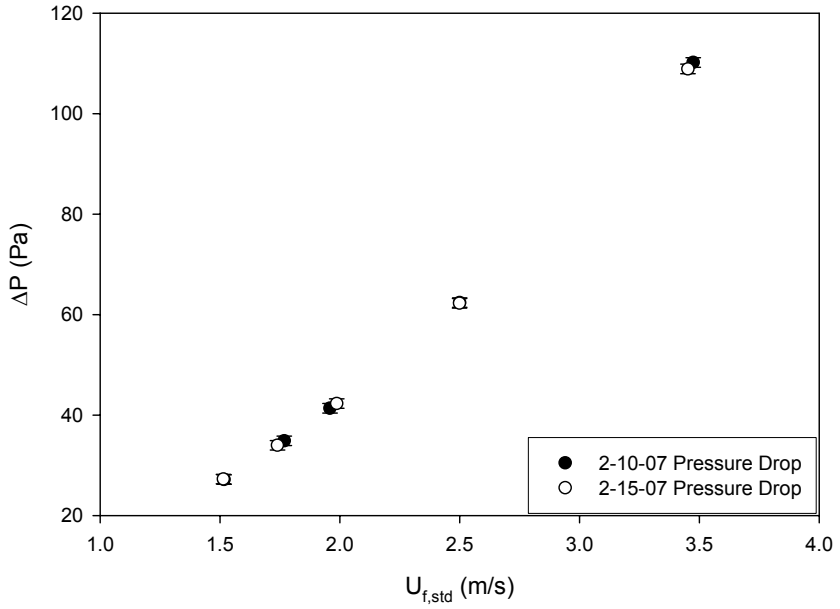

Fig. 37. Test #1 repeatability pressure drop results for the 03H047 Unit Cell coil.

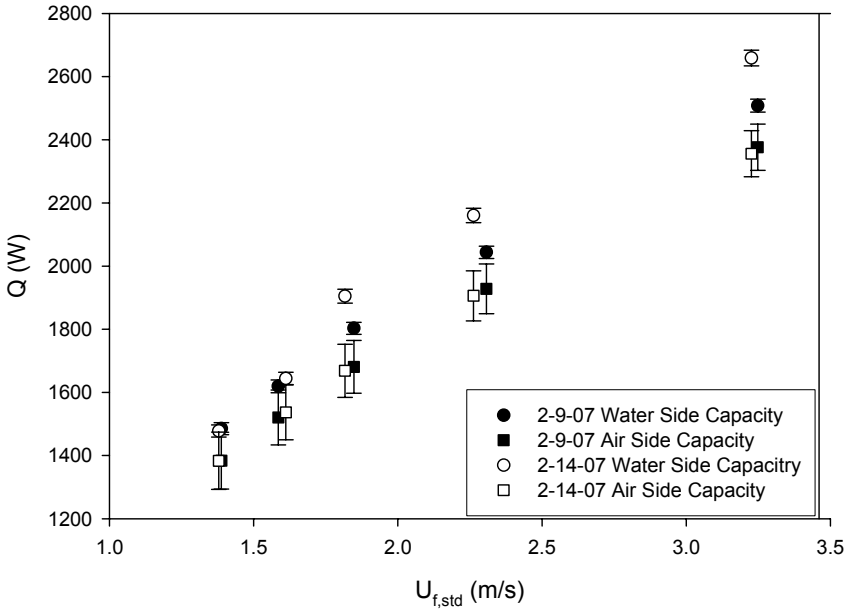

Fig, 38. Test #2 repeatability energy transfer results for the 03H047 Unit Cell coil.

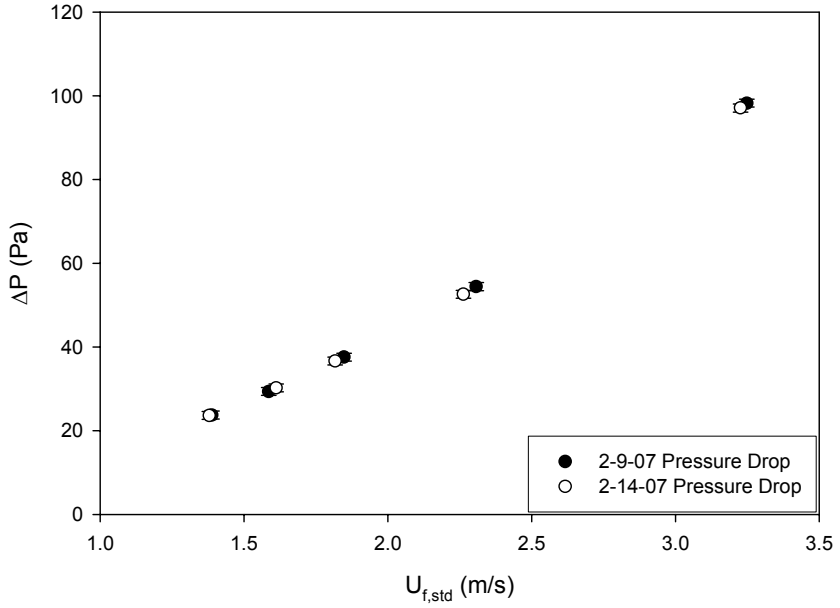

Fig. 39. Test #2 repeatability energy transfer results for the 03H047 Unit Cell coil.

Table 2. Repeatability Experiments Results.

Test Measurement	Test #1		Test #2	
	Average Error (%)	Maximum Error (%)	Average Error (%)	Maximum Error (%)
$T_{db,in}$ (°C)	0.09	0.19	0.11	0.33
$T_{wb,in}$ (°C)	0.40	1.24	0.23	0.81
$T_{db,out}$ (°C)	0.24	0.56	0.23	0.64
$T_{wb,out}$ (°C)	1.32	2.92	0.72	1.55
$\vec{v}_{air,std}$ (m/s)	0.20	1.60	0.68	1.95
$T_{H_2O,in}$ (°C)	0.00	0.61	0.08	0.26
$T_{H_2O,out}$ (°C)	0.02	0.65	0.21	0.58
$\dot{m}_{H_2O}$ (kg/min)	0.19	0.35	0.29	0.63
ΔP (Pa)	0.27	2.62	0.92	3.41
Q_{air} (W)	0.16	1.03	0.35	1.15
Q_{H_2O} (W)	0.32	1.56	3.58	5.84

Table 3. Repeatability Test Uncertainties.

Test Measurement	Test #1		Test #2	
	Average	Maximum	Average	Maximum
$T_{db,in}$ (°C)	± 0.046	± 0.046	± 0.046	± 0.046
$T_{wb,in}$ (°C)	± 0.055	± 0.059	± 0.055	± 0.060
$T_{db,out}$ (°C)	± 0.083	± 0.084	± 0.083	± 0.083
$T_{wb,out}$ (°C)	± 0.089	± 0.099	± 0.088	± 0.098
$\vec{v}_{air,std}$ (m/s)	± 0.09	± 0.10	± 0.09	± 0.10
$T_{H_2O,in}$ (°C)	± 0.063	± 0.068	± 0.063	± 0.074
$T_{H_2O,out}$ (°C)	± 0.098	± 0.104	± 0.098	± 0.100
$\dot{m}_{H_2O}$ (kg/min)	± 0.01	± 0.01	± 0.01	± 0.01
ΔP (Pa)	± 0.996	± 0.996	± 0.996	± 0.996
Q_{air} (W)	± 79.9	± 88.0	± 82.7	± 90.7
Q_{H_2O} (W)	± 20.55	± 22.58	± 20.6	± 24.6

Because the unorthodox "zeroing" method was implored for the testing it is necessary to see how this plays a role in calculation of heat transfer properties. Looking at zeroed and non-zeroed heat transfer rates from the Test #2 repeatability data, Fig. 40, little effect by the "zeroing" can be seen in the heat transfer rates of the air and liquid capacitates. In fact "zeroing" typically only quantifies only 10-20 W of the 2 kW heat transfer rate. This corresponds to about 2-3% improvement in the overall heat balance. At the low velocities this percentage is the greatest at 0.62%, Table 4, in the water side heat transfer. While for the test performed in this investigation, zeroing can be deemed as a non-critical measurement, at low air face velocities, sub 0.5 m/s, or for tests using coils smaller than the 15.24 cm by 15.24 cm surface dimensions, the heat transfer is low enough that the "zeroing" technique again become an important parameter. To help compare present results to coils in the future, all data presented in this investigation are zeroed.

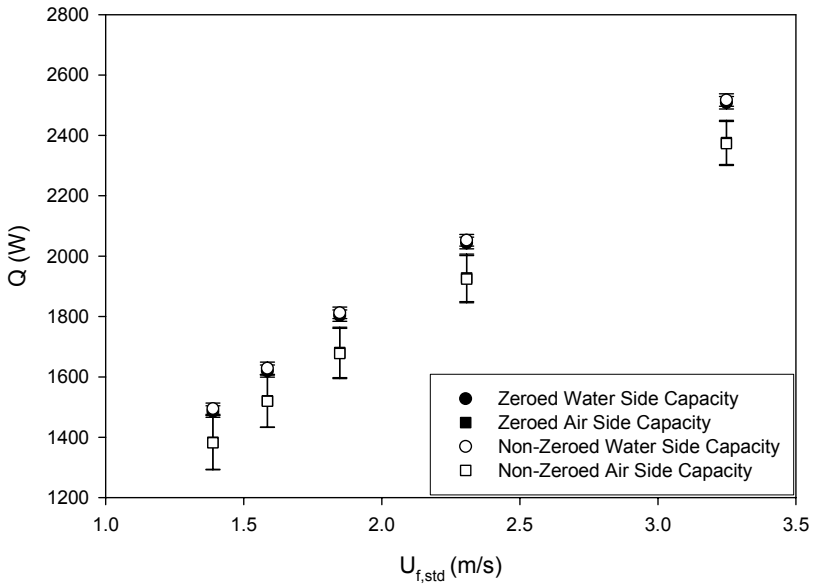

Fig. 40. Comparison of "Zeroing" effects on Air and Water side heat transfer.

Table 4. Effects of Zeroing on Heat Transfer.

$\vec{v}_{air,std}$ (m/s)	Change in Q_{air} (%)	Change in Q_{H_2O} (%)
1.39	0.14	0.62
1.59	0.10	0.57
1.85	0.19	0.51
2.31	0.21	0.45
3.25	0.15	0.36

With the validity of the system confirmed, it is important to show how different inlet conditions will affect the overall heat transfer and pressure drop across the coil. Because the current air handler was unavailable for a majority of the research, humidity control was also unavailable. Thus a parametric study was performed in how the inlet wet bulb temperature affected the pressure drop and overall heat transfer of the coil. Again the Trane 03H047 Unit Cell coil was used as the test coil. The coil was subjected to an inlet air with a dry bulb temperature of 26.7 °C and an actual air face velocity varying from 1.5 m/s to 3.5 m/s. The water had an inlet temperature of 82.2 °C and flowed with a Reynolds's number of approximately 29,500. Two separate humidities were investigated:

1. A wet bulb temperature of 22.5 °C, which corresponds to a humidity ratio of 15.7 g/kg.
2. A wet bulb temperature of 13.3 °C, which corresponds to a humidity ratio of 4.2 g/kg.

Which such a wide variance in the wet bulb temperatures and humidity ratios, any effect that these parameters have on the pressure drop and heat transfer should be evident. In Fig. 41, the affect of humidity on the pressure drop across the coil can be seen during sensible heat tests. For heating tests, there is no relative effect on the pressure drop

across the coil. Even with a 373% increase in water moisture content in the air, no variation in the pressure drop was measured.

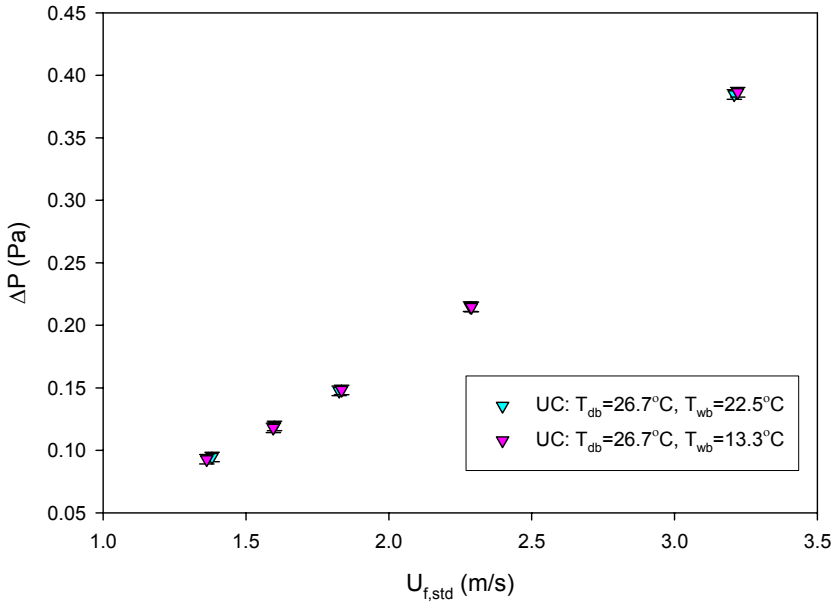

Fig. 41. Pressure drop vs. standard air face velocity results for the 03H047 Unit Cell test coil. (Heating Test)

The heat transfer however was affected slightly by the increased in humidity, Fig. 42. In all cases the heat transfer coefficient increased by at least 1.3%. This increase in heat transfer as humidity increases is in line with Still, Venzke, Durst and Melling [13] where they observed "an increase of the heat transfer… with increasing humidity." These findings show that the system behavior is reasonable to other standard based tests. It also shows that matching inlet conditions are important in comparison of the standard coil to the Unit Cell coil.

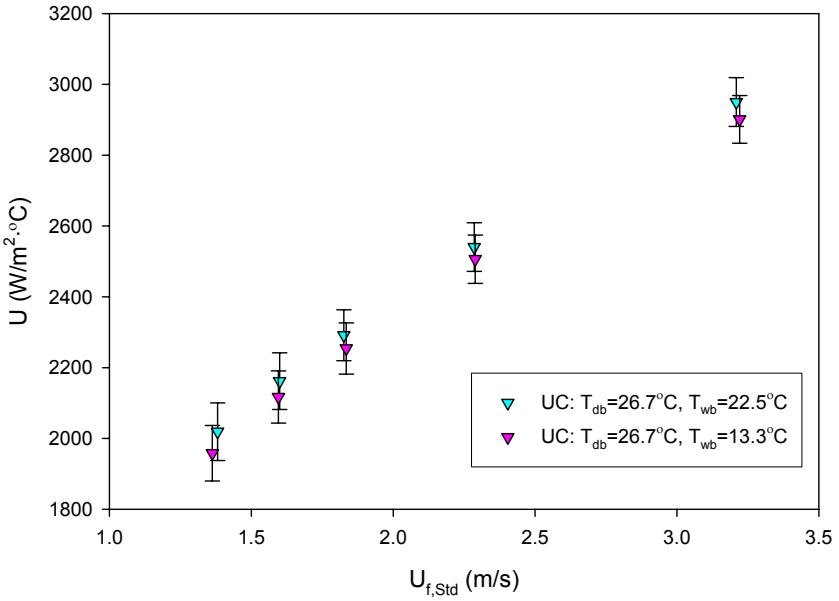

Fig. 42. Heat transfer coefficient vs. standard air face velocity results for the 03H047 Unit test coil. (Heating Test)

The humidity has an even stronger affect on the Unit Cell coil when tested under cooling conditions. The Trane 03H047 Unit Cell coil was tested at an inlet air temperature of 26.7 °C and various face velocities between 1.5 and 4.0 m/s. The water flowed through the coil with a Re value of 7,500 and an inlet temperature of 7.2 °C. Again two humidities were investigated:

1. A wet bulb temperature of 19.4 °C, which corresponds to a humidity ratio of 11.3 g/kg.
2. A wet bulb temperature of 15.2 °C, which corresponds to a humidity ratio of 6.2 g/kg.

Unlike the sensible heating tests, the pressure drop is very much affected by the amount of humidity in the air, Fig 43. By increasing the humidity of the incoming air the saturation temperature of the air rises. If this saturation temperature is higher than that of the coil fins, condensate formation on the coil will lead to a much greater frictional pressure drop. Similar trends are also shown for heat transfer increase with humidity

increase for the cooling tests, Fig. 44. The wet bulb temperature, or more specifically the moisture content in the air, has a significant impact on the energy transfer and pressure drop. Thus, now that humidity control has been established in the wind tunnel system, it is necessary to match the moisture content in the air to effectively utilize the Unit Cell concept for future air-to-liquid heat exchanger R&D.

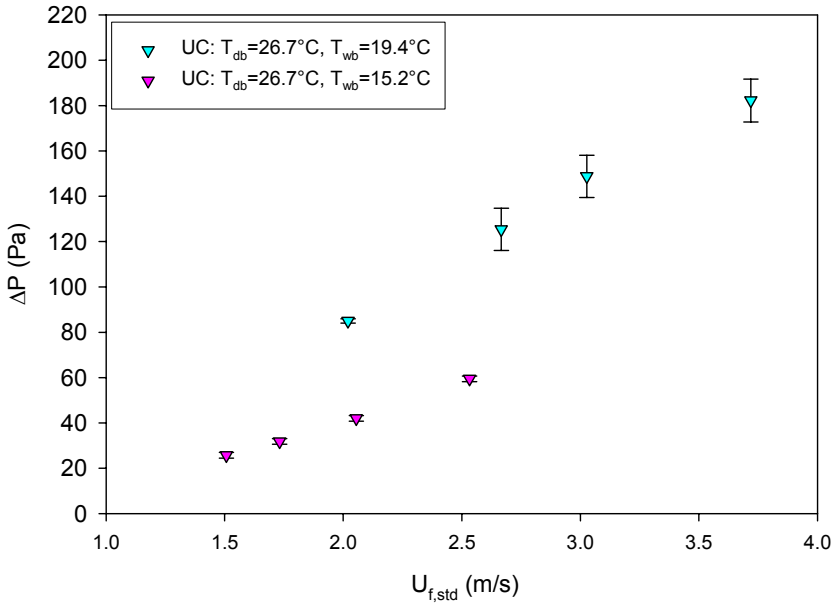

Fig. 43. Pressure drop vs. standard air face velocity results for the 03H047 Unit Cell test coil. (Cooling Test)

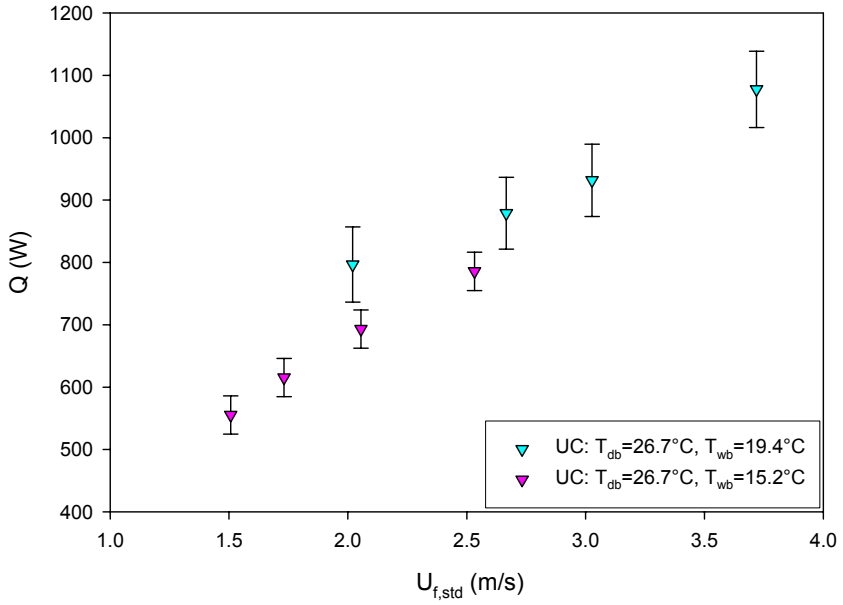

Fig. 44. Energy transfer vs. standard air face velocity results for the 03H047 Unit Cell test coil. (Cooling Test)

To show the effectiveness in the Unit Cell concept a total of three unit coils were tested and compared to their standard coils. The first coil, the TRANE 03H047, was tested at the inlet air conditions of a dry bulb and wet bulb temperature 26.7 °C and 18.6 °C, respectively. The air velocity was varied between 1.5 and 4.0 m/s. The inlet water conditions for the coil were a Re of 29,500 and an inlet water temperature of 82.2 °C. The results of comparative pressure drop and heat transfer coefficient can be seen in Figs. 45 and 46. Results for the standard coil were provided by AHT [14, 15].

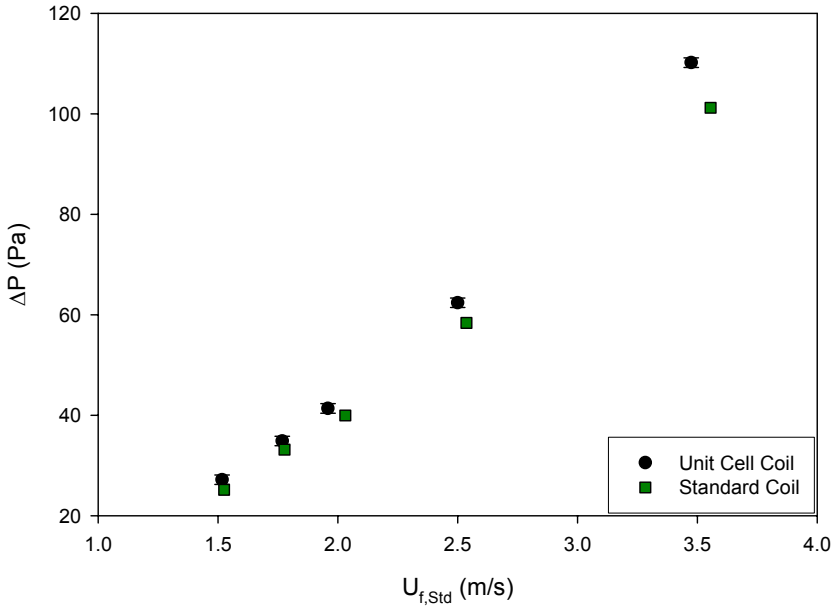

Fig. 45. Pressure drop vs. standard air face velocity results for the 03H047 Unit Cell and Standard test coil. (Heating Test)

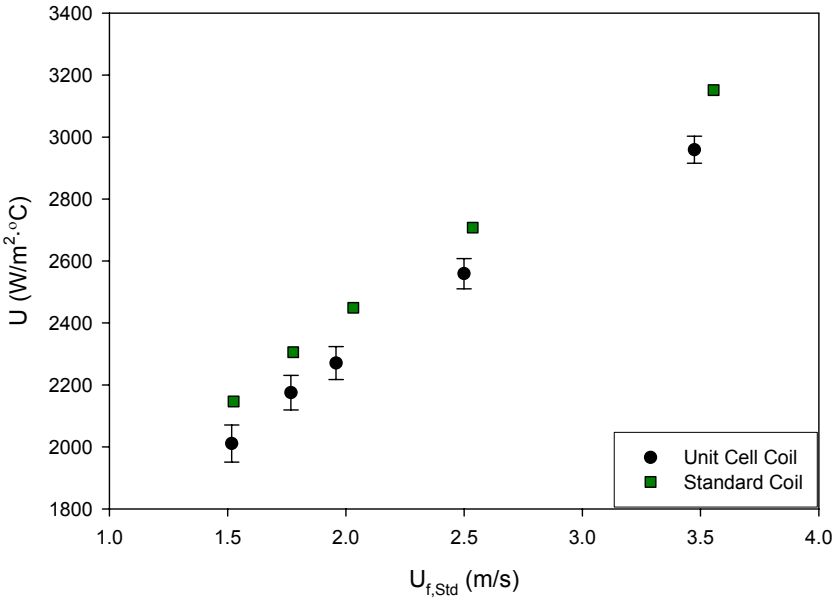

Fig. 46. Heat Transfer Coefficient per unit area vs. standard air face velocity results for the 03H047 Unit Cell and Standard test coil. (Heating Test)

Looking more closely at the results from the Unit Cell comparison the predicted pressure drop from the Unit Cell coil is nominally 6.27% higher than the standard coil.

The Unit Cell sensible heat transfer coefficient is nominally 6.37% lower than standard coil. The actual water side heat transfer rate was almost directly matched with only a 1.32% average difference for all five air velocity. Unfortunately, the lower air side heat transfer rate influenced the $U_{sensible}$ to be lower than it should have been. However, considering the face area of the coil was reduced by from 1.497 m^2 to 0.022 m^2, a 6-7% difference of performance measures relatively remarkable. As for the system, it was easily capable of matching all Unit Cell conditions to that of the standard coil tests. All temperatures were matched within 1.79% and flow rates within 3.66%.

Table 5. Unit Cell Comparison Test Results.

Test Measurement	Average Difference from Standard Coils (%)	Maximum Difference from Standard Coils (%)
$T_{db,in}$ (°C)	0.00	0.27
$T_{wb,in}$ (°C)	0.72	1.79
$T_{db,out}$ (°C)	5.82	6.17
$T_{wb,out}$ (°C)	0.08	1.42
$\vec{v}_{air,std}$ (m/s)	1.73	3.66
$T_{H_2O,in}$ (°C)	0.07	0.26
$T_{H_2O,out}$ (°C)	4.37	5.73
Re	1.07	1.50
ΔP (Pa)	6.27	8.50
Q_{air} (W)	9.03	11.32
Q_{H_2O} (W)	1.36	3.68
$U_{sensible}$ (W/m^2· °C)	6.37	7.55

Table 6. Unit Cell Comparison Test Uncertainties.

Test Measurement	Average	Maximum
$T_{db,in}$ (°C)	± 0.046	± 0.046
$T_{wb,in}$ (°C)	± 0.053	± 0.055
$T_{db,out}$ (°C)	± 0.083	± 0.084
$T_{wb,out}$ (°C)	± 0.089	± 0.099
$\vec{v}_{air,std}$ (m/s)	± 0.09	± 0.10
$T_{H_2O,in}$ (°C)	± 0.061	± 0.065
$T_{H_2O,out}$ (°C)	± 0.098	± 0.101
$\dot{m}_{H_2O}$ (kg/min)	± 0.01	± 0.01
ΔP (Pa)	± 0.996	± 0.996
U (W/m^2· °C)	± 52.22	± 59.88

The other two Unit Cell coils were tested at similar dry bulb and air face velocities. Data was again supplied by AHT [16]. Because these tests were preformed prior to the wind tunnel having humidity control, there was slight variation in the wet bulb temperature. The inlet water temperature set to again to 82.2 but here Re was cut to 12,500. These Unit Cell comparative results can be seen in Fig. 47. In all three comparative tests the results of the Unit Cell tests matched the standard coil tests relatively well. From the additional two prototype coils there is a maximum variation of 10.46% and 16.82% in ΔP respectively for each coil, Table 7. Like previous Trane 03H047 Unit Cell coil, the standard coil pressure drop was matched more closely at lower air velocities, 0-2.0 m/s. This may show that there is a limiting velocity in which the Unit Cell concept can accurately predict pressure drop for a standard coil. There is also a difference in heat transfer rates per area rates, up to 12.12% and 14.28% respectively for each coil, however this discrepancy is most likely due to the raised wet

bulb temperature at the inlet conditions. It is important to note that it is being assumed that the standard coil test results are accurate.

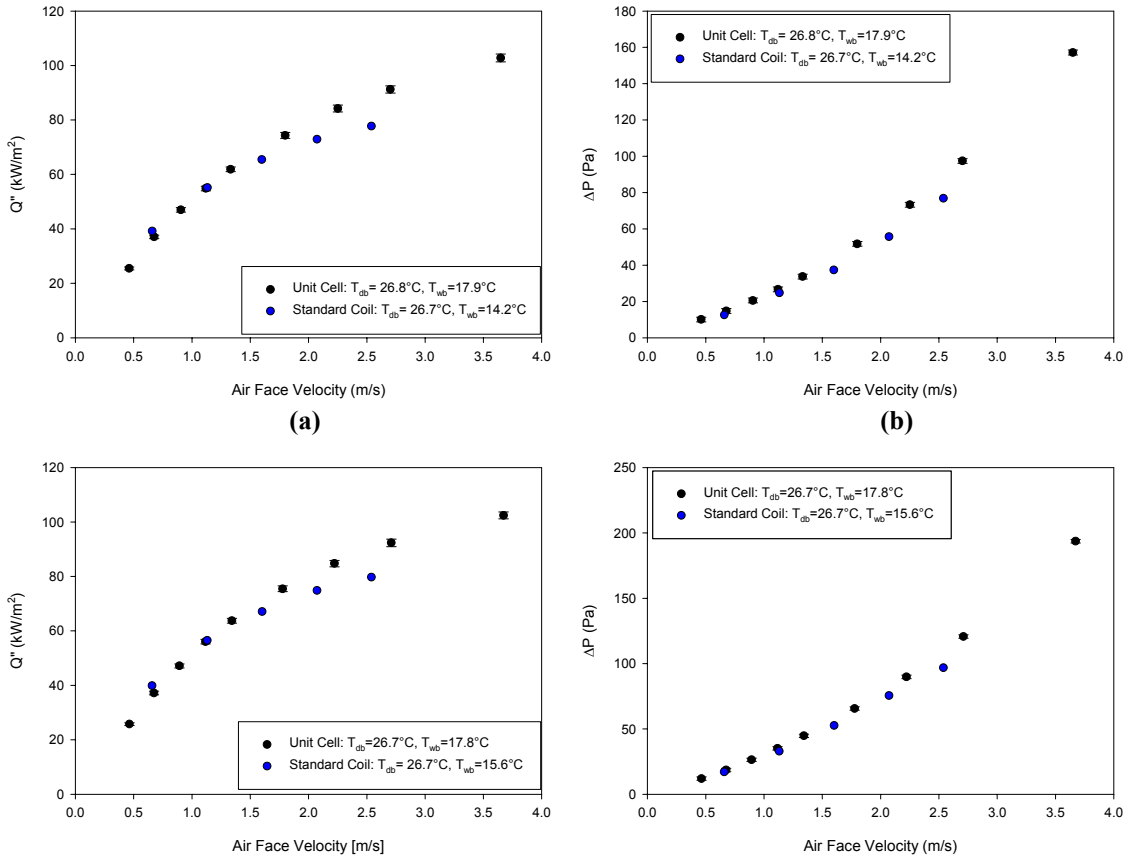

Fig. 47. (a) Heat flux versus face velocity for prototype coil 'A'. (b) Pressure drop across Prototype 'A' versus face velocity. (c) Heat flux versus face velocity for prototype coil 'B'. (d) Pressure drop across prototype 'B' versus face velocity.

Table 7. Supplemental Unit Cell Comparison Test Results.

Test Measurement	Prototype 'A'		Prototype 'B'	
	Ave. Diff. from S.C. (%)	Max. Diff. from S.C. (%)	Ave. Diff. from S.C. (%)	Max. Diff. from S.C. (%)
Re	0.87	1.90	0.78	1.40
ΔP (Pa)	7.52	10.46	13.53	16.82
Q" (W)	3.52	12.12	4.32	14.28

Beyond matching air side inlet conditions, two other factors must be addressed to ensure Unit Cell and standard coil results are comparable. First, all sources of air by-pass need to be eliminated, ensuring all air passes through coil. Second, because the size reductions in the Unit Cell coil, the circuitry of the coil is typically different from the standard coil. Thus, matching tube side Reynolds number is the most critical to match the tube side heat transfer characteristics.

5. CONCLUSION

In general it has been determined that the Unit Cell concept will work and will be effective and efficient method for future coil R&D. The Unit Cell concept was verified against four standard scale coils, Trane 03H047 and two aluminum prototype coils, recognizing there was uncertainty in the standard coil test results and the difference in size between the Unit Cell coil and the standard coil was significant. The multifunctional wind tunnel, although constantly upgraded, has currently met ASHRAE Standards, developed for full size coils, and has performed well to be able to test the Unit Cell concept. The abilities of test apparatus have also been verified through the heat transfer energy balances between air and liquid and through compatibility with the full scale results from Outokumpu-Heatcraft data. Heat transfer rates, heat transfer coefficients, and pressure drops measured by the Unit Cell wind tunnel have been reasonably accurate and can be used to predict full scale coil performances.

To better improve the overall performance and quality of the system several recommendations have been made. Because there is some underlying biased in airside temperature measurements, which cause the airside heat transfer to be lower than the water side heat transfer during heating tests and higher for cooling tests, adjustments to the measuring the device need to be made. By creating an array of thermistors or thermocouples directly inside the duct work a better T_{db} could be established. The current system for measuring T_{db} and T_{wb} could be used to find the inlet and outlet W used in calculation of the psychrometric properties of the air.

Improvements in the airside flow rate measurements should also be considered. Because the current method cannot always conform to ASHRAE standard uncertainty criteria, the uncertainty due to instrumentation must be improved. Although the production of nozzles can probably avoided, it is recommended that a more accurate and better calibrated pressure transducer is used for measuring pressure drop across the LFE. Currently the transducer's large instrumentation uncertainty has the greatest effect on the total airside flow measurement uncertainty, thus improvements in this transducer will greatly reduce uncertainty in the measurement.

REFERENCES

1. Jeom-Yul Yun, Kwan-Soo Lee. 1999. Investigation of heat transfer characteristics on various kinds of fin-and-tube heat exchangers with interrupted surfaces. *International Journal of Heat and Mass Transfer.* 42:2375-2385.

2. Jeom-Yul Yun, Kwan-Soo Lee. 2000. Influence of design parameters on the heat transfer and flow friction characteristics of the heat exchanger with slit fins. *International Journal of Heat and Mass Transfer.* 43:2529-2539.

3. Ju-Suk Buyn, Jinho Lee, Chang-Duk Jeon, Jinho Mok. 2006. A study on airside performance of geometry combination fins using large scale model. *International Journal of Refrigeration*. 29: 1034-1042.

4. H.C. Kang, M.H. Kim. 1999. Effect of strip location on the air-side pressure drop and heat transfer in stip fin-and-tube heat exchanger. *International Journal of Heat and Mass Transfer.* 22:302-312.

5. ARI. 2001. Standard 410: Forced Circulation Air-Cooling and Air-Heating Coils. Arlington, Virginia: Air Conditional and Refrigeration Institution.

6. ANSI/ASHRAE. 2000. Standard 33-2000: Method of Testing Forced Circulation Air Cooling and Air Heating Coils. Atlanta: American Society of Heating and Refrigerating and Air-Conditioning Engineers, Inc.

7. ANSI/ASHRAE. 1987. Standard 41.2-1987: Standard Method for Laboratory Airflow Measurement. Atlanta: American Society of Heating and Refrigerating and Air-Conditioning Engineers, Inc.

8. *Laminar Flow Elements: Installation and Operation Instructions.* File No. 501:440-10. http://www.meriam.com/downloads/pdf/Manuals/lfe_manual.pdf. (8/31/2005)

9. Auld, D.J., K.Srinivas. *Aerodynamics.* 2007. http://www.ae.su.oz.au/aero/contents.html (1/29/2006).

10. Kestin, J., J.H. Whitelaw. 1964. The viscosity of dry and humid air. *International Journal of Heat and Mass Transfer.* 7:1245-1255.

11. ASHRAE. 2001. 2001 ASHRAE Handbook-Fundamentals. Atlanta: American Society of Heating and Refrigerating and Air-Conditioning Engineers, Inc.

12. Incropera, Frank P., David P. DeWitt. 2002. Introduction to Heat Transfer, 4th Edition. 2002. New York: John Wiley & Sons, Inc.

13. Still M., H. Venzke, F. Durst, A. Melling. 1998. Influence of humidity on the convective heat transfer from small cylinders. *Experiments in Fluids*. 24:141-150.

14. Heidenreich, Mike. Advanced Heat Transfer LLC. 7/05-1/07. Memphis, Tennessee. (Personal Communication).

15. Winebrenner, Bill. Supervisor, Lab Operations Outokumpu Heatcraft. 4/25/2006. Grenada, Mississippi. (Personal Communication).

16. Wu, Hailing. Advanced Heat Transfer LLC. 7/10/06. Memphis, Tennessee. (Personal Communication).

17. Buckon, Leo J. Technical Services Manager, Meriam Process Technologies. 8/31/2005. Cleveland, Ohio. (Personal Communication).

18. Beckwith, Thomas G., Roy D. Marangoni, John H. Lienhard V. 1993. Mechanical Measurements, 5th Edition. Reading, Massachusetts: Addison-Wesley Publishing Company, Inc.

APPENDIX A

Appendix A contains all AutoCAD prints for the wind tunnel test section and coil encasing and instructions for mounting and installation.

A.1 Construction of the Test Section

The Unit Cell test section (See Fig. 8) was created out of sixteen 1.27 cm (0.50 in.) clear acrylic pieces. The entire modular section measures 58.42 cm (23.00 in.) in length and is divided into three segments; the front, the back and the flange segment. The front segment of the test section is created out of four pieces 22.86 cm (9.00 in.) in length. The back section is created out of two 22.86 cm (9.00 in.) for the top and bottom pieces and two 17.78 cm (7.00 in.) pieces for the sides. The non uniform lengths of the back segment were designed to allow for later insertion of the Unit Cell coil. For both the front and back segments, the acrylic pieces are arranged in a configuration to create a 15.24 cm by 15.24 cm (6.00 in. by 6.00 in.) duct for air flow. In both the front and back segments four 0.15 cm (0.06 in.) pressure taps were drilled in each. All joints permanent joints were bonded and sealed using methanol chloride. For additional support and connection to the rest of the wind tunnel ducting the two segments were fitted with 1.27 cm (0.50 in.) aluminum end plates. Like the other acrylic ducting of the wind tunnel, the end plates were connected to a 2.54 cm (1 in.) square steel tubing structure. This steel assembly separated the front and back segments creating a 17.78 cm (7.00 in.) void in the section. The void is intended to be enclosed by the flange section and the Unit Coil

encasing described below. The flange section is created out of two 24.13 cm by 36.83 cm (9.50 in. by 14.50 in.) acrylic pieces used for the top and bottom. Flange side walls are inserted perpendicular to the duct flow for stability in the flange and to hold insulation for the manifold sections in the Unit Cell coils. A back sealing wall is used for close the final gap between the recessed back side walls and the Unit Cell encasing. This sealing wall can be expanded or reduced depending on the width of the Unit Cell coil's fins. To allow for deconstruction of the flange segment all joints are connected by 10-24 socket head cap screws. The use of screws for construction of the flange segment also allow for redesign of the flange walls which can be increased in height to allow for larger coil manifolds and configurations.

A.2 Construction of the Coil Mounting

Because the Unit Cell coils that are tested are all differently shaped it was necessary top develop a standard coil encasing that could be easily manufactured and fit the Unit Cell test section. The encasing designed and described below took in account for various coil sizes, geometries and flange and manifold configurations. To correctly encase the test coil all any preexisting flanges on the coil are removed and/or sealed behind acrylic sections to prevent heat transfer from flange. The encasings were constructed out of two 1.27 cm (0.50 in.) acrylic pieces used for the top and bottom of the structure. The 1.27 cm (0.50 in.) thickness was found to have more structural stability and sealed much easier in the test section. The sides of the encasing are constructed out of 0.32 cm (0.13 in.) thick acrylic pieces. The encasing is constructed as shown in the drawings in C.3. The coil is recessed from the front of the casing by 3.81 cm (1.50 in.)

for standardizing the coil placement inside each encasing. However if warranted by the larger coil dimensions, sliding the coil forward or backwards in the encasing should have no effect on the tests. The 10.48 cm (4.13 in.) thick section allows the encasing to slide into the place between the front segment and the flange sealing wall of the test section. The height of this section must be at least 15.24 cm (6.00 in.). These dimensions are critical because the securing sealing wall acts almost as a tolerance fit for the coil. Any additional air gaps in this fit can be sealed with vacuum tape. Again this area can be expanded or contracted depending on the coil dimensions, but a new flange sealing wall must be designed and built. Like the test section all acrylic pieces are connected with a small amount of menthol chloride. Manifold areas are then insulated with Great Stuff® expanding foam. To prevent air flow bypass the coils are sealed along the coil/acrylic joints. Additionally any gaps along the outside edges due to the coil construction are also sealed. Due to non standard inlet/outlet tubing diameters in the Unit Cell coils, compression fittings were used to connect the manifolds to the liquid conditioning loop. The sizes of the fittings could easily be changes in the 'T' coupler so that a large variety of tube diameters could be connected.

Coils that do not meet the 15.24 cm by 15.24 cm (6.00 in. by 6.00 in.) coil surface area specifications can also be tested. However coils that are larger than the 15.24 cm by 15.24 cm (6.00 in. by 6.00 in.) section can not currently be tested in the wind tunnel, unless the outlying areas can be insulated from the air stream or the test section/wind tunnel section rebuilt. An inclined angle of 5° or less recommended for changing the dimensions of the coil duct size. This angle will help decrease the effect of the contraction/expansion of the duct dimensions on the pressure drop across the coil.

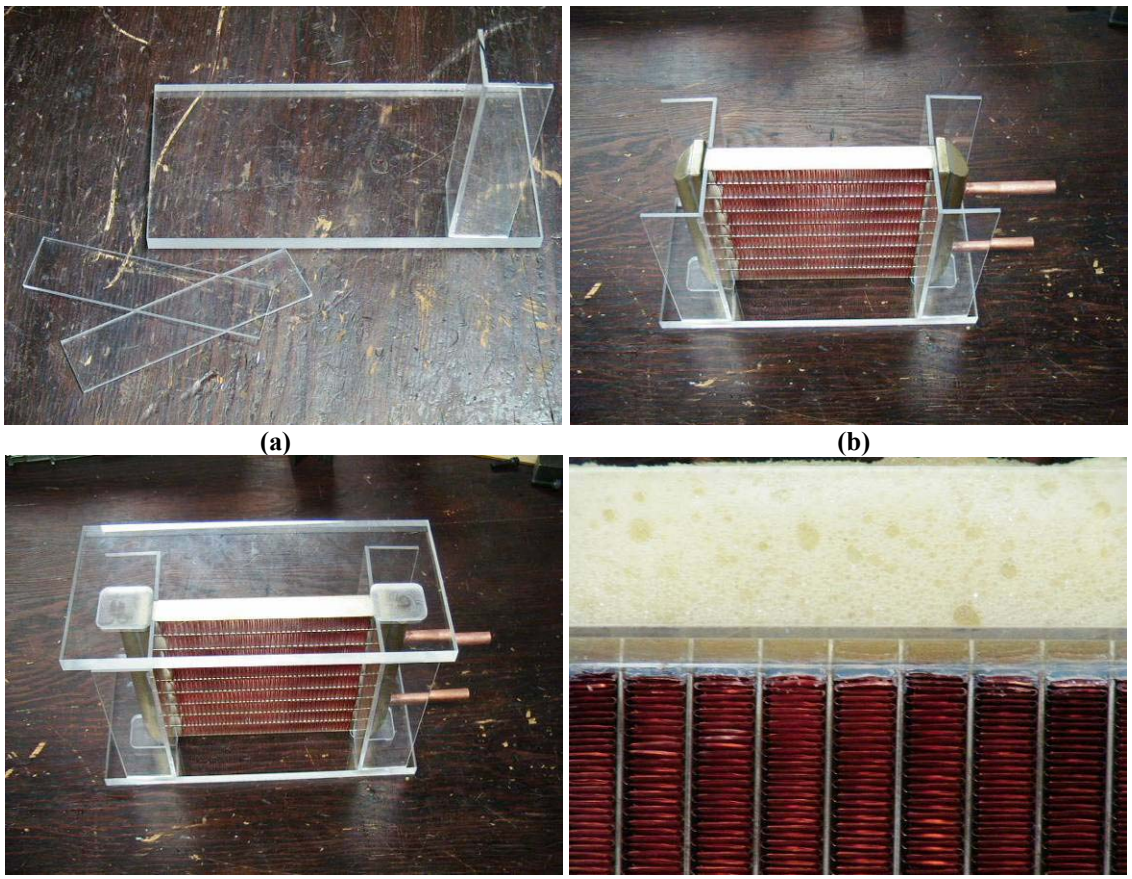

(a) **(b)**

(c) **(d)**

Figure A1. Construction of coil encasing. (a) Encasing is constructed out of 1/2" and 1/8" clear acrylic. (b) Walls are formed out of acrylic surrounding the coil. (c) Top is attached to coil encasing. (d) Coil outlying areas are sealed and insulated.

A.3 Test Section and Supplemental Drawings

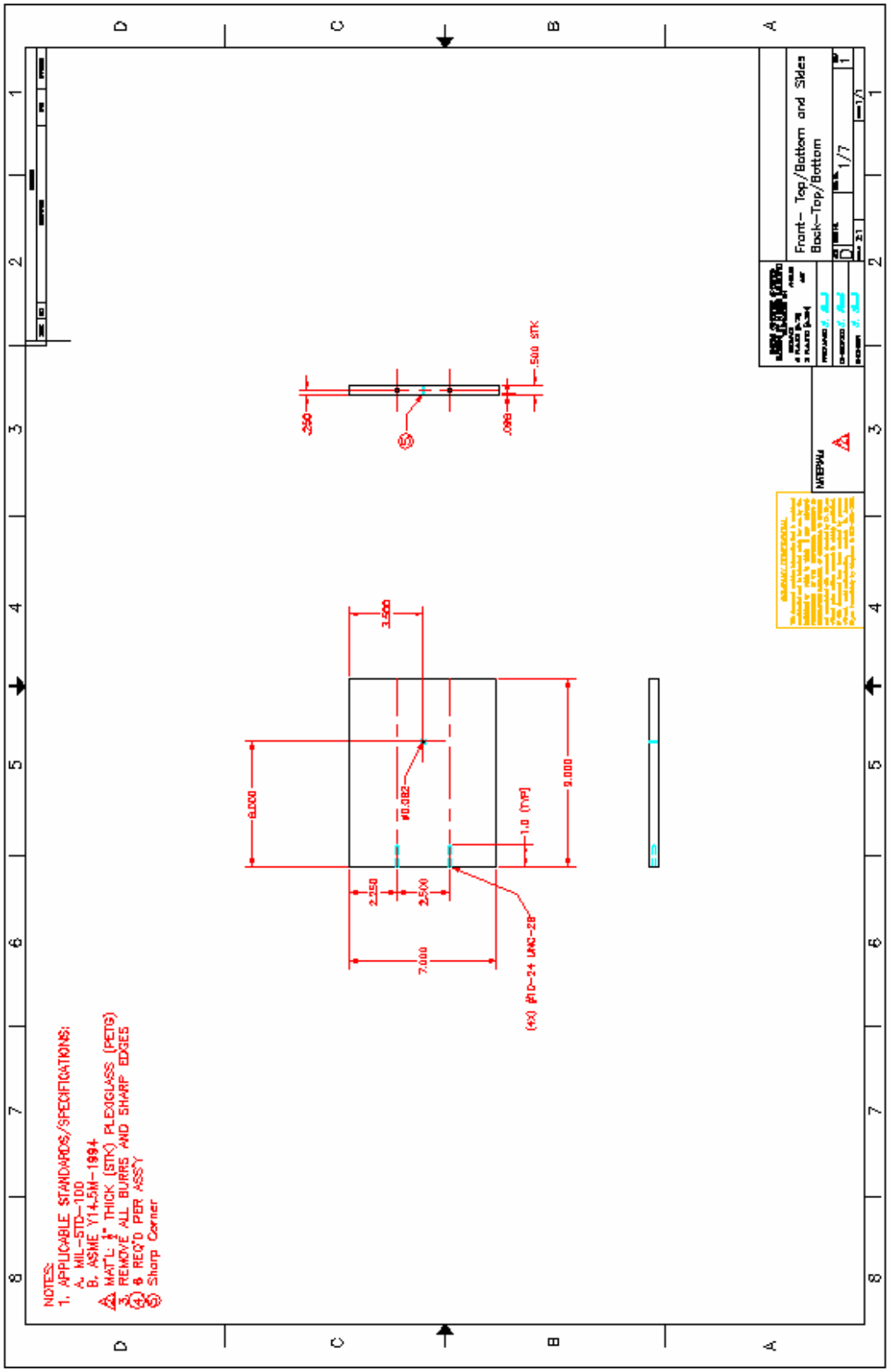

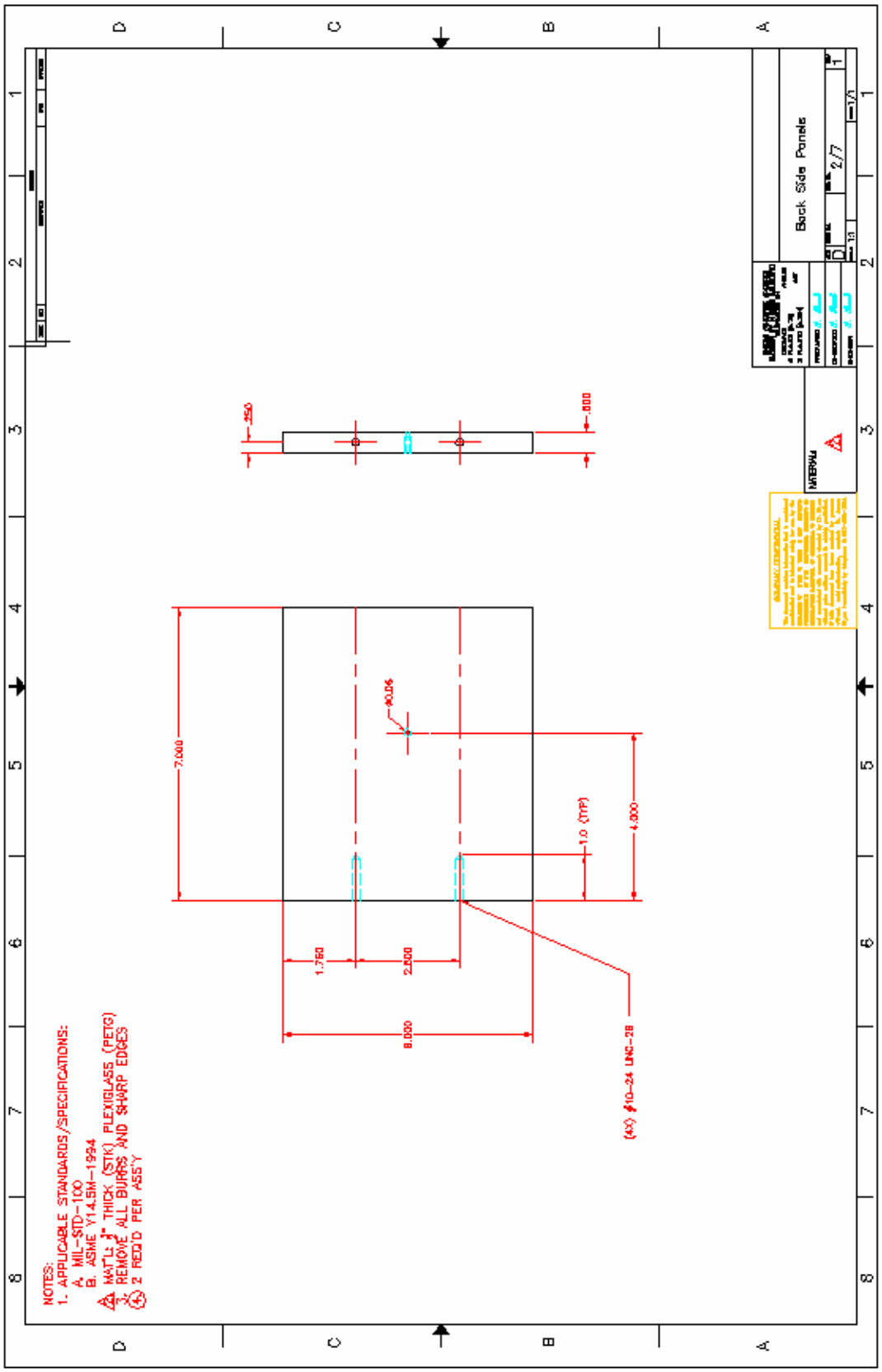
Back Side Panels
NOTES:
1. APPLICABLE STANDARDS/SPECIFICATIONS:
A. MIL-STD-100
B. ASME Y14.5M-1994
MAT'L: 1/4" THICK (STK) PLEXIGLASS (PETG)
REMOVE ALL BURRS AND SHARP EDGES
2 REQ'D PER ASS'Y
7.000
4.000
1.0 (TYP)
1.750
2.500
8.000
(4X) #10-24 UNC-2B

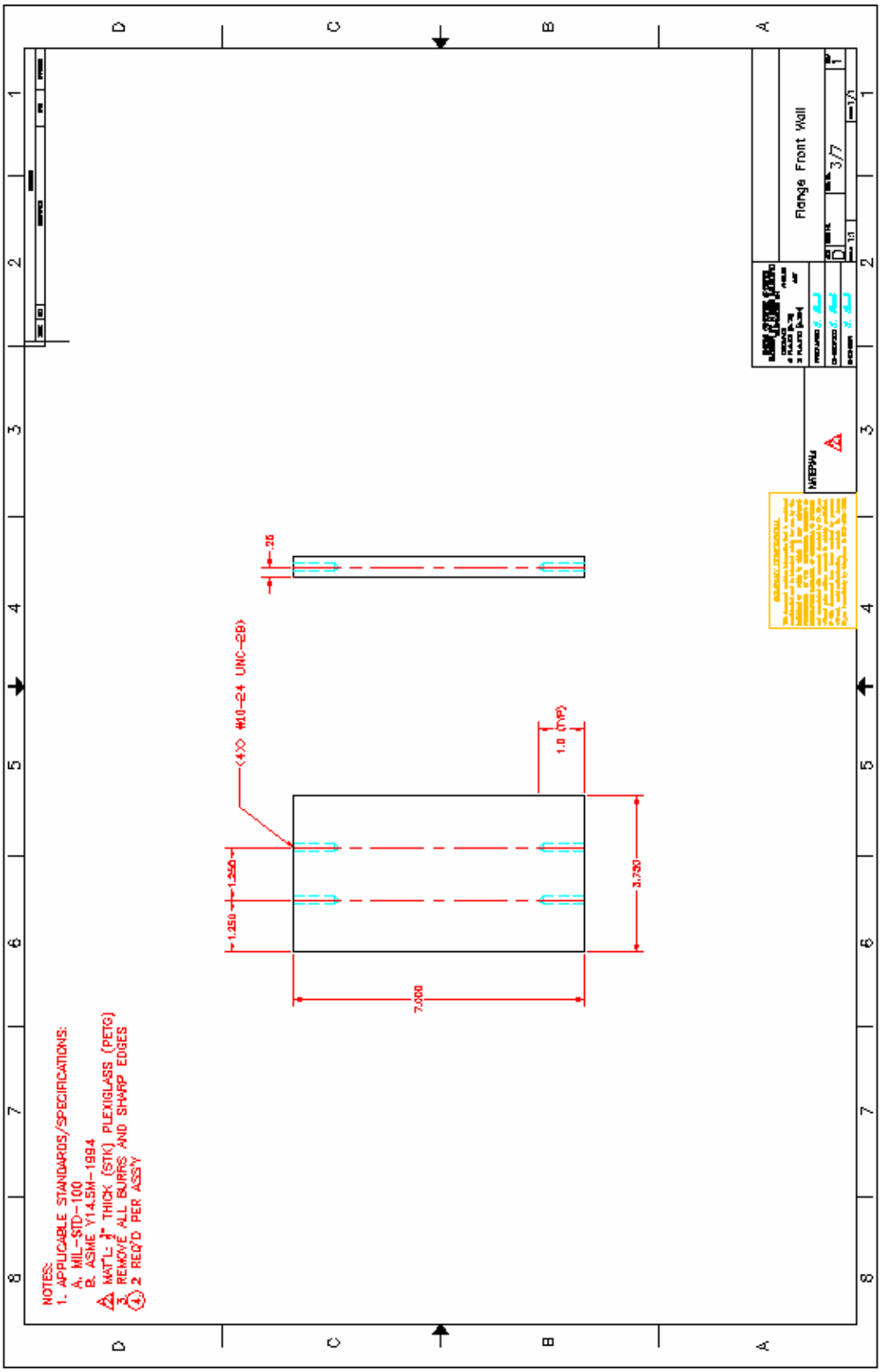
Flange Front Wall
3/7
NOTES:
1. APPLICABLE STANDARDS/SPECIFICATIONS:
A. MIL-STD-100
B. ASME Y14.5M-1994
2. MATL: ¼" THICK (STK) PLEXIGLASS (PETG)
3. REMOVE ALL BURRS AND SHARP EDGES
4. 2 REQ'D PER ASSY
(4X) #10-24 UNC-2B
.25
1.0 (TYP)
1.250
1.250
3.750
7.000

NOTES:
1. APPLICABLE STANDARDS/SPECIFICATIONS:
   A. MIL-STD-100
   B. ASME Y14.5M-1994
2. MAT'L: ¼" THICK (STK) PLEXIGLASS (PETG)
3. REMOVE ALL BURRS AND SHARP EDGES
4. 2 REQ'D PER ASS'Y

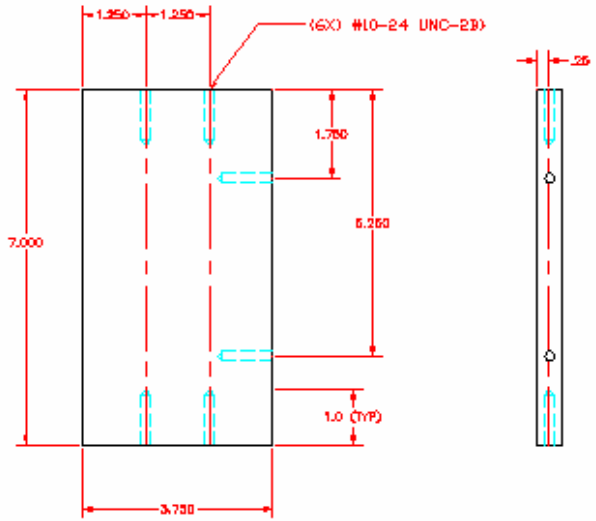

Flange Back Wall

4/7

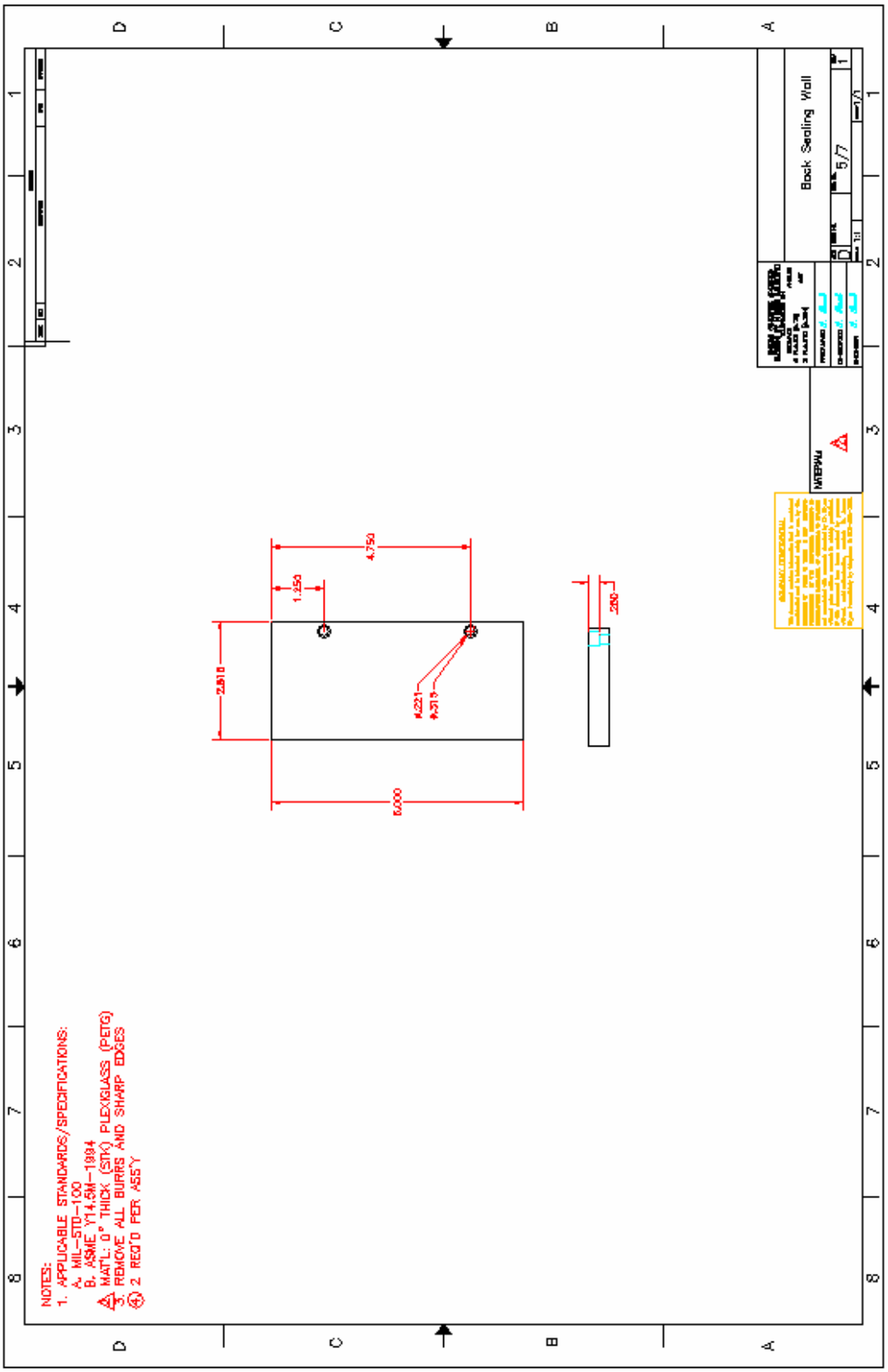
NOTES:
1. APPLICABLE STANDARDS/SPECIFICATIONS:
A. MIL-STD-100
B. ASME Y14.5M-1994
3. MAT'L: 0° THICK (STK) PLEXIGLASS (PETG)
5. REMOVE ALL BURRS AND SHARP EDGES
4 2 REQ'D PER ASS'Y
4.750
1.250
2.510
6.000
.250
Back Sealing Wall
5/7

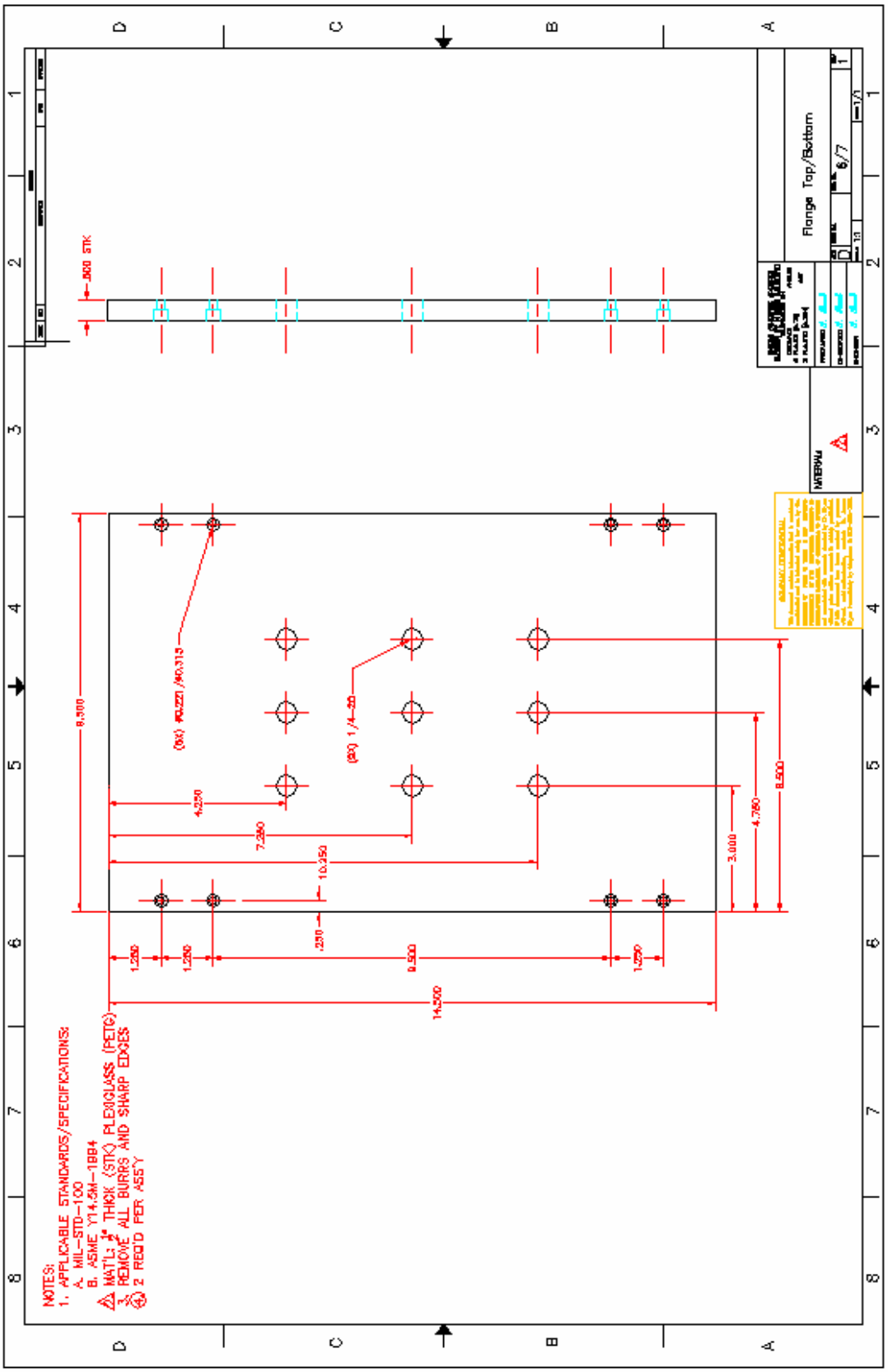
Flange Top/Bottom
NOTES:
1. APPLICABLE STANDARDS/SPECIFICATIONS:
A. MIL-STD-100
B. ASME Y14.5M-1994
2. MAT'L: 1/4" THICK (STK) PLEXIGLASS (PETG)
3. REMOVE ALL BURRS AND SHARP EDGES
4. 2 REQ'D PER ASS'Y

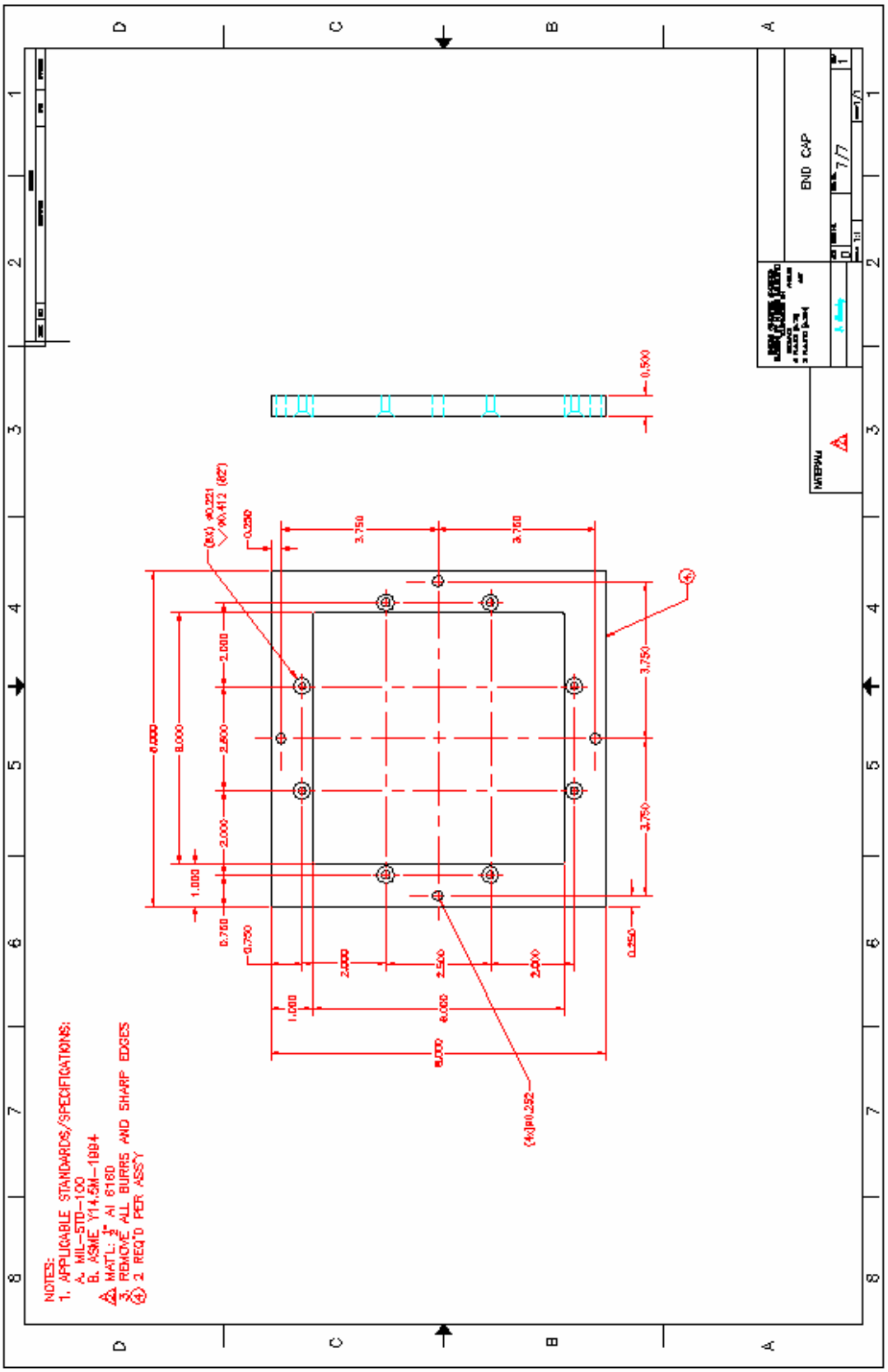
END CAP
NOTES:
1. APPLICABLE STANDARDS/SPECIFICATIONS:
A. MIL-STD-100
B. ASME Y14.5M-1994
2. MATL: ½" Al 6160
3. REMOVE ALL BURRS AND SHARP EDGES
4. 2 REQ'D PER ASSY

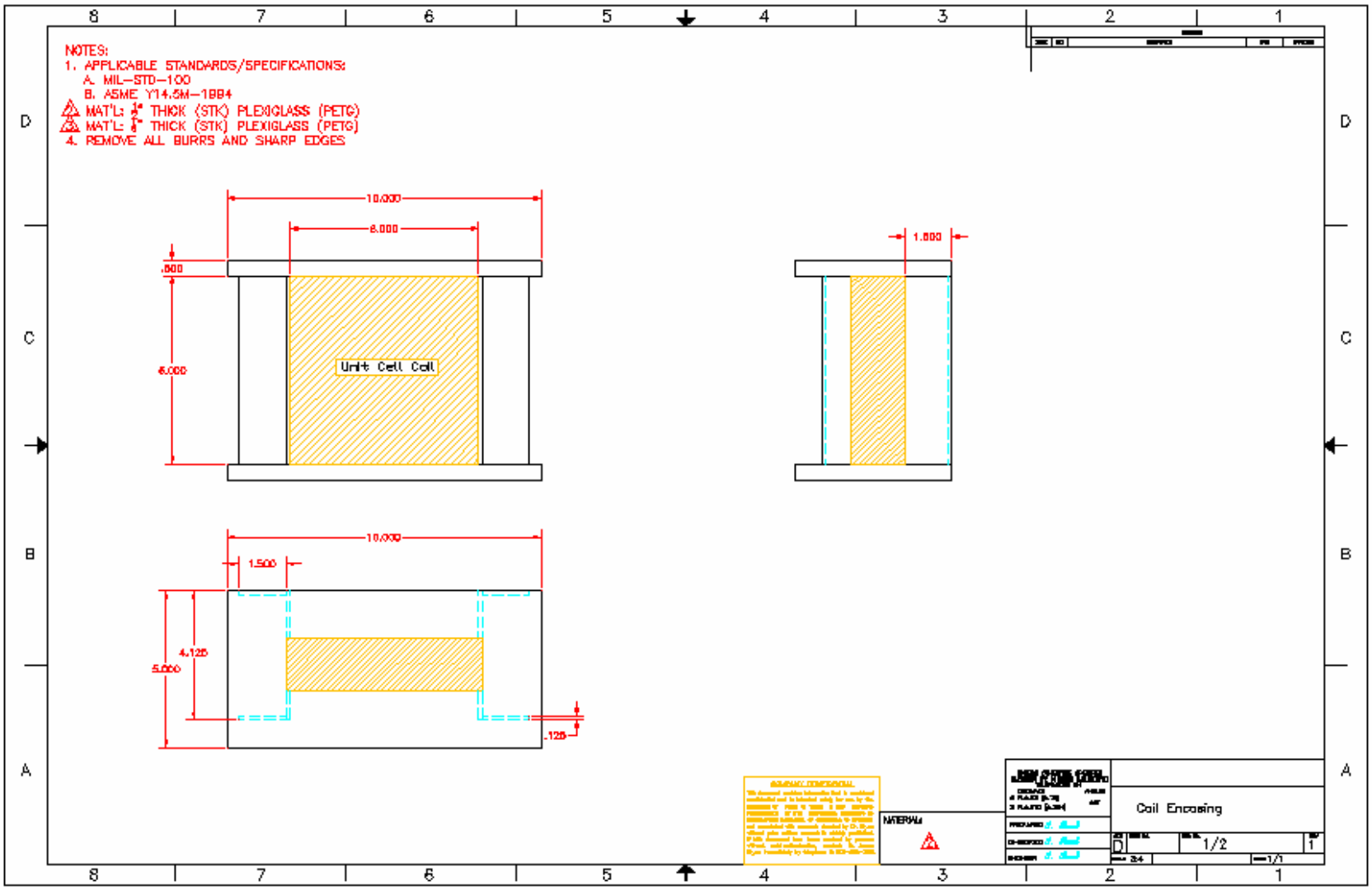
NOTES:
1. APPLICABLE STANDARDS/SPECIFICATIONS:
A. MIL-STD-100
B. ASME Y14.5M-1994
MAT'L: 1/4" THICK (STK) PLEXIGLASS (PETG)
MAT'L: 1/8" THICK (STK) PLEXIGLASS (PETG)
4. REMOVE ALL BURRS AND SHARP EDGES
10.000
8.000
.500
5.000
Unit Cell Coil
1.000
10.000
1.500
4.125
5.000
.125
Coil Encasing
1/2

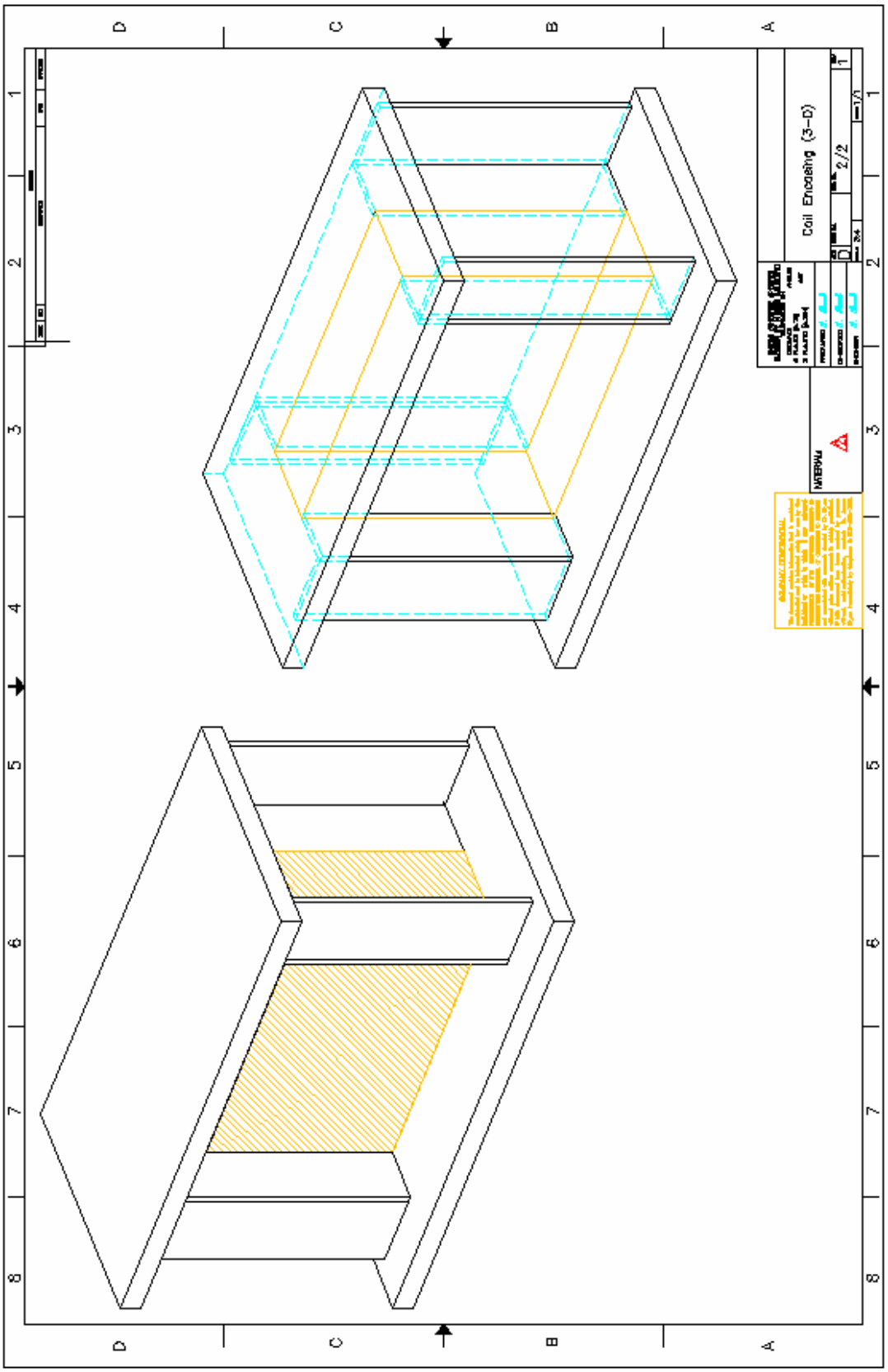
Coil Enclosing (3-D)
2/2
MATERIAL

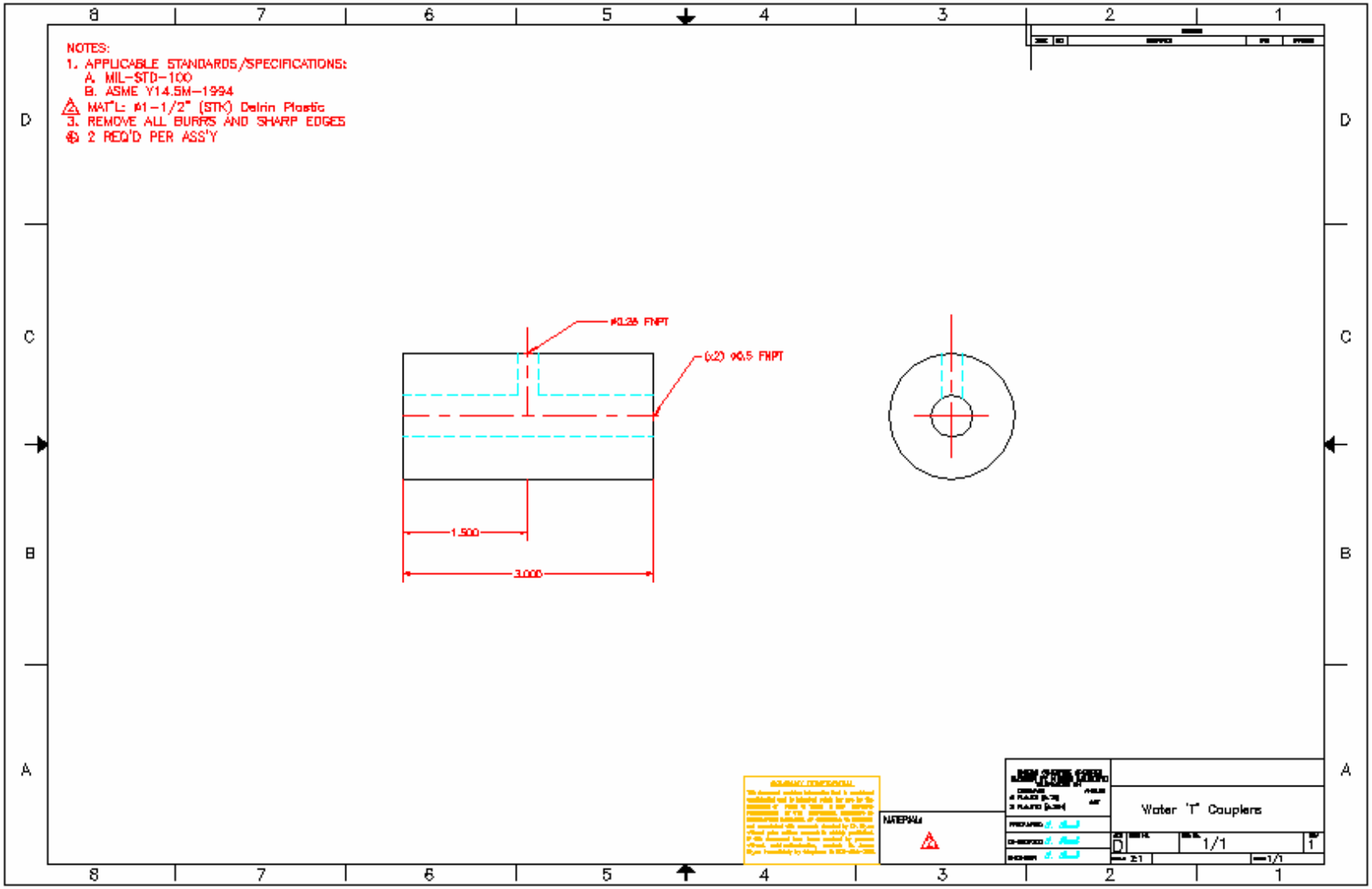
NOTES:
1. APPLICABLE STANDARDS/SPECIFICATIONS:
A. MIL-STD-100
B. ASME Y14.5M-1994
2. MAT'L: ø1-1/2" (STK) Delrin Plastic
3. REMOVE ALL BURRS AND SHARP EDGES
4. 2 REQ'D PER ASS'Y
ø0.25 FNPT
(x2) ø0.5 FNPT
1.500
3.000
Water 'T' Couplers
1/1

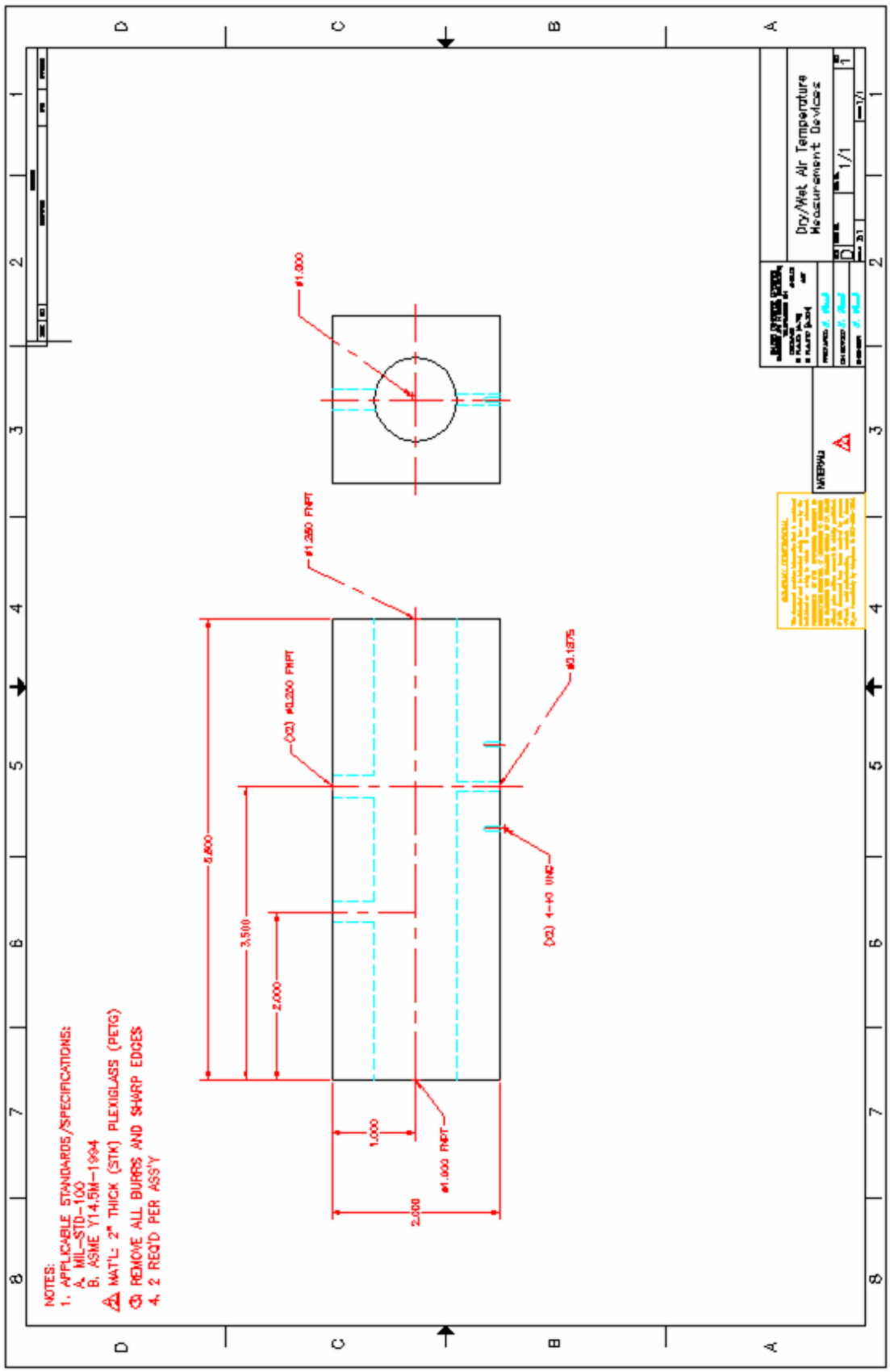
Dry/Wet Air Temperature Measurement Devices
NOTES:
1. APPLICABLE STANDARDS/SPECIFICATIONS:
A. MIL-STD-100
B. ASME Y14.5M-1994
2. MAT'L: 2" THICK (STK) PLEXIGLASS (PETG)
3. REMOVE ALL BURRS AND SHARP EDGES
4. 2 REQ'D PER ASS'Y
5.500
3.500
2.000
1.000
2.000
(02) #0.1875
(02) 4-40 UNC

APPENDIX B

B.1 Calibration Curves

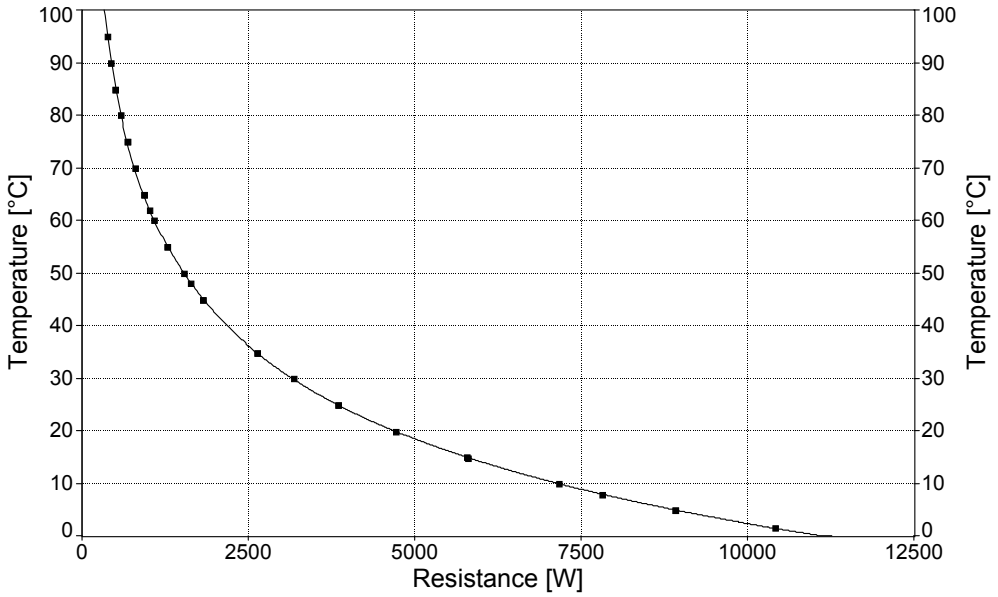

Fig. B1. Calibration curve for thermistor liquid temperature measurement at inlet of Unit Cell coil, Thermistor 03.

Curve fit results:

$$T_{H_2O,in} = 113.71108 - 0.00071546492R_x - 1.8597361\ln(R_x)^2 + 0.46008194R_x^{1/2} + \frac{763.80718}{R_x^{1/2}}, [°C] \quad \text{(B1)}$$

$r^2 = 0.99999943$, Fit Error = ±0.023139307 °C

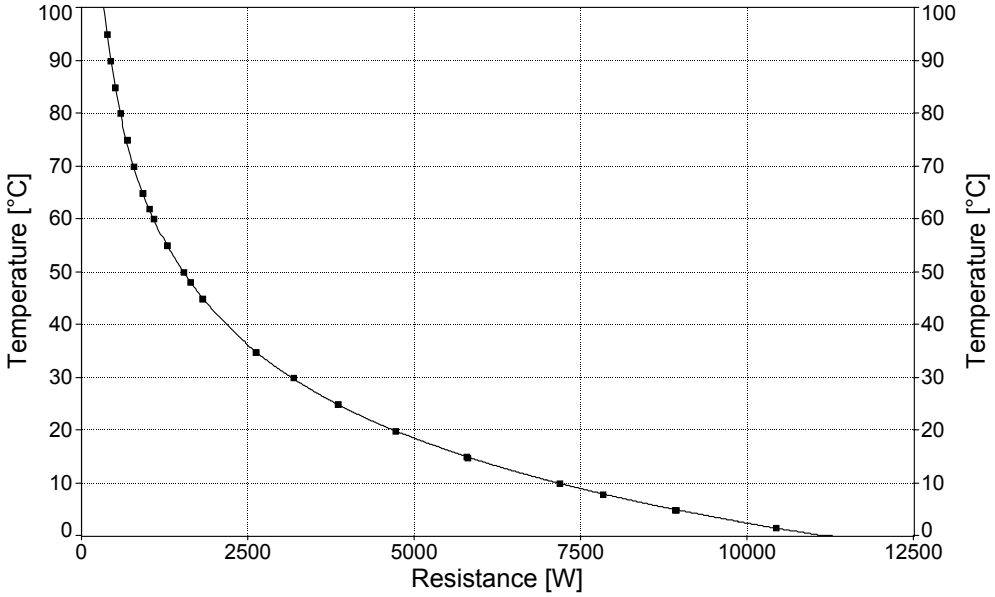

Fig. B2. Calibration curve for thermistor liquid temperature measurement at outlet of Unit Cell coil, Thermistor 02.

Curve fit results:

$$T_{H_2O,out} = 113.47824 - 0.00069285596R_x - 1.8502718\ln(R_x)^2 + 0.4528775R_x^{1/2} + \frac{759.64283}{R_x^{1/2}}, [°C] \quad \text{(B2)}$$

$r^2 = 0.99999931$, Fit Error = ±0.024140901°C

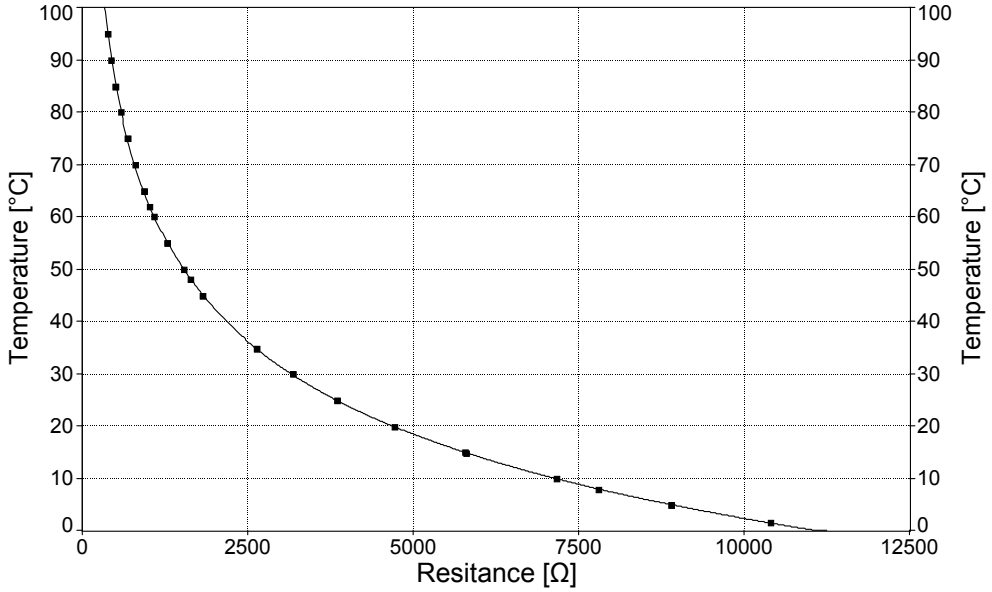

Fig. B3. Calibration curve for thermistor dry bulb temperature measurement at entrance of Unit Cell coil, Thermistor 05.

Curve fit results:

$$T_{db,in} = 113.58891 - 0.00072555816R_x - 1.8607934\ln(R_x)^2 + 0.46242089R_x^{1/2} + \frac{767.83469}{R_x^{1/2}}, [°C] \quad \text{(B3)}$$

$r^2 = 0.99999959$, Fit Error = ±0.019533228°C

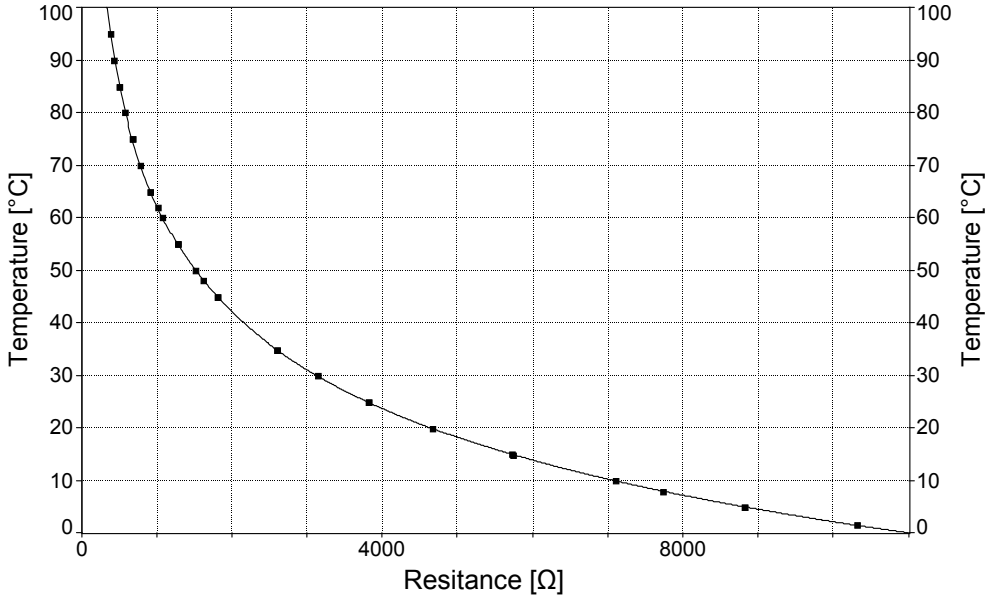

Fig. B4. Calibration curve for thermistor wet bulb temperature measurement at entrance of Unit Cell coil, Thermistor 13.

Curve fit results:

$$T_{wb,in} = 114.55212 - 0.00077249748R_x - 1.8881801\ln(R_x)^2 + 0.48083624R_x^{1/2} + \frac{746.67237}{R_x^{1/2}}, [°C] \quad \text{(B4)}$$

$r^2 = 0.99999946$, Fit Error = ±0.02243783°C

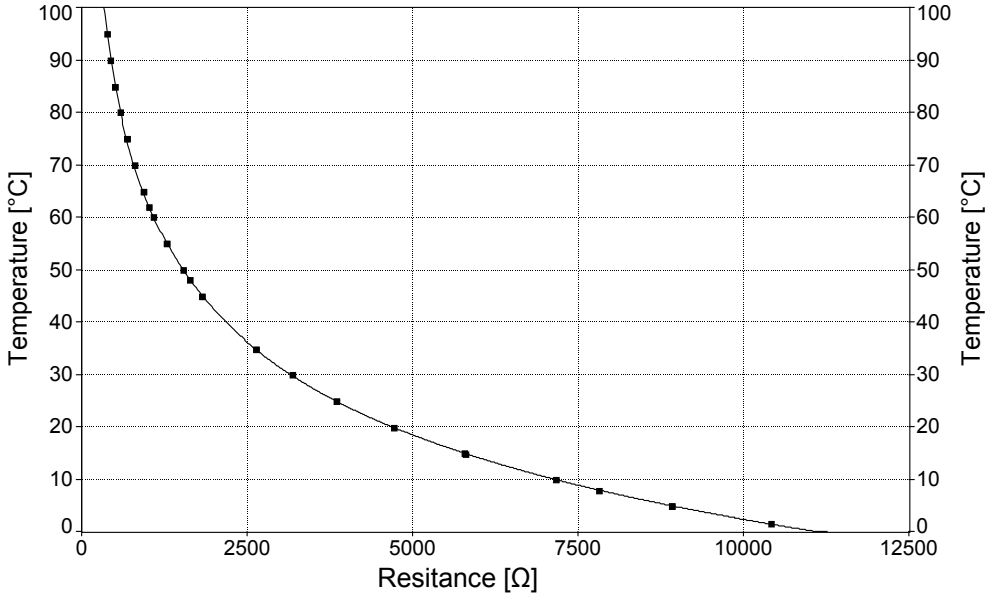

Fig. B5. Calibration curve for thermistor dry bulb temperature measurement at exit of Unit Cell coil, Thermistor 12.

Curve fit results:

$$T_{db,out} = 113.77966 - 0.00072733091 R_x - 1.863571 \ln(R_x)^2 + 0.46384128 R_x^{1/2} + \frac{763.83747}{R_x^{1/2}}, [°C] \quad \text{(B5)}$$

$r^2 = 0.99999951$, Fit Error = ±0.021404824°C

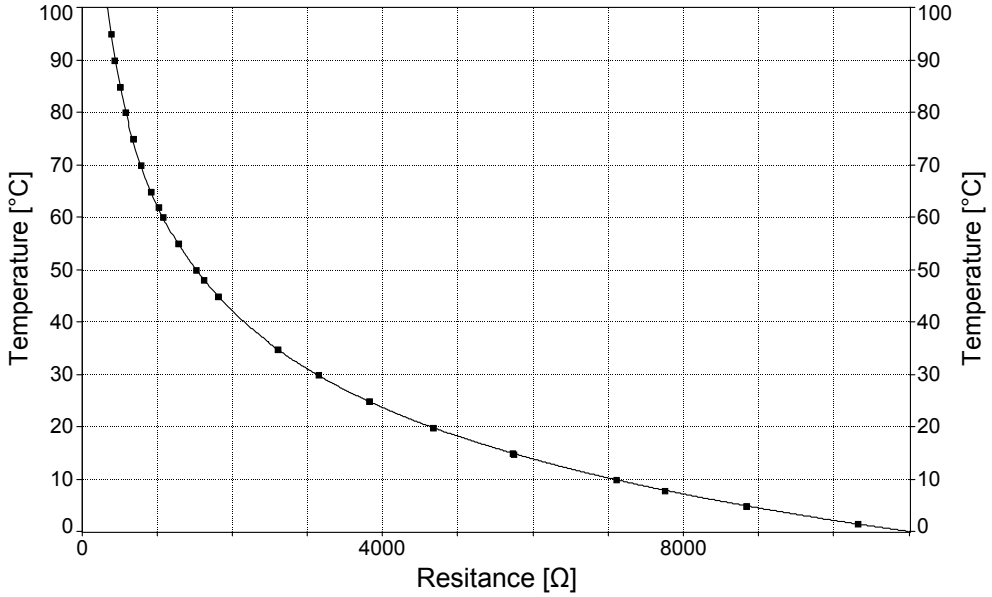

Fig. B6. Calibration curve for thermistor wet bulb temperature measurement at exit of Unit Cell coil, Thermistor 11.

Curve fit results:

$$T_{wb,out} = 111.54607 - 0.000631955R_x - 1.8094344\ln(R_x)^2 + 0.42788409R_x^{1/2} + \frac{771.02275}{R_x^{1/2}}, [°C] \quad \text{(B6)}$$

$r^2 = 0.99999964$, Fit Error = ±0.018255735°C

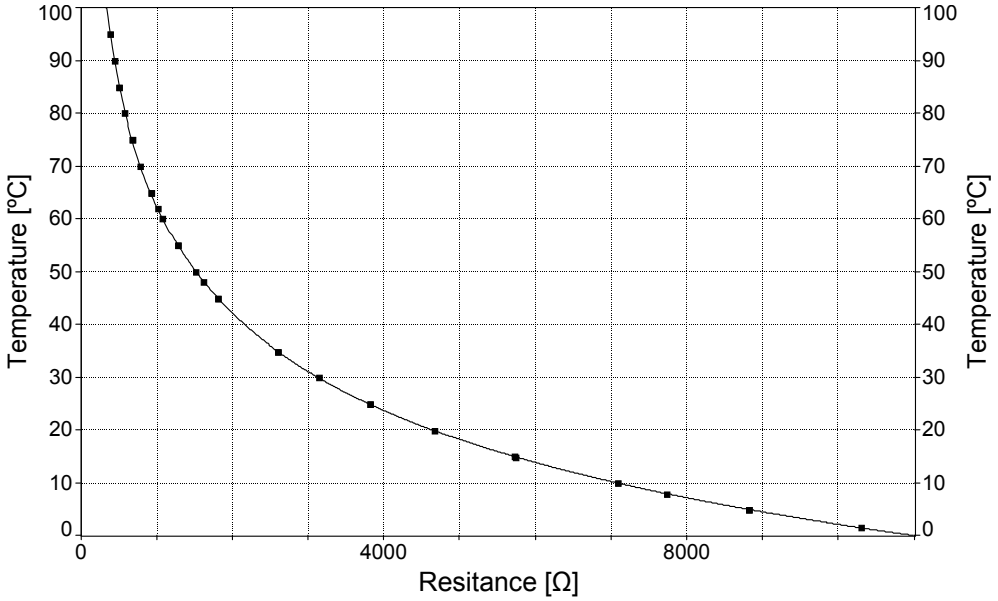

Fig. B7. Calibration curve for thermistor dry bulb temperature measurement at exit of LFE, Thermistor 07.

Curve fit results:

$$T_{db,LFE} = 114.66075 - 0.00077512961R_x - 1.8919729\ln(R_x)^2 + 0.48273276R_x^{1/2} + \frac{749.59643}{R_x^{1/2}}, [°C] \quad \text{(B7)}$$

$r^2 = 0.99999953$, Fit Error = ±0.020964312°C

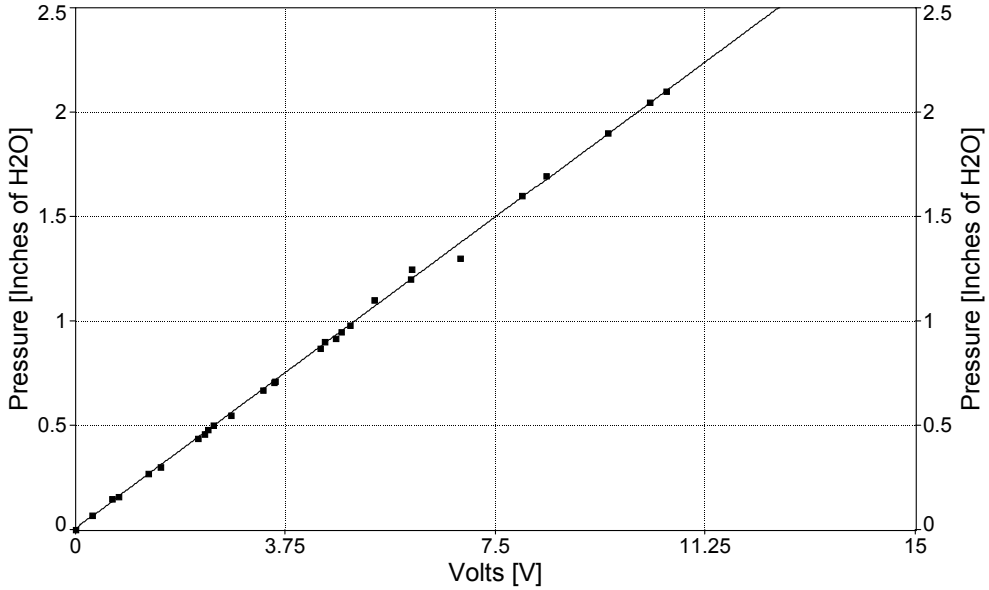

Fig. B8. Calibration curve for high pressure transducer across Unit Cell coil.

Curve fit results:

$$\Delta P_{high} = 0.0067979735 + 0.1987901 V_x, \left[\text{inches of } H_2O\right] \tag{B8}$$

$r^2 = 0.9991105$, Fit Error = ± 0.018731318 inches of H_2O

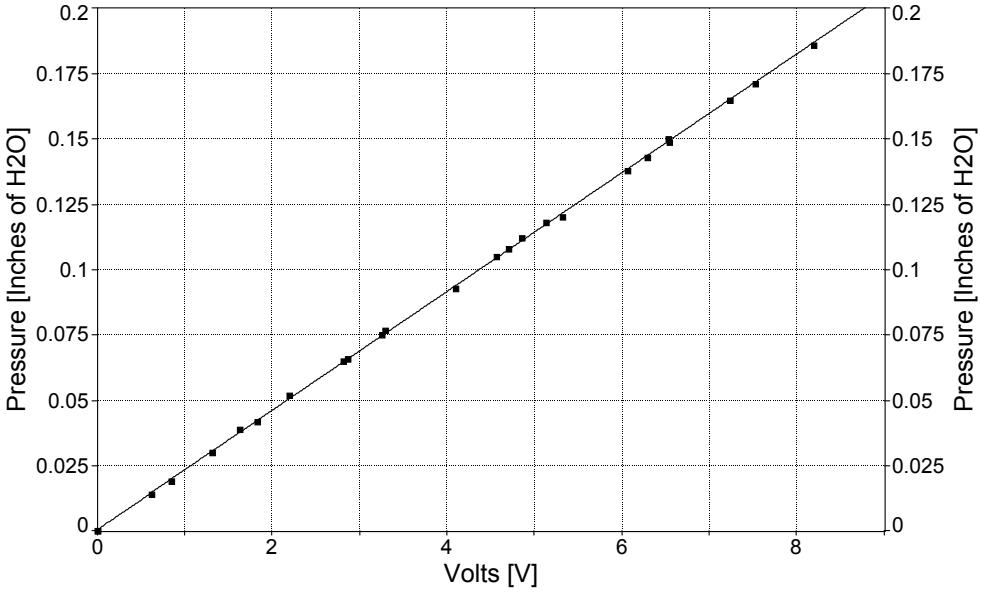

Fig. B9. Calibration curve for low pressure transducer across Unit Cell coil.

Curve fit results:

$$\Delta P_{low} = 0.00060798952 + 0.022712102 V_x, \left[\text{inches of } H_2O\right] \tag{B9}$$

$r^2 = 0.99978336,$ Fit Error = ± 0.00086336154 inches of H_2O

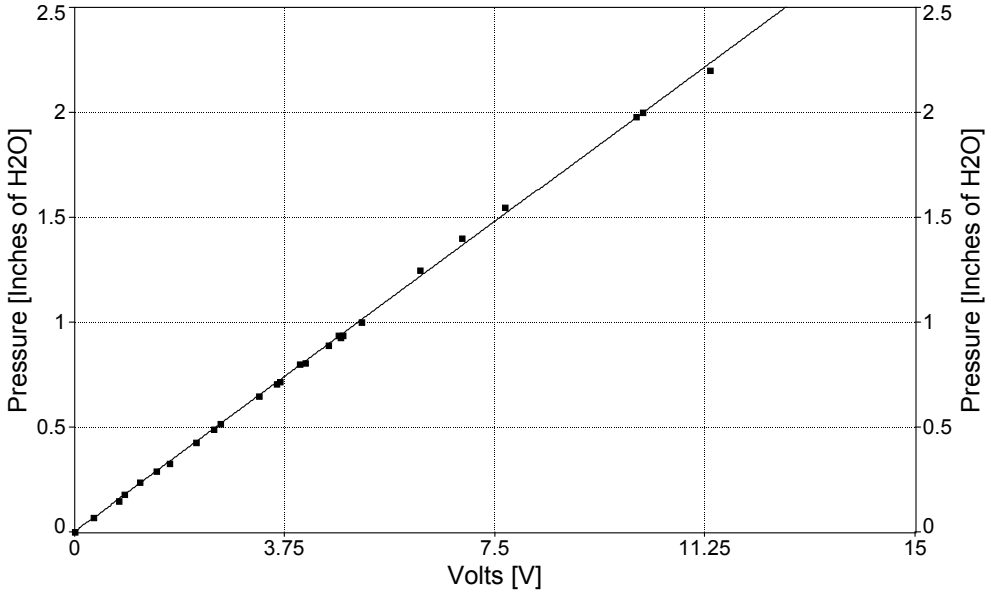

Fig. B10. Calibration curve for pressure transducer across the LFE.

Curve fit results:

$$\Delta P_{LFE} = 0.002012748 + 0.19710571 V_x, \left[\text{inches of } H_2O\right] \quad \text{(B10)}$$

$$r^2 = 0.99946949, \qquad \text{Fit Error} = \pm 0.01456268 \text{ inches of } H_2O$$

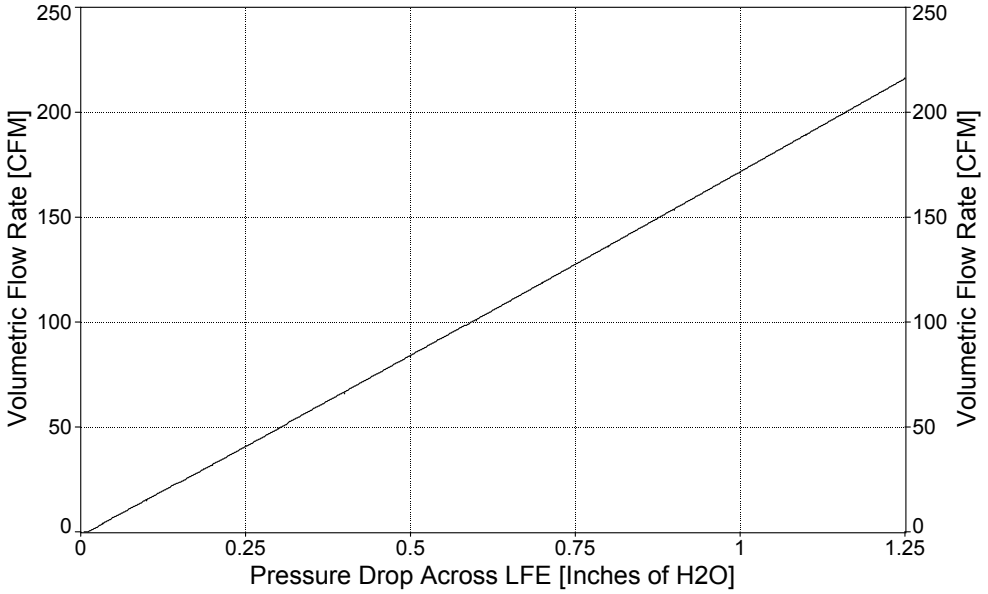

Fig. B11. Calibration curve for LFE with respect to pressure drop.

Curve fit results:

$$\dot{V}_{uncorrected} = -1.605079 + 168.6945\Delta P_{LFE} + 5.7677054\Delta P_{LFE}{}^{2} - 0.9937183\Delta P_{LFE}{}^{3}, \left[\mathrm{m}^3/\mathrm{s}\right], [17] \quad \text{(B11)}$$

$$\text{Instrument Bias} = \pm 0.0086 \times \dot{V}_{uncorrected}\ \mathrm{m}^3/\mathrm{s}$$

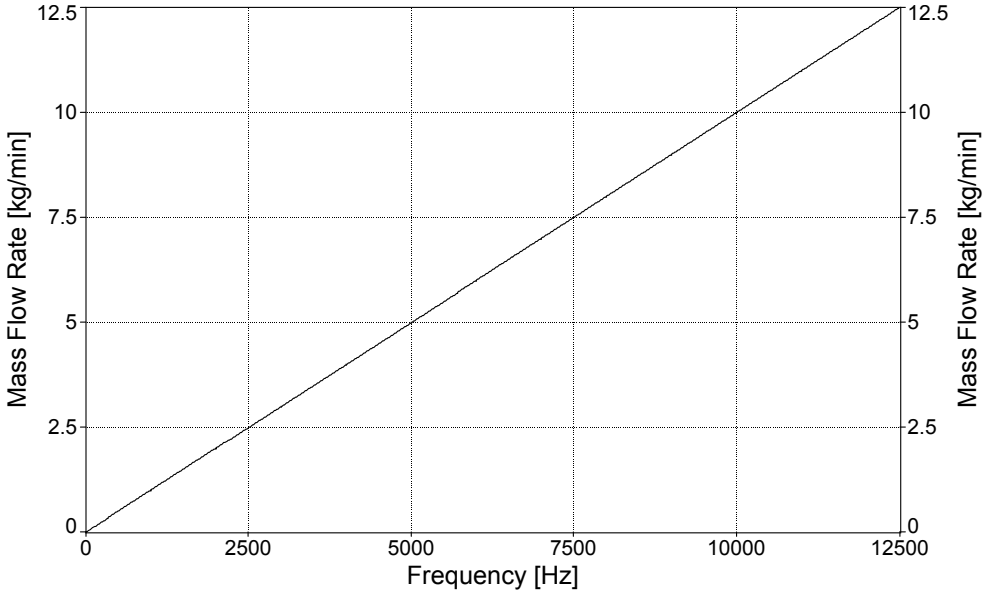

Fig. B12. Calibration curve for Micromotion flowmeter with respect to frequency.

Curve fit results:

$$\dot{m}_{H_2O} = 0.01\omega, \left[\text{kg/min}\right] \tag{B12}$$

$$\text{Instrument Bias} = \pm 0.0023 \times \dot{m}_{H_2O} \text{ kg/min}$$

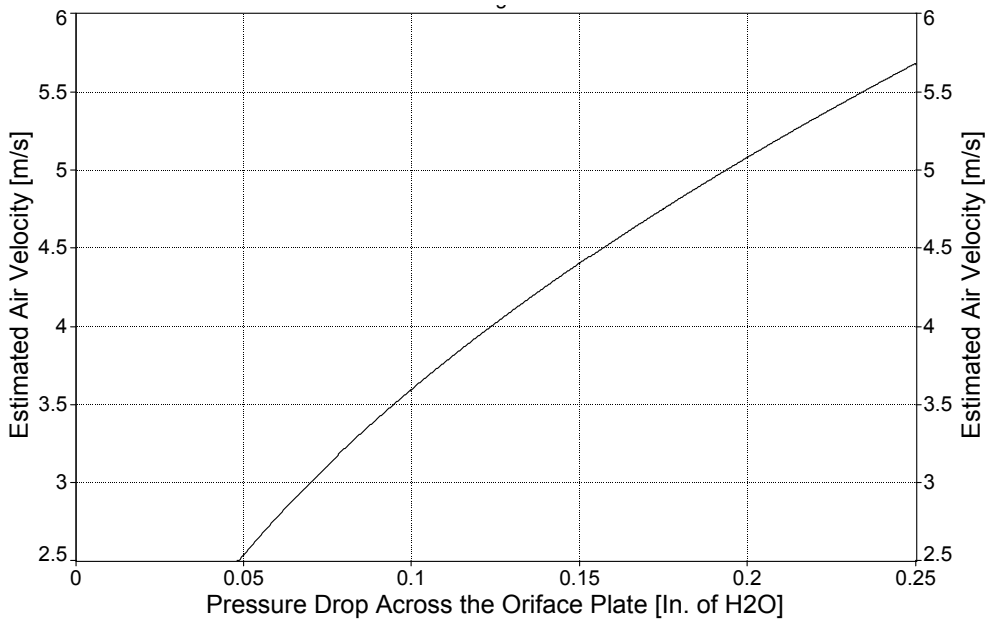

Fig. B13. Calibration curve for air regualtion oriface plates with respect to pressure drop.

Curve fit results:

$$\vec{v} = 11.3655\Delta P^{0.4998}, \left[\mathrm{m}^3/\mathrm{s}\right] \tag{B13}$$

B.2 Sample Uncertainty Calculation

The following is a sample uncertainty calculation for the inlet dry-bulb air temperature across the Unit Cell coil. The conditions for this test have moist air flowing with an actual face velocity of 1.5 m/s and an inlet air temperature of $T_{db,in}$=26.6 °C and $T_{in,wet}$=25.0 °C. Water, used as the liquid, flows through a copper coil at 4.5 kg/min with an inlet temperature of 82.2 °C.

To find the overall uncertainty for the inlet dry bulb temperature, the uncertainty in the thermistor resistance measurements from the DMM first must be calculated. Because the instrumentation was calibrated in place, there is no bias limit associated with the Keithley DMM in the readings, therefore only the precision limits are important. The precision limits associated with the DMM are calculated using the standard deviation of

the reading and confidence interval of 95%. A total of 99 resistance measurements give an average of 3602.398 Ω and standard a standard deviation of 2.492 Ω. Therefore, the precision limit can be calculated by,

$$P_{\text{DMM}} = \frac{\sigma_{\text{std}}}{\sqrt{n}} t_{v,95} = \frac{2.492}{\sqrt{99}}(1.96) = 0.491\,\Omega \tag{B14}$$

where n is the number of samples, σ_{std} is the measurement standard deviation, and $t_{v,95}$ is the t-distribution value at a 95% confidence interval. The degrees of freedom, v, for the t-distribution is calculated by

$$\nu = n - 1. \tag{A15}$$

From the t-distribution table in Mechanical Measurements, 5th Edition, [18] $t_{v,95} = 1.96$. Thus the total uncertainty concerned with the DMM in the calculation of the resistance of the dry bulb thermistor is

$$u_{\text{DMM}} = \sqrt{{P_{\text{DMM}}}^2 + {B_{\text{DMM}}}^2} = \sqrt{(0.491)^2 + (0)^2} = \pm 0.491\,\Omega. \tag{B16}$$

There are two forms of bias associated with the temperature measurement, the bias in the thermistors and the bias of the calibration instrument. For the inlet dry bulb temperature measurement these two biased limits are,

$$B_{\text{Instrument}} = 0.025°\text{C} \text{ and } B_{\text{Calibration}} = 0.0005°\text{C}. \tag{B17}$$

The two precision limits for the temperature uncertainty are the precision of the resistance measurement and the precision of the calibration curve. The precision in the resistance measurement can be calculated by,

$$P_{\text{Metric}} = \frac{\partial T_{db,in}}{\partial R_x} u_{\text{DMM}} = -0.007(0.491) = -0.001°\text{C} \tag{B18}$$

where $\frac{\partial T_{db,in}}{\partial R_x}$ is the partial derivative of Eq. (B3) with respect to resistance. The precision of the calibration curve is based upon the Standard Fit Error of the calibration curve, which is $\delta_{\text{STD Fit}} = \pm 0.019533228°\text{C}$ for the dry-bulb thermistor. Since 32 samples were taken during the calibration process the *v* for the calibration precision is 31. The overall calibration precision can be calculated by,

$$P_{\text{Calibration}} = \delta_{\text{STD Fit}}\left(t_{v,95}\right) = 0.0195(1.96) = 0.038°\text{C} \tag{B19}$$

where again $t_{v,95} = 1.96$. Finally the overall uncertainty for the inlet dry bulb temperature is

$$u_{\text{T}_{\text{db,in}}} = \sqrt{B_{\text{Instrument}}{}^2 + B_{\text{Calibration}}{}^2 + P_{\text{Calibration}}{}^2 + P_{\text{Metric}}{}^2} = \pm 0.046°\text{C}. \tag{B20}$$

The following is a sample calculation for the total air side heat transfer under the same test conditions as described above. The total air side heat transfer can be calculated using Eq. (2)

$$Q_{air} = \dot{m}_{air}\left(h_{out} - h_{in}\right).$$

Assuming that the uncertainties for the measured quantities were calculated as described above the mass flow rate and enthalpies can be calculated as

$$\begin{aligned} \dot{m}_{air} &= 0.037 \pm 0.001\,\text{kg/s} \\ h_{in} &= 77.185 \pm 0.202\,\text{kJ/kg} \\ h_{out} &= 114.853 \pm 0.445\,\text{kJ/kg}. \end{aligned} \tag{B21}$$

Thus the air side energy transfer is

$$Q_{air} = \dot{m}_{air}\left(h_{out} - h_{in}\right) = 0.037(114.853 - 77.185) = 1409.301\,\text{W}. \tag{B22}$$

To determine the uncertainty for this air side energy transfer measurement the following equation must be used:

$$u_{Q_{air}} = \sqrt{\left[\left(\frac{\partial Q_{air}}{\partial \dot{m}_{air}}\right)u_{\dot{m}_{air}}\right]^2 + \left[\left(\frac{\partial Q_{air}}{\partial h_{out}}\right)u_{h_{out}}\right]^2 + \left[\left(\frac{\partial Q_{air}}{\partial h_{in}}\right)u_{h_{in}}\right]^2}\,. \tag{B23}$$

where u_x represents the uncertainty of each measurement and the partial derivative of each is calculated

$$\frac{\partial Q_{air}}{\partial \dot{m}_{air}} = h_{out} - h_{in} = 37667.9\ \text{J/kg}\,, \tag{B24}$$

$$\frac{\partial Q_{air}}{\partial h_{out}} = \dot{m}_{air} = 0.0374\ \text{kg/s}\,, \tag{B25}$$

and

$$\frac{\partial Q_{air}}{\partial h_{in}} = -\dot{m}_{air} = -0.0374\ \text{kg/s}\,. \tag{B26}$$

Thus the total uncertainty of the air side energy transfer is calculated by,

$$\begin{aligned} u_{Q_{air}} &= \sqrt{\left[(37667.9)0.001\right]^2 + \left[(0.0374)219.133\right]^2 + \left[(-0.0374)202.049\right]^2}\,. \\ &= \pm 30.866\ \text{W} \end{aligned} \tag{B27}$$

APPENDIX C

Appendix C contains detailed calibration and test procedures used in testing the Unit Cell coil.

C.1 Calibration of Thermistors

For accurate temperature measurements for energy balance calculations test coil the thermistors which supply this data must be properly calibrated. The procedure for each pressure transducer calibration is described below.

1) Ensure that the wind tunnel Model 7701 card is inserted in card slot #2. Power up the DAQ. The DAQ needs to be on for at least four hours to achieve thermal equilibrium before use.
2) Power up the computer and open *TunnelSystem 3.4.xls*. This spreadsheet was developed with ExcelLink capabilities to perform the data collection. During calibration only the **DMM Scan** page is needed.
3) Submerge the thermistor probe tips into a temperature controlled water bath. For this system the Neslab RTE-111 was used as the temperature bath.
4) Next set up the Kaye® Model M2801 Intelligent reference RTD so that the tip of the sensor is completely submerged into the bath.
5) Set the bath to the desired starting temperature.
6) Use the DMM to record at a total 35 of readings for each thermistor at the given temperature.
7) Record the IRTD reference temperature in a .txt file to as it changes with time. The variation in the water temperature is typically less than 0.01˚C at each temperature interval.
8) Average the DMM resistance readings for each thermistor and reference them to the average IRTD temperature.
9) Complete up and down the temperature scale, and then take random points to have a full scale temperature range. For standard calibration the water temperature was varied from 1.5 to 95 ˚C at increments of 5 ˚C.
10) Using 2-D Table Curve Software, curve fit each thermistor's resistance with the IRTD temperature measurement in the form of,

$$T = a + bR_x + c\ln(R_x)^2 + dR_x^{1/2} + \frac{e}{R_x^{1/2}}$$

where where T is the tempeature in ˚C, R_x is the measures resistance, and a, b, c, d, and e are constants.
11) Calculate the calibration constants and standard fit error, for use in data reduction and uncertainty measurements. The results of the thermistor calibrations can be seen in Appendix B.

Fig. C1. Calibration of Thermistors using Kaye Intelligent RTD Temperature Probe.

C.2 Calibration of Pressure Transducers

For accurate flow measurements with the LFE and pressure drop measurements across the test coil the pressure transducers which supply this data must be properly calibrated. The procedure for each pressure transducer calibration is described below.

1) Ensure that the wind tunnel Model 7701 card is inserted in card slot #2. Power up the DAQ. The DAQ needs to be on for at least four hours to achieve thermal equilibrium before use.
2) Power up the computer and open *TunnelSystem 3.4.xls*. This spreadsheet was developed with ExcelLink capabilities to perform the data collection. During calibration only the **DMM Scan** page is needed.
3) The high side of the transducer is connected to the high side of the manometer with rubber tubing, while the low side of the transducer and manometer left open to the ambient air. For the low pressure transducer the high side was connected to a 0-2 in. of H_2O scale manometer, Fig. C2a. For the high pressure and LFE transducer the high side was connected to a 0-5 in. of H_2O scale manometer, Fig C2b.
4) At zero pressure the bypass valve was opened and the zero potentiometer was adjusted to a DMM reading of ±0.01Vdc by turning the demodulator potentiometer clockwise for an increase in output and counter-clockwise for a decrease.
5) Once the DMM reading reads nominally zero, pressure was increased to the full scale pressure by slowly applying pressure with a syringe to the opening low side of the transducer.

6) The bypass valve is quickly closed to maintain pressure on the high side of the transducer and the syringe is removed, opening the low side to ambient.
7) The span potentiometer on the demodulator is adjusted to 10±0.01Vdc.
8) Steps 4-7 repeated until there is no interaction between the adjustments.
9) Again pressurize the system recording the transducer voltage for 35 measurements. Line up your eye with the reflective strip in the Heise gauge and record the current pressure manually into excel.
10) Complete up and down the temperature scale, and then take random points to have a full scale pressure range. The pressure transducer output voltage is averaged and referenced to the manual manometer reading.
11) Using 2-D Table Curve Software, curve fit the transducer's resistance with the manometer pressure measurement in the form of,

$$\Delta P = a + bV_x$$

where ΔP is the pressure difference of the transducer in inches of H_2O, V_x is the transducer output voltage and a and b are constants.
12) Calculate the calibration constants and standard fit error, for use in data reduction and uncertainty measurements. The results of the pressure transducer calibrations can be seen in Appendix B.
13) Repeat this process for all three transducers.

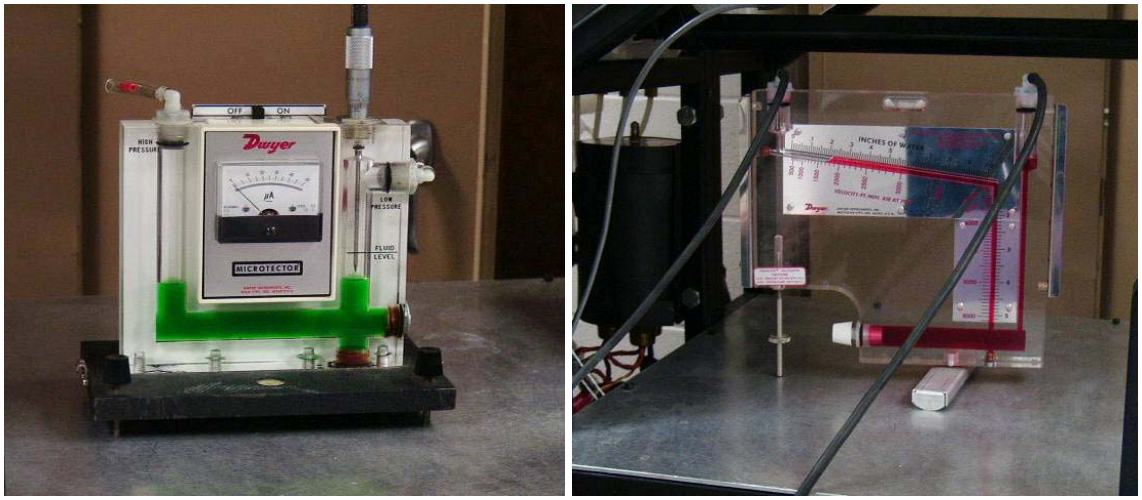

(a) **(b)**

Fig. C2. Manometers used for transducer calibration.
(a) Dwyer Microtector Manometer Model 1430. (b) Dwyer Inclined Manometer Model 421-5.

C.3 Unit Cell Test Procedure

To determine the performance of each Unit Cell coil, tests were performed with the custom built wind tunnel. The procedure for using the wind tunnel and procedure for each Unit Cell test is described below.

1) Begin DAQ collection.

a. Ensure that the wind tunnel Model 7701 card is inserted in card slot #2. Power up the DAQ. The DAQ needs to be on for at least four hours to achieve thermal equilibrium before use.
b. Power up the computer and open *TunnelSystem 3.4.xls*. This spreadsheet was developed with ExcelLink capabilities to perform the data collection. The file consists of five pages the **Test Info**, **DMM Config**, **DMM Scan**, **DATAConv**, and **HUD** all of which are important to the data collection.
    i. **Test Info**. The first page in the *TunnelSystem 3.4.xls* document is the Test Info Page, Fig. C3. This page mostly used for informational purposes and used for test organization. Here the target test parameters can be written. Test type and barometric pressure must be specified
    ii. **DMM Config.** DMM Instrumentation page in which measurement instruments can be added and their measurement settings changed.
    iii. **DATA SCAN.** The Scan page is where the data collection takes place and DMM measurements are originally displayed. Measurement display can also be changed.
    iv. **DATAConv**. Customized page which redisplays DMM measurements and converts the data using calibration equations. When recalibration is preformed calibration and equations need to be changed (columns AI and AJ).
    v. **HUD**. The Heads Up Display page shows the measured data graphically according to time. Convenient for knowing when system reaches steady-state.
c. On the **Test Info** page update coil information and desired wind tunnel conditions. Specify the type of test with an 'X' on either "Zero Test", "Hot Water Test" or "Cold Water Test". Record the barometric pressure and temperature on the **Test Info** which is used in calculations of air flow rates.
d. Begin data collection on the **DMM Scan** page. Data is preset to record 3000 measurements for each instrument, roughly 550 minutes of data collection. Switch either to the **DATAConv** or **HUD** page for monitoring of the system.

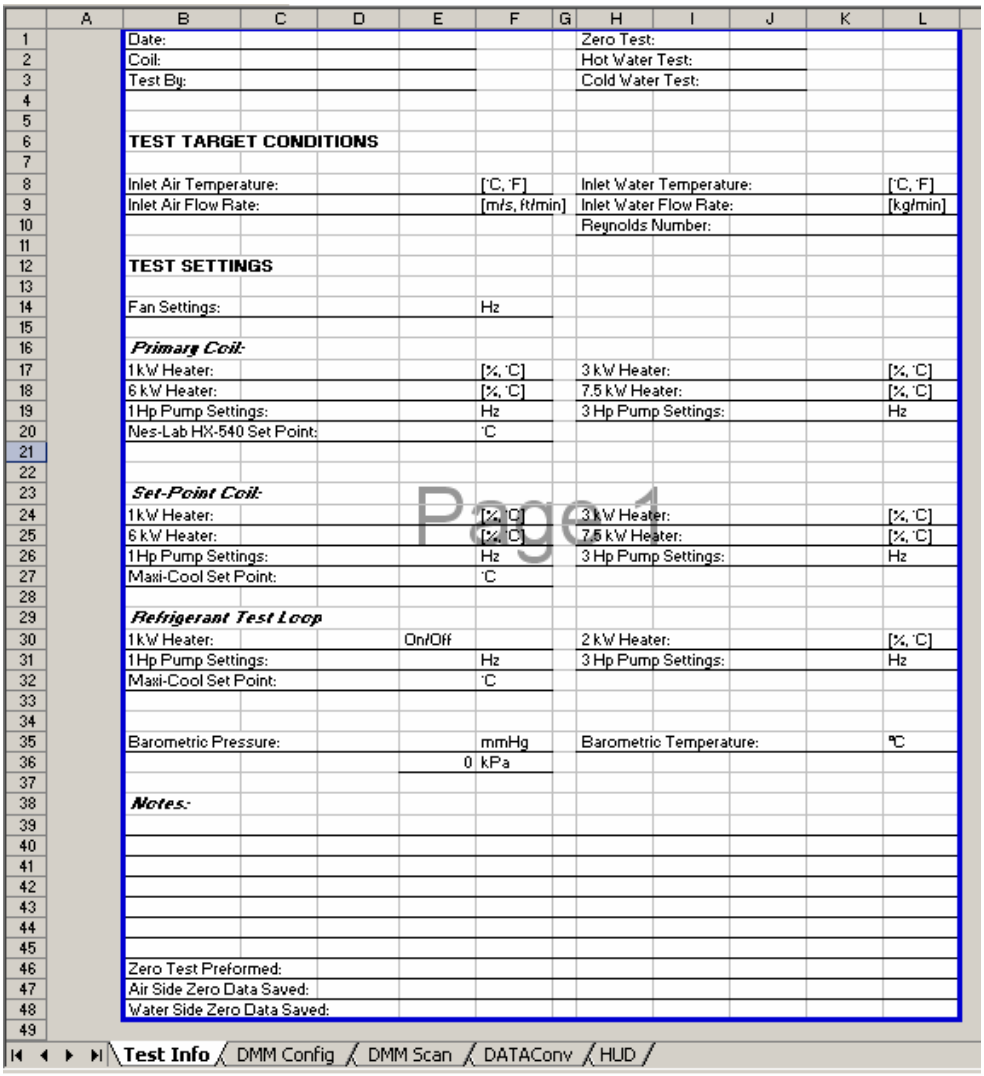

1	Date:						Zero Test:				
2	Coil:						Hot Water Test:				
3	Test By:						Cold Water Test:				
4											
5											
6	**TEST TARGET CONDITIONS**										
7											
8	Inlet Air Temperature:				[°C, °F]		Inlet Water Temperature:				[°C, °F]
9	Inlet Air Flow Rate:				[m/s, ft/min]		Inlet Water Flow Rate:				[kg/min]
10							Reynolds Number:				
11											
12	**TEST SETTINGS**										
13											
14	Fan Settings:				Hz						
15											
16	***Primary Coil:***										
17	1 kW Heater:				[%, °C]		3 kW Heater:				[%, °C]
18	6 kW Heater:				[%, °C]		7.5 kW Heater:				[%, °C]
19	1 Hp Pump Settings:				Hz		3 Hp Pump Settings:				Hz
20	Nes-Lab HX-540 Set Point:				°C						
21											
22											
23	***Set-Point Coil:***										
24	1 kW Heater:				[%, °C]		3 kW Heater:				[%, °C]
25	6 kW Heater:				[%, °C]		7.5 kW Heater:				[%, °C]
26	1 Hp Pump Settings:				Hz		3 Hp Pump Settings:				Hz
27	Maxi-Cool Set Point:				°C						
28											
29	***Refrigerant Test Loop***										
30	1 kW Heater:			On/Off			2 kW Heater:				[%, °C]
31	1 Hp Pump Settings:				Hz		3 Hp Pump Settings:				Hz
32	Maxi-Cool Set Point:				°C						
33											
34											
35	Barometric Pressure:				mmHg		Barometric Temperature:				°C
36				0	kPa						
37											
38	***Notes:***										
39											
40											
41											
42											
43											
44											
45											
46	Zero Test Preformed:										
47	Air Side Zero Data Saved:										
48	Water Side Zero Data Saved:										
49											

Test Info | DMM Config | DMM Scan | DATAConv | HUD

Fig. C3. The Test Info Page in the TunnelSystem 3.4.xls.

2) Bring air handler to steady-state.
   a. Close BV21 on the wind tunnel control panel to ensure LFE pressure drop will be read correctly.
   b. Turn on air handler using PowerFlex 4 located on the air handler control panel. The frequency can be adjusted from 0-60 Hz until desired air velocity is achieved. Consult the **DATAConv** or **HUD** screen for the actual or standard velocity.
   c. Turn on both blowers for the air temperature measurement systems. The switches for the blowers are located on the wind tunnel control panel.
   d. Remove plugs and connect an inclined manometer to the orifice plate for the inlet temperature measurement system.
   e. Adjust regulation gate valves, GV7 until there is 0.2 in. of H_2O pressure drop across the orifice plate.
   f. Repeat the process for the outlet orifice plate; however, adjusts GV8 until a pressure drop of 0.2 in. of H_2O is reached.
   g. Return plugs to both sets of orifice plates.

h. Before the air handler can be temperature controlled, prepare the Air Handler Conditioning Loops for Temperature Regulation. Ensure that the Conditioning loops are filled to capacity and connected to their respective air handler coils. If the loop is low on water open water tank valves BV7 and BV8. Return to closed position if loop is filled.
i. Ensure valves BV6 and BV14 are open.
j. Power up loop control panel.
k. Control flow for each conditioning loop by using the 1 and 3 hp pump for each system. Additional control of flow can be gained in using bypass valves, BV1-5 and BV9-13; however for Unit Cell tests they were not necessary.
l. Adjust conditioning loop outlet temperature with Watlow® controllers. Depending on controller settings either desired temperature (0-85.0 °C) or desired output (0-100%) can be set for each heater.
m. To use the loop for cooling purposes, the FTS® Maxi-Cool and NESLAB HX540 for their respective conditioning loops can be turned on and their temperature adjusted accordingly. Ensure facility water is flowing though each chiller prior using them. For Unit Coil Tests the NESLAB® HX540 was found unnecessary and not used.
n. If humidity control is needed turn on DriSteem® Humidifier and power supply located on the air handler control panel.
o. If air flow rate is to low an error message will appear on the Humidifier controller and the air flow override switch, located on steel expansion section downstream of the test section, must be turned on.
p. Adjust Humidifier supply rate from 0-10 VDC.
q. Constantly monitor the **DATAConv** or **HUD** until air inlet conditions reach steady-state. Because of room conditions changing during tests, temperatures and flow rates may need to be adjusted throughout testing.

Fig. C4. Wind tunnel control panel.

Fig. C5. Air handler control panel.

Fig. C6. Picture of Air Handler Conditioning Loop 1 control panel.

3) Bring Unit Cell Conditioning Loop to steady-state.
    a. During Unit Cell Coil Tests, the alternate outlet is not used. Therefore BV18 and BV20 must be closed.
    b. Connect the inlet and outlet fittings to the Unit Cell coil. If a zero test is being performed the recirculating loop is not connected to the coil. Instead the inlet fitting is connected directly to the outlet fitting.
    c. Open BV17 and remove SV1 and fill the system until the clear accumulator is ¾ full.
    d. Replace SV1 with Teflon tape to ensure an air tight seal.
    e. Pressurize the recirculating loop by hooking up facility air to SV1. A recommended setting is to 10-15 psi; however, DO NOT exceed 20 psi.
    f. To maintain pressure throughout the tests close BV17.
    g. Control the flow rate of the water by using the controllers for each pump. The frequency can be adjusted from 0-60 Hz until desired mass flow rate is achieved. The mass flow rate can be monitored by the MicroMotion® Totalizer on the wind tunnel control panel or by looking at the **DATAConv** or **HUD** display screen.

h. For the pump not in use, ensure that the ball valve downstream of that pump, BV15 and BV16, is closed.
i. Using the total pressure gage on the back side of the pumps check for positive pressure. If the pressure drops too far, the water may cavitate inside the pump heads and flow may stop. When the flow stops, the chance of overheating a element heater rises.
j. Remove any air from the system by slowly loosening the inlet and outlet thermistor compression fittings. When water begins to spill from the fittings retighten.
k. To use the loop for heating purposes, the 2 kW heater may be turned on by using the switch located on the wind tunnel control panel.
l. The 2 kW heater can be adjusted form 0-100% on the Watlow® controller until desired temperature is achieved.
m. For supplemental heat the 1 kW heater switch may be turned on.
n. To use the loop for cooling purposes, the FTS® Maxi-Cool can be turned on and their temperature adjusted accordingly. Ensure facility water is flowing though each chiller prior using them. (The Maxi-Cool may also be used for supplemental heating if needed.
o. Monitor the total pressure throughout heating tests on the various total pressure gages on the system. If it rises dramatically (~50psi) re-open BV17 and SV1 to slowly depressurize the system.
p. Constantly monitor the **DATAConv** or **HUD** until Unit Cell conditioning loop inlet conditions reach steady-state. Because of room conditions changing during tests, temperatures and flow rates may need to be adjusted throughout testing.

4) Control differential pressure transducers.
   a. Open BV25, and Close BV22, BV23, and BV24.
   b. Check pressure drop across the High Differential Pressure Transducer on the **DATAConv**.
   c. If the pressure of the HDP is lower than 0.35 in. of H_2O, close BV25 and open BV23 and BV25. This will prevent potential damage to the transducers.
5) Collect test data once inlet and outlet conditions reach steady state. To ensure a reasonable uncertainty, specified by ASHRAE, collect data for at least 32 measurements for each instrument, roughly 6 minutes. (All Unit Cell tests are run for 100 measurements, 20 minutes.)

C.4 Data Transfer and Reduction Procedure

Once the data a test has been completed and saved using the *TunnelSystem 3.4.xls*, it is necessary to reduce the basic measurements into useful quantities such as heat transfer rates and UA values. Thus a spreadsheet has been developed to post-process the data for further study. All equations and calculations used are as described previously. The following is a procedure to move the raw *TunnelSystem 3.4.xls* data to the *Analyzed Data 3.4.xls* file. As long as at least 35 measurements have been made for each instrument all calculations and uncertainty measurements should be correct.

1) Power up the computer and open *Analyzed Data 3.4.xls*. This spreadsheet was developed with to be used with the *TunnelSystem 3.4.xls* to perform data reduction. The file has a total of six pages which are:
    a. **IP.** The IP displays analyzed data in English units. No changes should be made to this page.
    b. **SI.** The SI displays analyzed data in standard Metric units. This page only demands slight changes for each test.
    c. **DATA.** Raw data and measurements for Unit Cell tests.
    d. **Air Zero DATA**. Raw data and measurements for air side temperature measurement 'zero' tests, if necessary.
    e. **Fluid Zero DATA**. Raw data and measurements for water side temperature measurement 'zero' tests, if necessary.
    f. **Equations**. Displays calibration curves and error constants. When instrumentation is recalibrated, calibration constants and standard fit error need to be changed for accurate data and uncertainty analysis. DO NOT change the fluid properties.
2) On the **SI** page update test information and coil information.
    a. Update test information: coil number, date, and the tech that performed the test.
    b. Update coil geometric parameters: Coil Face Area, Tube inside Diameter, and the number of tubes in which the water flows through the coil.
    c. If the data was zeroed then place an 'X' next to this option.
    d. Specify the type of test with an 'X' on either "Hot Water Test" or "Cold Water Test".
3) Switching to the **DATA** page, the raw experimental data must be inserted into the spreadsheet.
    a. Input the barometric pressure and barometric pressure that was recorded on the **Test Info** page of *TunnelSystem 3.4.xls.*
    b. Copy the entirety of the raw data displayed on the **DATAConv** in the *TunnelSystem 3.4.xls* file that is wished to be analyzed to the **DATA** page. This includes columns A-AF.
        i. To correctly copy this data 'right click' in cell B14 on the **DATA** page and select *Insert Copied Cells…* and *Shift cells Down.* This will update the spreadsheet with formulas, but not the actual data. This step is necessary to ensure that important cells are not over written.
        ii. Again click on cell B14 on the **DATA** page and 'right click' and select *Paste Special*….Under the Paste Options select *Values.* This will update the spreadsheet with the correct raw data.
    c. Copy the entirety of the instrument data on the **DATAConv** in the *TunnelSystem 3.4.xls* file that is wished to be analyzed to the **DATA** page. This includes columns AM-BZ.
        i. To correctly copy this data 'right click' in cell AN14 on the **DATA** page and select *Insert Copied Cells…* and *Shift cells Down.* This will update the spreadsheet with formulas, but not

the actual data. This step is necessary to ensure that important cells are not over written.

ii. Again click on cell AN14 on the **DATA** page and 'right click' and select *Paste Special*….Under the Paste Options select *Values.* This will update the spreadsheet with the correct raw data.

4) Switching to the **Air Zero DATA** page, the raw air data must be inserted into the spreadsheet. If the system was not zeroed this step can be ignored.
   a. Copy the entirety of the raw data displayed on the **DATAConv** in the *TunnelSystem 3.4.xls* file that is wished to be analyzed to the **Air Zero DATA** page. This includes columns A-B and Q-AD.
      i. To correctly copy this data 'right click' in cell B14 on the **Air Zero DATA** page and select *Insert Copied Cells…* and *Shift cells Down.* This will update the spreadsheet with formulas, but not the actual data. This step is necessary to ensure that important cells are not over written.
      ii. Again click on cell B14 on the **Air Zero DATA** page and 'right click' and select *Paste Special*….Under the Paste Options select *Values.* This will update the spreadsheet with the correct raw data.
      iii. A similar process must be done for the other thermistors data in columns D-R.
   b. Copy the entirety of the instrument data on the **DATAConv** in the *TunnelSystem 3.4.xls* file that is wished to be analyzed to the **Air Zero DATA** page. This includes columns AM-AN and BK-BX.
      i. To correctly copy this data 'right click' in cell X14 on the **Air Zero DATA** page and select *Insert Copied Cells…* and *Shift cells Down.* This will update the spreadsheet with formulas, but not the actual data. This step is necessary to ensure that important cells are not over written.
      ii. Again click on cell X14 on the **Air Zero DATA** page and 'right click' and select *Paste Special*….Under the Paste Options select *Values.* This will update the spreadsheet with the correct raw data.
      iii. A similar process must be done for the other thermistors data in columns Z-AM.

5) Switching to the **Fluid Zero DATA** page, the raw fluid data must be inserted into the spreadsheet. If the system was not zeroed this step can be ignored.
   a. Copy the entirety of the raw fluid zero data displayed on the **DATAConv** in the *TunnelSystem 3.4.xls* file that is wished to be analyzed to the **Fluid Zero DATA** page. This includes columns N-Q.
      i. To correctly copy this data 'right click' in cell B14 on the **Fluid Zero DATA** page and select *Insert Copied Cells…* and *Shift cells Down.* This will update the spreadsheet with formulas, but not the actual data. This step is necessary to ensure that important cells are not over written.

ii. Again click on cell B14 on the **Fluid Zero DATA** page and 'right click' and select *Paste Special*….Under the Paste Options select *Values.* This will update the spreadsheet with the correct raw data.

b. Copy the entirety of the fluid zero instrument data on the **DATAConv** in the *TunnelSystem 3.4.xls* file that is wished to be analyzed to the **Fluid Zero DATA** page. This includes columns BG-BJ.
   i. To correctly copy this data 'right click' in cell L14 on the **Fluid Zero DATA** page and select *Insert Copied Cells…* and *Shift cells Down.* This will update the spreadsheet with formulas, but not the actual data. This step is necessary to ensure that important cells are not over written.
   ii. Again click on cell L14 on the **Fluid Zero DATA** page and 'right click' and select *Paste Special*….Under the Paste Options select *Values.* This will update the spreadsheet with the correct raw data.